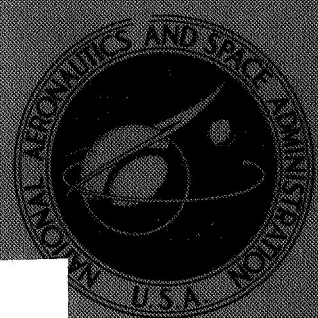


NASA CONTRACTOR REPORT



NASA CR-1024

NASA CR-1024

GPO PRICE \$ _____

CFSTI PRICE(S) \$ _____

Hard copy (HC) _____

Microfiche (MF) _____

ff 653 July 65

N 68-23560

FACILITY FORM 602

(ACCESSION NUMBER) _____ (THRU) _____

146 (PAGES) _____ (CODE) _____

(NASA CR OR TMX OR AD NUMBER) _____ (CATEGORY) 17

ULTRAVIOLET-PROTON RADIATION EFFECTS ON SOLAR CONCENTRATOR REFLECTIVE SURFACES

by *R. B. Gillette*

Prepared by
THE BOEING COMPANY
 Seattle, Wash.
 for Langley Research Center



ULTRAVIOLET-PROTON RADIATION EFFECTS ON
SOLAR CONCENTRATOR REFLECTIVE SURFACES

By R. B. Gillette

Distribution of this report is provided in the interest of information exchange. Responsibility for the contents resides in the author or organization that prepared it.

Prepared under Contract No. NAS 1-5251 by
THE BOEING COMPANY
Seattle, Wash.

for Langley Research Center

NATIONAL AERONAUTICS AND SPACE ADMINISTRATION

For sale by the Clearinghouse for Federal Scientific and Technical Information
Springfield, Virginia 22151 - CFSTI price \$3.00

... ..

... ..

... ..

... ..

... ..

... ..

TABLE OF CONTENTS

	Page
1.0 SUMMARY	1
2.0 INTRODUCTION	2
3.0 TEST SAMPLES	3
4.0 APPARATUS	8
4.1 Charged Particle Radiation Facility	8
4.2 Ultraviolet Radiation Facility	8
4.3 Reflectometers	12
4.4 In-Situ Reflectance Measurement/Irradiation Facility	12
5.0 PROCEDURES	15
5.1 Charged Particle Irradiation and Dosimetry	15
5.2 Ultraviolet Irradiation and Dosimetry	17
5.3 Combined Proton-Ultraviolet Irradiation and Dosimetry	23
5.4 In-Situ Reflectance Measurement Experiment	25
5.5 Electron Photomicrographs	26
5.6 Reflectance Data Acquisition and Reduction Procedures	26
6.0 RESULTS AND DISCUSSION	29
6.1 Contamination of Test Samples	29
6.2 Electroformed-Nickel Mirrors	32
6.3 Stretch-Formed Aluminum Mirrors	69
6.4 Magnesium Substrate Mirrors	98
6.5 Space Radiation Effects	103
7.0 CONCLUSIONS	116
8.0 RECOMMENDATIONS	117
9.0 REFERENCES	118
10.0 APPENDICES	121
Tables of data for all tests	
ABSTRACT	139

LIST OF ILLUSTRATIONS

Figure	Title	Page
1.	Schematic of Low-Energy Particle Accelerator	9
2.	Ultraviolet Test Chamber	10
3.	Ultraviolet Test Setup	11
4.	Schematic of Ultraviolet Irradiation/In-Situ Reflectance Measurement Facility	13
5.	Typical Proton Flux Distribution Across Sample	18
6.	Variation of Intensity Along Length of UA-II Mercury Lamp	19
7.	Spectral Distribution of Ultraviolet Lamps	22
8.	Schematic of Combined Proton/Ultraviolet Test Setup	24
9.	Relationship of Specularly Reflected Beam to Entrance Port of Gier-Dunkle Integrating Sphere	27
10.	Spectral Reflectance of Typical Electroformed Nickel Mirror Samples	33
11.	Effect of Proton Energy on Silicon-Oxide Overcoated, Nickel Substrate Mirrors	35
12.	Effect of Protons on Spectral Reflectance of Bare Aluminum Coated, Nickel Substrate Mirrors	37
13.	Effect of Protons on Solar Specular Reflectance of Aluminum Coated, Nickel Substrate Mirrors	39
14.	Effect of Protons on Spectral Reflectance of Si ₂ O ₃ Overcoated, Nickel Substrate Mirrors	40
15.	Effect of Protons on Solar Specular Reflectance of Si ₂ O ₃ Overcoated, Nickel Substrate Mirrors	41
16.	Photomicrograph of Unirradiated Silicon-Oxide Surface	44
17.	Photomicrograph of Silicon-Oxide Surface Irradiated with 4.7×10^{16} Protons cm^{-2} (16 keV 0°C)	44
18.	Photomicrograph of Silicon-Oxide Surface Irradiated with 1×10^{17} Protons cm^{-2} (16 keV 0°C)	45
19.	Photomicrograph of Silicon-Oxide Surface Irradiated with 2×10^{17} Protons cm^{-2} (16 keV 0°C)	45
20.	Effect of Protons on Spectral Reflectance of 8000Å Si ₂ O ₃ Overcoated, Nickel Substrate Mirrors	46
21.	Effect of Protons on the Infrared Reflectance of Si ₂ O ₃ Overcoated, Nickel Substrate Mirrors	48
22.	Effect of Protons on Solar Specular Reflectance of 8000Å Si ₂ O ₃ Overcoated, Nickel Substrate Mirrors	49
23.	Effect of Protons on Spectral Reflectance of 17000 Å SiO ₂ Overcoated, Nickel Substrate Mirrors	50
24.	Effect of Protons on the Infrared Reflectance of SiO ₂ Overcoated, Nickel Substrate Mirrors	51
25.	Effect of Protons on Solar Specular Reflectance of SiO ₂ Overcoated, Nickel Substrate Mirrors	53

LIST OF ILLUSTRATIONS (Cont.)

Figure	Title	Page
26.	Effect of Ultraviolet Radiation on Solar Specular Reflectance of Nickel Substrate Mirrors	54
27.	Effect of Ultraviolet Radiation on Solar Specular Reflectance of Nickel Substrate Mirrors	55
28.	Effect of Ultraviolet Radiation on Solar Specular Reflectance of Nickel Substrate Mirrors	56
29.	Effect of Ultraviolet Radiation on Solar Specular Reflectance of Nickel Substrate Mirrors	57
30.	In-Situ Reflectance Data on SiO ₂ Overcoated Nickel Mirror	60
31.	In-Situ Reflectance Data on 8000Å -Thick Si ₂ O ₃ Overcoated Nickel Substrate Mirrors	61
32.	Effect of Combined Proton-Ultraviolet Radiation Environment on Aluminum Coated, Electroformed Nickel Mirrors	63
33.	Effect of Proton Irradiation on Ultraviolet Degradation of Aluminum Coated, Nickel Substrate Mirrors	64
34.	Effect of Combined Proton-Ultraviolet Radiation Environment on Si ₂ O ₃ Overcoated, Electroformed Nickel Substrate Mirrors	65
35.	Effect of Proton Irradiation on Ultraviolet Degradation of Si ₂ O ₃ Overcoated Nickel Substrate Mirrors	66
36.	Spectral Reflectance of Typical Stretch-Formed Aluminum Mirror Samples	70
37.	Effect of Proton Angle of Incidence on Bare Aluminum Coated, Aluminum Substrate Mirrors	71
38.	Photomicrograph of Unirradiated Bare Aluminum Coated, Aluminum Substrate Mirror	72
39.	Photomicrograph of Bare Aluminum Coated, Aluminum Substrate Mirror Irradiated at Normal Incidence	72
40.	Photomicrograph of Bare Aluminum Coated, Aluminum Substrate Mirror Irradiated at 30 Degrees from Normal	73
41.	Photomicrograph of Bare Aluminum Coated, Aluminum Substrate Mirror Irradiated at 60 Degrees from Normal	73
42.	Effect of Proton Angle of Incidence on Blister Size Distribution on Bare Aluminum Coated, Aluminum Substrate Mirrors	74
43.	Proton Penetration in a Bare Aluminum Coated, Aluminum Substrate Mirror	76
44.	Effect of Proton Energy on Blister Formation in Bare Aluminum Coated, Aluminum Substrate Mirrors	78
45.	Photomicrograph of Bare Aluminum Coated, Aluminum Substrate Mirror Irradiated with 4 keV Protons	79
46.	Photomicrograph of Bare Aluminum Coated, Aluminum Substrate Mirror Irradiated with 6.4 keV Protons	80
47.	Photomicrograph of Bare Aluminum Coated, Aluminum Substrate Mirror Irradiated with 13.3 keV Protons	81

LIST OF ILLUSTRATIONS (Cont.)

Figure	Title	Page
48.	Photomicrograph of Bare Aluminum Coated, Aluminum Substrate Mirror Irradiated with 21.3 keV Protons	82
49.	Photomicrograph of Bare Aluminum Coated, Aluminum Substrate Mirror Irradiated with 27 keV Protons	83
50.	Effect of Protons on Solar Specular Reflectance of Bare Aluminum Coated, Aluminum Substrate Mirrors	85
51.	Effect of Protons on Solar Specular Reflectance of Silicon-Oxide Overcoated, Aluminum Substrate Mirrors	87
52.	Stretch Formed Aluminum Mirror after Heating to 100°C	89
53.	Stretch Formed Aluminum Mirror after Heating to 200°C	90
54.	Effect of Ultraviolet Radiation on Stretch-Formed Aluminum Mirrors	91
55.	Effect of Ultraviolet Radiation on Stretch-Formed Aluminum Mirrors	92
56.	Effect of Combined Proton-Ultraviolet Radiation Environment on Bare Aluminum Coated, Aluminum Substrate Mirrors	94
57.	Effect of Proton Irradiation on Ultraviolet Degradation of Bare Aluminum Coated, Aluminum Substrate Mirrors	95
58.	Effect of Combined Proton-Ultraviolet Radiation Environment on Si ₂ O ₃ Overcoated, Aluminum Substrate Mirrors	96
59.	Effect of Proton Irradiation on Ultraviolet Degradation of Si ₂ O ₃ Overcoated, Aluminum Substrate Mirrors	97
60.	Effect of Protons on the Spectral Reflectance of Magnesium Substrate Mirrors	99
61.	Effect of Protons on Solar Specular Reflectance of Silicon-Oxide Overcoated, Magnesium Substrate Mirrors	100
62.	In-Situ Reflectance Data on Magnesium-Substrate Mirrors	102
63.	Effect of Combined Proton-Ultraviolet Radiation Environment on Magnesium Substrate Mirrors	104
64.	Trapped Proton Spectra at Synchronous Altitude	106
65.	Proton Stopping Power in Silica	109
66.	Path Length and Penetration Depth of Protons in Silica	110
67.	Differential-Dose and Elastically-Deposited Energy to an Si ₂ O ₃ Surface at Synchronous Orbit	112
68.	Space Mission Equivalences for 16 keV Proton Test Data	115

LIST OF TABLES

		Page
I	Description of Solar Mirror Test Samples	3
II	Summary of Test Conditions in Proton Experiments	16
III	Summary of Test Conditions In Ultraviolet Experiments	20
IV	Emission Data for UA-II Mercury-Arc Lamp	21
V	Summary of Electron Irradiation Data	68

1.0 SUMMARY

The results of a research program conducted over the period beginning June 1965 to August 1967 under Contract NAS 1-5251 are presented in this final report.

The overall scope of the program was to study effects of protons and ultraviolet radiation on the specular and diffuse reflectances of stretch-formed aluminum, electro-formed nickel, and magnesium substrate solar concentrator surfaces. A limited number of electron radiation experiments was also performed. Spectral reflectances were measured over the wavelength region from 0.3 to 2.5 microns so that changes in the integrated reflectance for the solar spectrum could be calculated. Test samples, typical of the three types of solar concentrators, had reflective surfaces of either aluminum or aluminum overcoated with Si_2O_3 and SiO_2 films.

In proton experiments, test samples were irradiated with integrated fluxes varying from 1×10^{15} to 2×10^{17} protons cm^{-2} , energies in the range of 2 to 30 keV, and irradiation angles of incidence varying from 0 to 60 degrees from normal. In ultraviolet experiments, test samples were irradiated with exposures up to 9800 equivalent space sun hours (ESSH). The effects of varying temperature over the range of -195° to 200°C were evaluated in both proton and ultraviolet experiments. Additional experiments performed in the program included "in-situ" reflectance measurements in ultraviolet tests and combined radiation environment tests.

It was found that the stretch-formed aluminum and magnesium substrate solar concentrator surfaces showed severe reticulation at temperatures in excess of 50° to 80°C . The most severe mechanism of radiation-induced degradation was found to be proton blistering. The amount of reflectance degradation produced by blistering was shown to be highly temperature dependent and is a function of the proximity of the stopped protons to the site at which hydrogen agglomeration occurs. When blistering did not occur, the reflectance degradation was not strongly temperature-dependent and exhibited a saturation effect at relatively low exposures. An interesting minor effect noted was the decrease in diffuse reflectance of proton-irradiated silicon oxide overcoated surfaces. This was attributed to a smoothing or "ionic polishing" effect on the oxide surface.

In-situ reflectance measurements, made on selected test samples before and after ultraviolet irradiation, showed that no significant annealing of radiation-induced degradation occurred when the surfaces irradiated in vacuum were returned to ambient pressure. It was however noted that the silicon-oxide overcoated surfaces exhibited a shift in wavelength of interference maxima and minima during pumpdown, irradiation, and backfilling to ambient pressure.

2.0 INTRODUCTION

Over the past few years considerable effort has been expended on the development of solar radiation concentrators capable of operating in the space environment. These concentrators (mirrors) are being developed as a possible heat source for thermal-electrical conversion systems on spacecraft. A space-qualified solar mirror must be light in weight, structurally stable, geometrically accurate, and must possess high solar specular reflectance. This research effort has been involved with the latter of these requirements. The objectives of this program were to evaluate the combined and individual effects of ultraviolet radiation and protons on the specular and diffuse reflectance of various solar mirror coatings and substrates. Specifically, the dependence of reflectance changes on proton energy, proton angle of incidence, mirror temperature, integrated particle flux, and ultraviolet exposure are discussed. Results of combined proton/ultraviolet and electron radiation experiments are also presented.

Although a great variety of materials has been used for fabricating solar mirrors, three of the most promising concepts were chosen for evaluation in this program: stretch-formed aluminum, electroformed nickel, and magnesium substrate mirrors. All of these mirrors employ multilayer coatings for the purposes of enhancement of solar specular reflectance, thermal control, bonding, and protection of the metallic reflecting surfaces. Since it was anticipated that the effects of ultraviolet radiation and protons would be somewhat dependent on the specific combination of coatings used, several combinations of coatings on the aluminum and nickel substrates were evaluated. Solar mirror test samples were prepared with bare vacuum-deposited aluminum, both thin and thick silicon oxide overcoatings, and thick fused silica overcoatings.

Experiments in this program pertain primarily to solar mirrors; however, the results are somewhat useful for predicting radiation effects on other mirror surfaces in space.

3.0 TEST SAMPLES

Two basic types of solar mirror substrates were chosen for evaluation at the outset of the program: stretch-formed aluminum; and electroformed nickel. A magnesium substrate mirror was introduced later in the program. The overcoatings applied to these substrates were typical of those applied to actual solar mirrors for space application. The processes and materials used for fabricating the first two types of mirrors have been described in detail in References 1 and 2. A description of the magnesium substrate mirror is given below. The epoxy-coated aluminum substrates were prepared by TAPCO*; the electroformed nickel substrates were prepared by Spectrolab Inc. of Sylmar, California, and the magnesium substrates by NASA/Lewis Research Center. Vacuum deposited films on the two former substrates were applied by Spectrolab, and on the latter by the Kinney Vacuum Division of the New York Air Brake Co. A detailed description of the various combinations of substrates and coatings evaluated is given in Table I. Nominal coating thicknesses are also given in the table; however, specific thicknesses and vacuum coating data are given in Appendix A.

TABLE I -- DESCRIPTION OF SOLAR MIRROR TEST SAMPLES

Sample Type	A	B	C	D	E	F	G
Number of Samples	100	100	100	100	32	32	43
Layer 4	--	Si ₂ O ₃ (1800Å)	--	Si ₂ O ₃ (1800Å)	Si ₂ O ₃ (8000Å)	SiO ₂ (17,000Å)	Si ₂ O ₃ (1400Å)
Layer 3	Aluminum (1000Å)		Aluminum (1000Å)			Aluminum (1000Å)	
Layer 2	SiO (1500Å)		SiO (1500Å)			SiO (1500Å)	
Layer 1	Epoxy (0.002 cm)		Chromium (500Å)			Epoxy (0.004 cm)	
Substrate	Stretch-formed Aluminum (0.05 cm)		Electroformed Nickel (0.076 cm)			Magnesium (0.076 cm)	

* A division of Thompson Ramo Wooldridge, Inc., Cleveland, Ohio

3.1 Electroformed Nickel Test Samples

The electroformed-nickel mirror test samples were prepared as follows. A ground and polished Pyrex disc, 30.5 cm in diameter, was used as the optical master for electroforming. The Pyrex disc was cleaned and coated with silver prior to each electroforming operation. Then, a nominal thickness of 0.076 cm (30 mils) of nickel was plated onto the master in a conventional nickel-sulfamate bath. The sheet of nickel was separated from the glass master, the silver was chemically removed, and then 2.38 cm (15/16-inch) diameter test samples were cut out by a spark-discharge machining process. Although a nominal thickness of 0.076 cm was planned, it was found that the thickness varied by as much as ± 16 percent across the sheet.

The cleaning procedure used for the nickel mirror samples was as follows:

- 1) Following electroforming, the samples were thoroughly rinsed with distilled water;
- 2) The nickel sheets were then immersed in a water solution of ammonium hydroxide and hydrogen peroxide to remove the silver parting film;
- 3) Sheets were again rinsed with distilled water;
- 4) After spark-discharge machining, the samples were immersed in a proprietary cleaning solution (Eloxal No. 6) to remove the electrolyte;
- 5) Samples were then rinsed in two sequential toluene baths;
- 6) Samples were then immersed in a 10 percent liquid detergent solution for 2 minutes at 72°C;
- 7) Samples were then immersed in a sulfuric acid solution of 5 percent by volume;
- 8) Samples were then sprayed with deionized water;
- 9) Samples were rinsed in distilled water and blown dry with a syringe;
- 10) Immediately before vacuum deposition, samples were placed in a pure ethyl alcohol bath and scrubbed with long-fiber surgical cotton;
- 11) Samples were finally dried with an air blast and placed in the vacuum Chamber as soon as possible.

Prior to the vacuum coating operation, the nickel samples were subjected to glow-discharge cleaning for a period of 10 minutes at a pressure of 5×10^{-3} torr. The sample temperature was maintained at about 250°C during glow-discharge cleaning.

A summary of details of the vacuum coating operation and estimated coating thicknesses are given in Appendix A. All coatings were applied with an electron beam evaporator using standard procedures. Arrays of samples were rotated during deposition to obtain maximum uniformity of coating thicknesses. It should be noted that thicknesses of the 8000 Å Si_2O_3 films and the SiO_2 films (sample types E and F) were calculated from wavelength positions of reflectance interference maxima on the actual mirror samples, assuming an index of refraction of 1.5. The thicknesses of SiO and thin Si_2O_3 films were calculated from interference maxima obtained by monitoring the reflectance of a glass optical-flat during deposition with light of 5461 Å wavelength. Indices of refraction of 1.8 and 1.5 were assumed for calculating the respective film thicknesses.

It should be pointed out that there is reason to doubt the thickness values given in Appendix A for the thin Si_2O_3 coating on mirror types B and D. The fact that no optical interference was noted in the reflectance spectra of these mirrors indicates that the physical thickness is considerably smaller than the 1800 to 2000 Å value reported. Thickness measurements made with an interferometer and an electron microscope indicate a thickness of 900 - 1300 Å for the Si_2O_3 films on Type B and D mirrors. The discrepancy in film thickness appears to be due to a difference in the rate of deposition between the glass monitoring substrate and the mirror samples. For the benefit of future coating operations of this type, it is recommended that: (1) the reflectance of an actual mirror sample surface be monitored during deposition; and (2) control samples should be prepared which have a shielded or uncoated strip for interferometric thickness measurements.

The thicknesses of metallic films were calculated by the following procedure:

- 1) Reflectance was monitored versus time while the vacuum deposited film was building up to a thickness of about 200 Å;
- 2) Published data of reflectance versus thickness was then used to calculate the thickness versus time (or rate of deposition);
- 3) Based on this rate, the deposition was continued until the desired thickness was obtained.

For presentation purposes, the assumption has been made that the silicon oxide films are stoichiometric compounds of SiO , Si_2O_3 , and SiO_2 . The exact composition was not determined; however, far-infrared reflectance measurements on mirrors coated with 8000 Å of Si_2O_3 verified that the silicon oxide film was Si_2O_3 as determined in similar experiments by Bradford and Hass (Reference 3). Similar infrared reflectance measurements on the specimens coated with vacuum deposited fused silica revealed that those films were probably not the stoichiometric SiO_2 compound.

3.2 Stretch-Formed Aluminum Mirrors

The stretch-formed aluminum mirrors were prepared as follows:

- 1) The samples were made from 3003 "0" condition aluminum alloy that had been annealed at 410°C;
- 2) Sheets of aluminum, 0.05 cm thick, were uniaxially stretch-formed to a 2 percent elongation;
- 3) After stretch-forming the aluminum sheets were cleaned with an etching paste*, rinsed with water, and baked at 70°C;
- 4) The aluminum was then spray-coated with a high-temperature epoxy resin** to improve the specularity of the surface (0.002 cm thick);
- 5) Following spray coating, the epoxy coated sheets were subjected to a cure cycle of 1 hour at 43°C, 16 hours at 93°C, and 2 hours at 150°C.

The cleaning procedure used prior to vacuum coating was as follows:

- 1) Scrub in an Aerosol solution***;
- 2) Immerse in bath of distilled water;
- 3) Scrub under running, warm tap water to remove Aerosol solution;
- 4) Immerse in bath of distilled water;
- 5) Scrub lightly with cotton;
- 6) Immerse in another distilled water bath;
- 7) Remove from bath, shake off excess water, and dry with air.

After cleaning, the samples were immediately placed in the vacuum chamber for coating. The chamber was evacuated to 5×10^{-5} torr, backfilled with air, and a glow discharge was operated for about 30 seconds. Then the chamber pressure was lowered for the vacuum-coating process. A summary of the data from the vacuum coating process is given in Appendix A. It is significant to note that the stretch-formed aluminum samples were not heated during glow-discharge cleaning or vacuum coating in contrast to the nickel substrate mirrors. A thermocouple attached to one of the samples showed no deviation from ambient temperature.

* Hughson Chemical Co., Erie, Pennsylvania, Etching Paste No. EX-B727-6

** Emerson Cumming No. C-26 epoxy resin

*** Fischer Scientific Co. "OT" Aerosol solution, Catalog No. A-351-25% clear

3.3 Magnesium Mirrors

The magnesium-substrate solar mirror samples, supplied by NASA/Lewis Research Center, consisted of a magnesium substrate coated with epoxy, SiO₂, aluminum and Si₂O₃. The magnesium substrate was about 0.076 cm thick and was formed by machining discs from a solid rod. The discs were then ground to an acceptable finish and spray-coated with a 0.004 cm thick epoxy coating. The epoxy coating was cured to a maximum temperature of 90°C. Vacuum-deposited films were applied by the Kinney Vacuum Division of the New York Air Brake Company. Vacuum-coating data for these coatings are given in Appendix A.

The procedure followed for cleaning and vacuum coating was as follows.

1) Most of the epoxy-coated substrates were cleaned using a breath vapor pattern and cotton. The cleaning was necessary to remove fingerprints from the epoxy surfaces. This cleaning caused visible scratches to be formed on the surfaces. Substrates without fingerprints were not cleaned.

2) All substrates were placed in the vacuum chamber and glow-discharge cleaned. The pressure was first reduced to 8×10^{-5} torr and then was increased to 5×10^{-2} torr by backfilling with oxygen. The glow discharge was operated for 30 seconds.

3) Substrates were coated with SiO₂ and aluminum coatings.

4) The aluminum surface was then glow-discharge cleaned for 30 seconds.

5) The Si₂O₃ overcoating was applied and the mirror samples were removed from the chamber.

4.0 APPARATUS

4.1 Charged Particle Radiation Facility

A schematic of the low-energy particle accelerator used for experiments in this program is shown in Figure 1. The schematic shown was the setup for obtaining protons. Essentially the same setup was used for obtaining electrons except that an electron gun was used and the analyzing magnet was not used.

An ORTEC* ion source was used to generate hydrogen ions from commercial, ultrapure laboratory-grade hydrogen gas. This ion source utilizes an 80-Mc rf field to create a plasma containing H^+ , H_2^+ and H_2-H^+ ions (98 percent mass 1 and 2 with some mass 3 particles). Positive ions were electrostatically accelerated to the desired keV energy by applying appropriate potentials to accelerating electrodes and focusing lenses.

Experiments in this program were performed at energies varying from 2 to 30 keV. Mass, energy, and charge separation of the ions were accomplished by the use of a magnetic field and two limiting apertures of 1.9 cm diameter. A particle bend angle of about 25 degrees was used. The first aperture separated the ion-pumped portion of the beam tube from the turbo-molecular pumped portion of the system. The gate valve was closed whenever mirror samples were changed.

Mirror samples were individually mounted on a temperature-controlled copper heat sink. The temperature of the heat sink was varied from the liquid nitrogen boiling point, -195°C , to 200°C . Temperatures of 0° , 40° , 50° , 100° , and 200°C were obtained by passing either heated nitrogen or air through the sample holder.

In regard to the vacuum system employed, indium seals were used throughout the beam tube except in special cases where Viton -A or other polymeric "O" rings had to be used. An ion pump and a turbo-molecular pump were used for evacuation. Typical pressures during irradiation were in the order of 2×10^{-7} torr. A liquid nitrogen cold trap was located in the beam tube such that any volatiles from the ion source, the turbo-molecular pump, or the mirror samples would be adsorbed. This cold trap was removed and cleaned before it warmed up, each time a mirror sample was changed, to avoid contamination of the vacuum system.

4.2 Ultraviolet Radiation Facility

The facility used for performing ultraviolet tests in this program is shown in Figures 2 and 3. As noted in the figures, four independent arrays of mirror samples

* Oak Ridge Technical Enterprise Co.

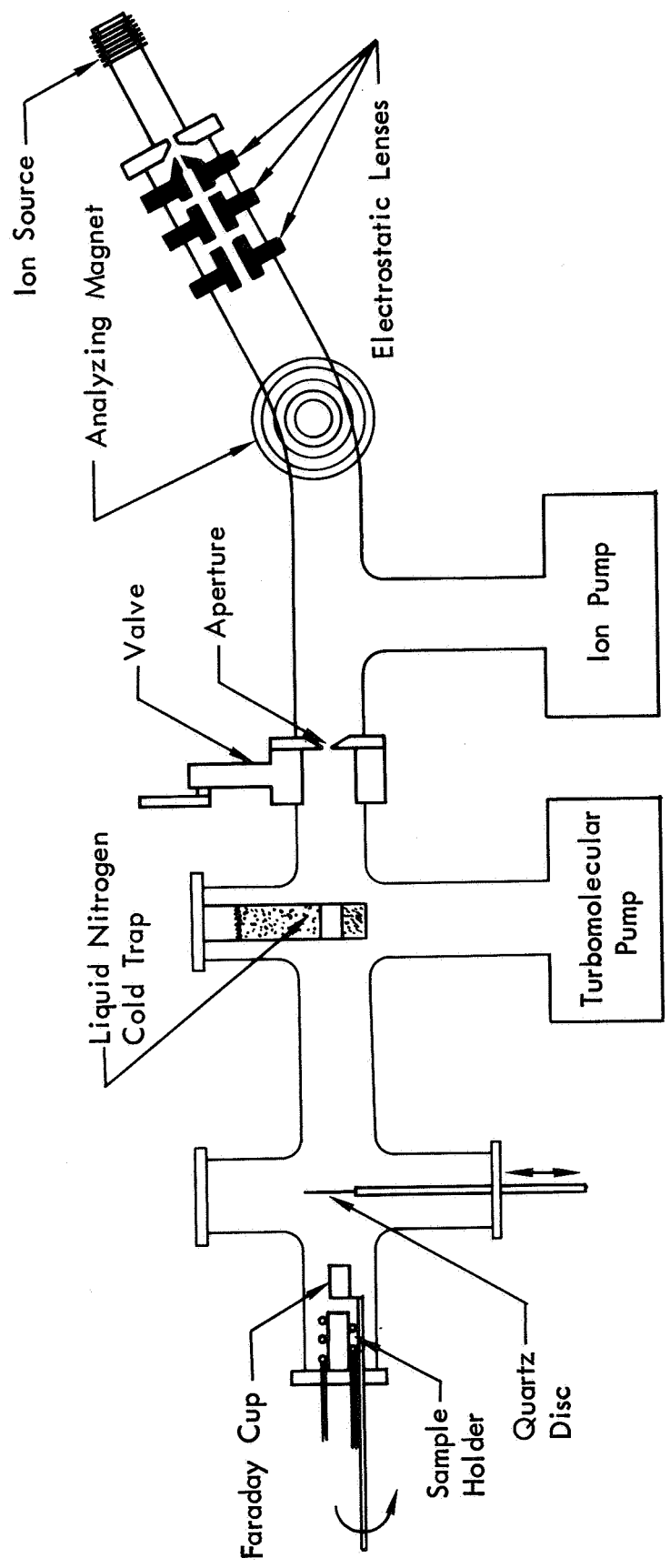


Figure 1: SCHEMATIC OF LOW-ENERGY PARTICLE ACCELERATOR

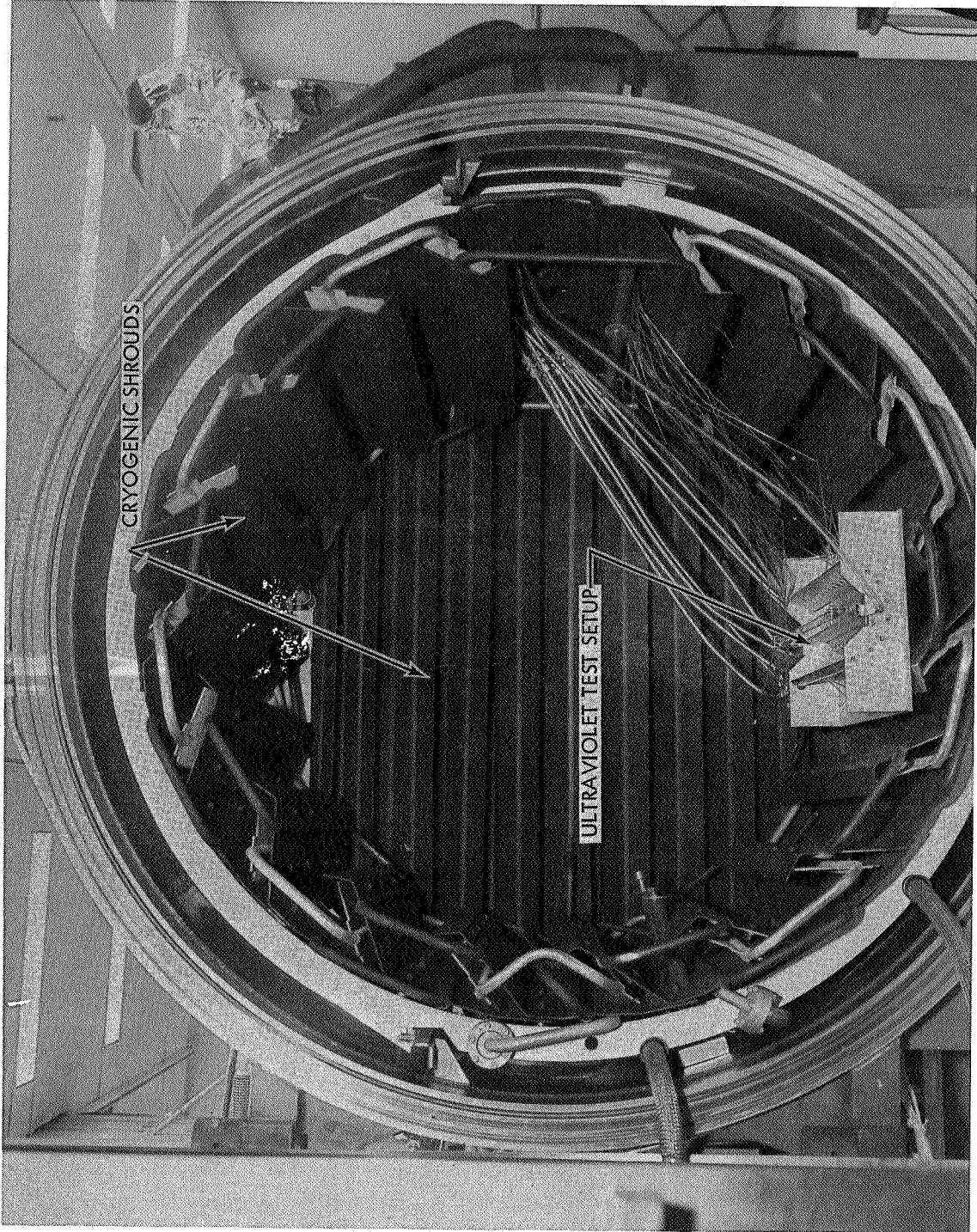


Figure 2: ULTRAVIOLET TEST CHAMBER

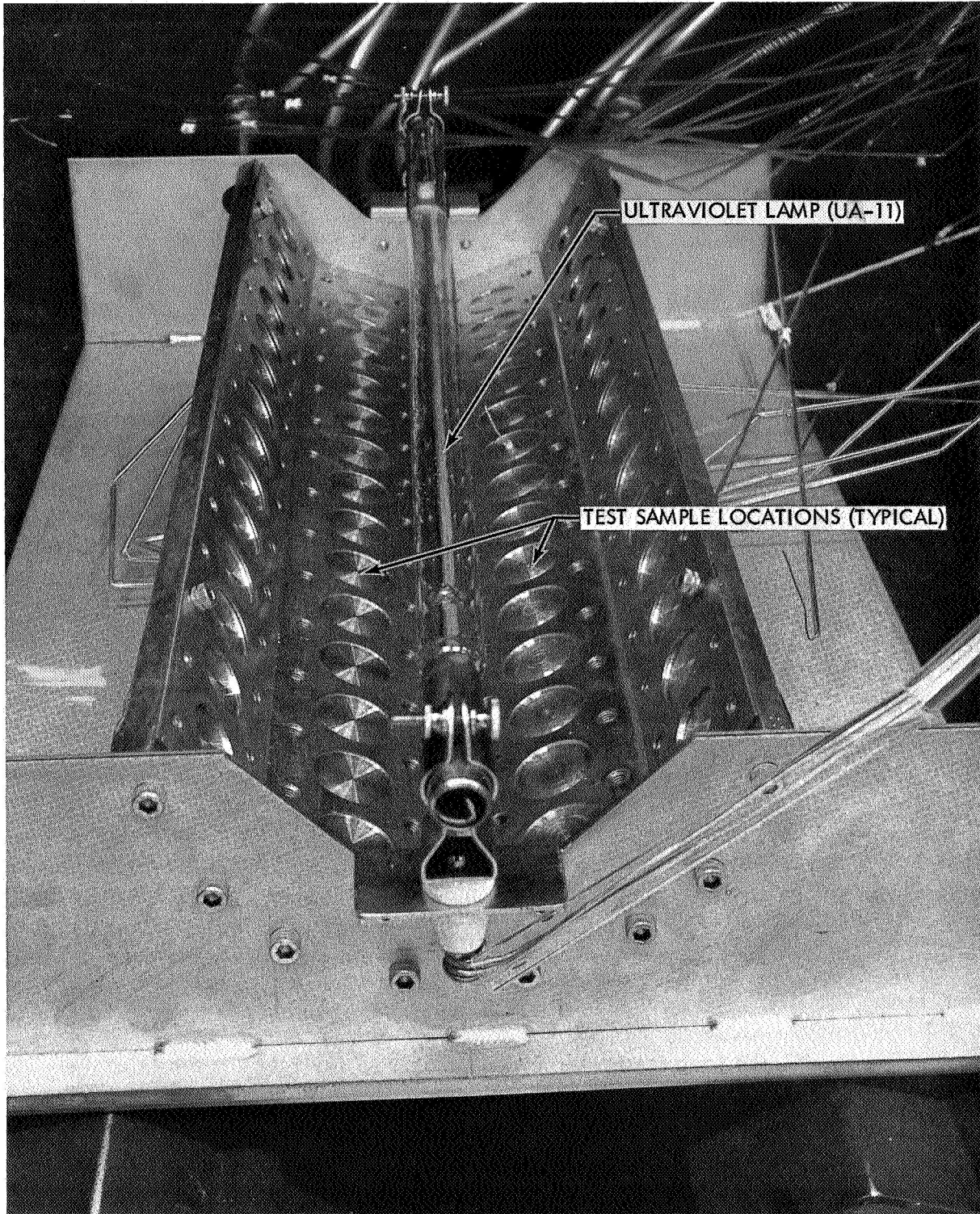


Figure 3: ULTRAVIOLET TEST SETUP

surrounded a UA-11* mercury arc lamp. The distance from the center of the lamp to the surfaces of the mirror samples was 7.1 cm. Fourteen samples were mounted on each sample holder. Each sample holder consisted of a 0.95 cm thick copper bar containing spot faced indentations for the mirror samples. A stainless-steel retainer plate was placed over the copper bar to hold the samples firmly against it. Holes in the retainer plate allowed ultraviolet radiation to strike the mirror surfaces. Copper tubing (a double pass coil) was brazed to the back side of each sample holder for conduction of heat transfer fluids.

4.3 Reflectometers

Reflectance measurements were obtained with a Gier-Dunkle Model AIS-6L Absolute Integrating Sphere Reflectometer (Reference 4) which was attached to a Perkin-Elmer Model 99 Monochromator. The Gier-Dunkle reflectometer provides absolute reflectance in point-by-point wavelength measurements over the region of about 0.30 to 2.5 microns. To minimize data acquisition time, a semi-automatic wavelength and reference mirror positioning system was developed and used in the program.

The infrared reflectance measurements performed in this program were made with a Perkin-Elmer Model IR-4 Spectrophotometer utilizing a heated Hohlraum reflectance attachment. This instrument provides reflectance data measured at near-normal incidence from a diffusely illuminated sample. Data were obtained covering the wavelength range from 1 to 15 microns.

4.4 In-Situ Reflectance Measurement/Irradiation Facility

During the course of this program it was planned to perform the ultraviolet radiation experiment, in which reflectance would be measured in-situ, in a large multiple-specimen irradiation facility. The experiment was indeed started in this facility; however, a vacuum seal failure prevented completion of the test. Because of the time required to repair the facility and schedule problems with another NASA contract, the ultraviolet radiation/in-situ reflectance experiment was run in a different facility. A schematic of this latter facility is shown in Figure 4.

The significant features of the facility are:

- 1) An A-H6* water-cooled ultraviolet lamp is used;
- 2) The ultraviolet intensity (in the wavelength region less than 0.4 micron) on the test sample is 6 to 7 equivalent space suns (ESS);

* Manufactured by the General Electric Co.

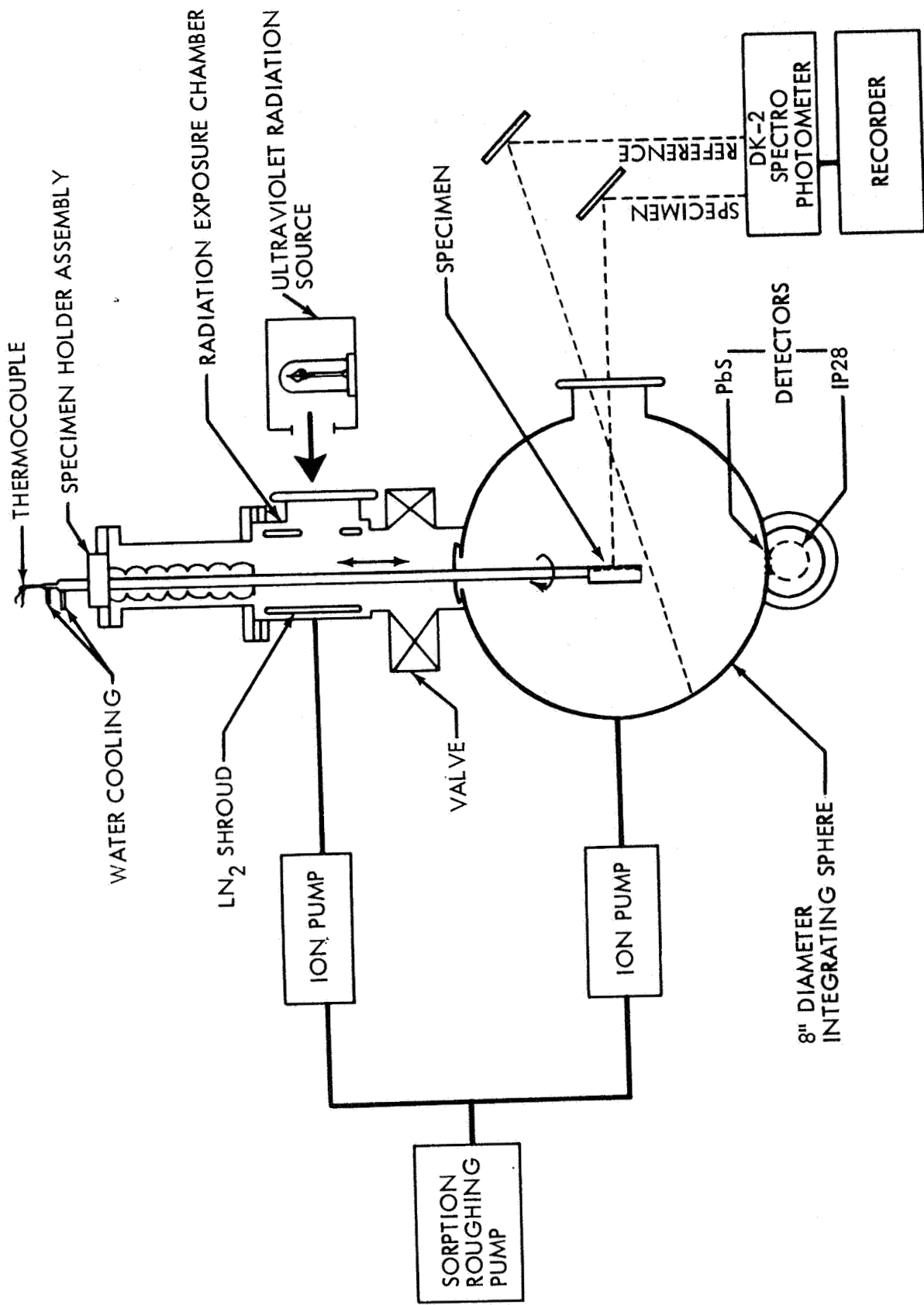


Figure 4: SCHEMATIC OF ULTRAVIOLET IRRADIATION/IN-SITU REFLECTANCE MEASUREMENT FACILITY

- 3) One sample is irradiated at a time;
- 4) A magnesium oxide coated Gier-Dunkle-type integrating sphere (Reference 4) is used in conjunction with a Beckman DK-2A Spectrophotometer; and
- 5) Adsorption and ion pumps are used for evacuation.

The use of an A-H6 mercury-arc lamp for this test provided a different ultra-violet spectrum for irradiation than the UA-11 lamp used in all other tests in the program; however, it was felt that the objective of the test could be accomplished with either lamp.

Both specular-plus-diffuse and diffuse reflectance measurements could be made in the in-situ reflectometer facility, although only the former was measured in these tests. The wavelength range of the instrument was about 0.22 to 2.7 microns; however, reflectance measurements could only be made over the range from 0.27 to 2.1 microns due to an optical lens problem. Inadequate time was available to correct the problem for these experiments.

In regard to cleanliness of the vacuum system, copper gasket and metal brazed seals were used throughout the system with the exception of one rotating seal on the sample holder assembly and the three roughdown valves on the adsorption pumps which were made of Viton-A. During irradiation and measurement of the test sample, only the one rotating seal was exposed to the high vacuum system. To further reduce the possibility of test sample contamination during irradiation, a liquid nitrogen cooled shroud was installed around the test sample as shown in Figure 4.

5.0 PROCEDURES

5.1 Charged Particle Irradiation and Dosimetry

A summary of the various test conditions which the mirror samples were exposed to in the proton tests is given in Table II. As noted in the table the proton integrated flux was varied from 1×10^{15} to 2×10^{17} , although the bulk of the tests were run in the 5×10^{16} to 2×10^{17} protons-cm⁻² range. Lower integrated flux values were run early in the program to determine the threshold of measurable damage. Proton energies were varied from 2 to 30 keV with the majority of the samples being exposed to 16 keV protons. Temperatures were varied from -195° to 50°C on the stretch-formed aluminum mirrors, -195 to 40°C on the magnesium substrate mirrors and -195° to 200°C on the nickel substrate mirrors. The lower maximum temperature on the epoxy-coated mirrors was dictated by a film failure problem as will be discussed in a subsequent section. A multiplicity of three samples for each data point was utilized for the majority of the tests.

In addition to the items shown in Table II, a limited number of proton exposures were conducted at angles of incidence of 30 and 60 degrees from normal on samples of the first four types. Also not given in the table are electron irradiation tests conducted on the fifth and sixth types of samples. The conditions prevailing in the electron exposures were a temperature of 0°C, integrated fluxes of 5×10^{16} , 1×10^{17} , and 2×10^{17} electrons-cm⁻², and an energy of 16 keV.

The procedure followed for charged particle irradiation of mirror samples is outlined below. Reflectance measurements were made on each mirror sample before irradiation. The individual sample to be irradiated was then installed on the temperature-controlled copper holder in the low energy particle accelerator. A scribe mark was placed on the test sample and oriented in a specific direction so that the position of the monochromatic light beam in subsequent reflectance measurements could be superimposed on the irradiated area. A threaded ring was used to clamp the sample onto the holder.

The test-end of the accelerator was then evacuated with the turbo-molecular pump. Care was taken during pump-down to start the turbo-molecular pump at a pressure of about 1000 microns of mercury to avoid backstreaming of oil into the system. When a pressure in the 10^{-6} torr range was reached, the gold trap (Figure 1) was filled with liquid nitrogen. When a pressure of about 1×10^{-7} torr was obtained the mirror sample temperature was established at the desired value, the gate valve was opened, and the exposure was started.

TABLE II. SUMMARY OF TEST CONDITIONS IN PROTON EXPERIMENTS

Mirror Substrate	Surface Coating	Integrated Particle Flux, p-cm ⁻²						Particle energy, KeV						Temperature, °C				
		1x10 ¹⁵	5x10 ¹⁵	5x10 ¹⁶	1x10 ¹⁷	2x10 ¹⁷		2	4	8	16	30	-195	0	40	50	100	200
Stretch-Formed Aluminum	Aluminum	x	x	x	x			x	x	x	x		x					
Stretch-Formed Aluminum	1800Å Si ₂ O ₃	x	x	x	x			x	x	x	x		x					
Electroformed Nickel	Aluminum	x	x	x	x			x	x	x	x		x					x
Electroformed Nickel	1800Å Si ₂ O ₃	x	x	x	x			x	x	x	x		x					x
Electroformed Nickel	8000Å Si ₂ O ₃			x	x			x										
Electroformed Nickel	17000Å SiO ₂			x	x			x										
Magnesium	1400Å Si ₂ O ₃			x	x			x					x					x

A Faraday cup having a 0.486 cm diameter aperture was used for dosimetry of both the proton and electron beams. A particle flux of 1×10^{13} protons-cm⁻²-sec⁻¹ was established at the beginning of the run. A beam uniformity of better than ± 10 percent was maintained across the portion of the test sample which was subsequently illuminated in the reflectance measurement. Figure 5 shows both the path of the Faraday cup aperture and the relative size of the reflectometer light beam with respect to the mirror sample. A typical proton flux distribution is also given. Similar beam flux profiles were made at regular intervals throughout the test run. The average proton flux was calculated for the area viewed by the reflectometer light beam at various times during the exposure. Then the integrated flux was calculated by integrating the average proton flux with respect to time. Typical test runs varied in length from about 1.3 to 5.2 hours for integrated flux levels of 5×10^{16} to 2×10^{17} protons-cm⁻², respectively.

When the desired integrated flux level was achieved the gate valve in the beam tube was closed, the test sample temperature was returned to ambient, and the beam tube was backfilled with dry nitrogen. Again, care was taken to begin backfilling the system before the turbo-molecular pump was completely stopped. The test sample was then removed from the system and stored in a dark container until reflectance measurements could be made. Immediately following each test, the cold trap was removed from the system and cleaned with hot water and aluminum oxide abrasive. It was then placed back in the accelerator beam tube for the next run. This procedure for warming and cleaning the cold trap prevented re-evaporation of adsorbed organic molecules into the vacuum system.

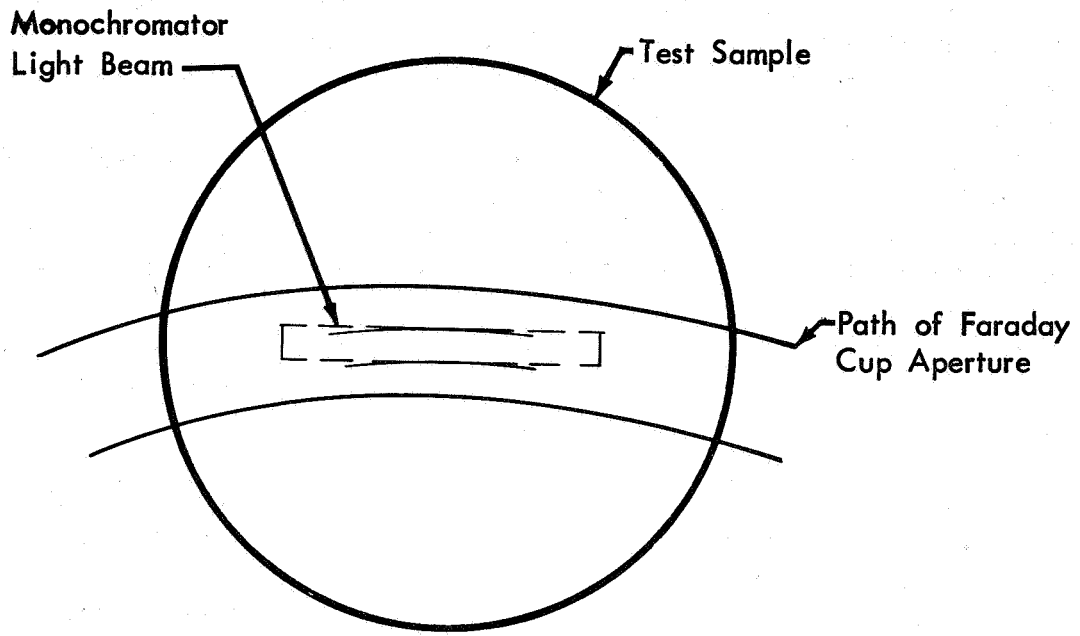
5.2 Ultraviolet Irradiation and Dosimetry

A summary of test conditions including temperatures and exposure increments for ultraviolet experiments is given in Table III. It should be noted that the exposure increments given in the table are only nominal values. Exact values for each mirror sample are given in Appendix B.

At the beginning of the program the ultraviolet intensity of the UA-11 lamp was mapped along the axis of the lamp so that the exposure rate of each sample would be known. A wide angle (135 degrees) radiometer* was used with and without appropriate filters** to establish the absolute output of the lamp in the wavelength region below 0.4 micron. The variation in intensity along the axis of the lamp plotted in equivalent space suns (ESS) is shown in Figure 6. As noted in the figure, the intensity varied from 11.2 ESS near the center of the lamp to 8.5 ESS at the ends of the lamp. In comparing data between test samples it has been assumed that reciprocity exists over this intensity range. Additional experiments should be run, however, to establish whether any exposure "rate effects" exist.

* Thompson-Ramo-Wooldridge Co. Model DR-2 Blackbody Thermopile

** Corning Filters 0-51 and 7-54



PATH OF FARADAY CUP APERTURE AND RELATIVE SIZE OF MONOCHROMATOR LIGHT BEAM WITH RESPECT TO MIRROR SAMPLE

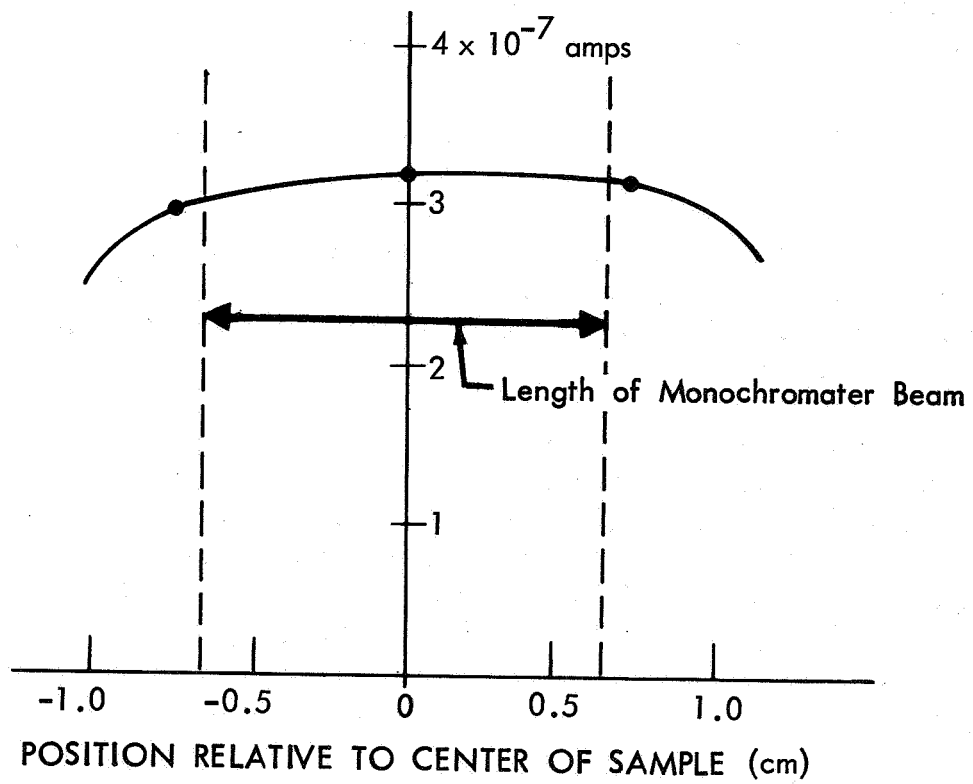
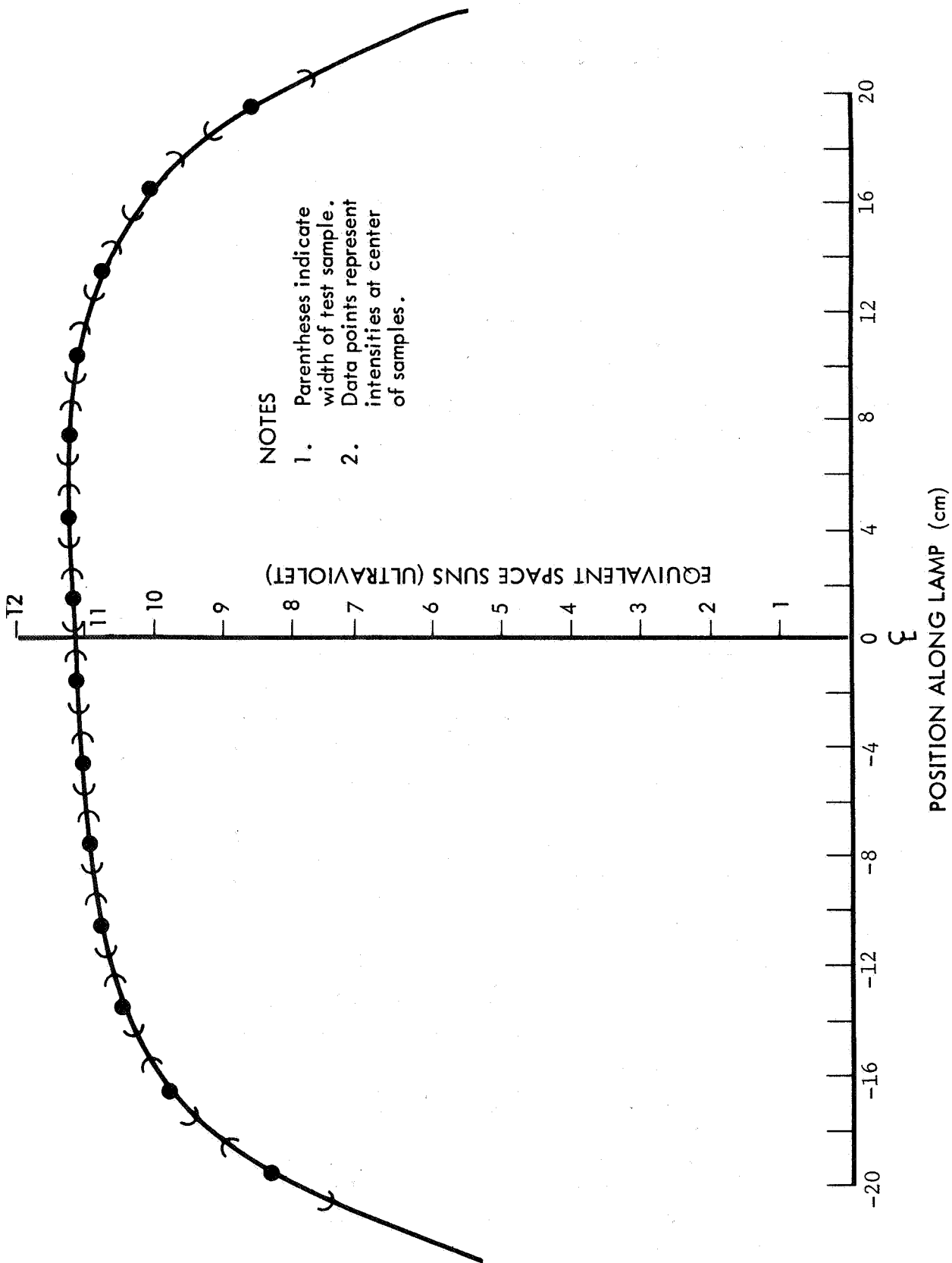


Figure 5: TYPICAL PROTON FLUX DISTRIBUTION ACROSS SAMPLE



NOTES
 1. Parentheses indicate width of test sample.
 2. Data points represent intensities at center of samples.

Figure 6: VARIATION OF INTENSITY ALONG LENGTH OF UA-11 MERCURY LAMP

TABLE III SUMMARY OF TEST CONDITIONS IN ULTRAVIOLET EXPERIMENTS

Mirror Substrate	Surface Coating	Temperature, °C						Nominal Exposure Increments, ESSH							
		-195	0	50	100	200	0	500	1000	2500	3500	8700			
Stretch-Formed Aluminum	Aluminum	x	x	x			x								
Stretch-Formed Aluminum	1800Å Si ₂ O ₃	x	x		x						x	x		x	x
Electroformed Nickel	Aluminum	x	x		x	x					x	x		x	x
Electroformed Nickel	1800Å Si ₂ O ₃	x	x	x				x					x		
Electroformed Nickel	8000Å Si ₂ O ₃		x											x*	
Electroformed Nickel	17000Å SiO ₂		x											x*	x
Magnesium	1400Å Si ₂ O ₃	x	x	x										x*	x

*In-situ reflectance measurements performed in these tests

A relative spectral distribution plot on a UA-11 lamp was also measured at the beginning of the program using a Beckman DK-1A Spectrophotometer. A plot of the spectral distribution of this lamp, the space solar spectrum, and an A-H6 mercury-arc lamp (used in the in-situ reflectance experiment) is shown in Figure 7. The relative amount of energy in each spectral line of the UA-11 lamp is given in Table IV. Also shown in the table are the ratios of energy in each lamp emission line to the energy in the space solar spectrum in the same wavelength region. It is significant to note that the energy in several of the lines exceeds the energy of the solar spectrum by greater than 100 times. Because of the relatively poor match between the UA-11 lamp and the solar spectrum it is recommended that either (1) spectral degradation sensitivity measurements be made on mirror samples using a line spectrum lamp with narrow band pass filters, or (2) degradation experiments be performed using a close-match solar spectrum and the amount of degradation be compared to the present measurements.

TABLE IV -- EMISSION DATA FOR UA-11 MERCURY-ARC LAMP

Wavelength, Å	Percent of Total	Equivalent Space-Sun Intensity
2527 - 2637	8.82	123.8
2637 - 2675	5.80	157.8
2690 - 2718	0.88	28.8
2748 - 2772	0.76	32.0
2791 - 2832	2.35	41.4
2882 - 2913	1.17	15.0
2913 - 2942	0.38	4.6
2955 - 2988	3.01	26.1
2998 - 3053	5.61	30.7
3108 - 3167	11.80	56.1
3318 - 3365	1.64	7.3
3616 - 3723	18.78	39.6
4003 - 4136	4.73	3.9
4301 - 4432	9.45	7.8
5340 - 5563	11.82	5.3
5621 - 5901	13.00	5.7

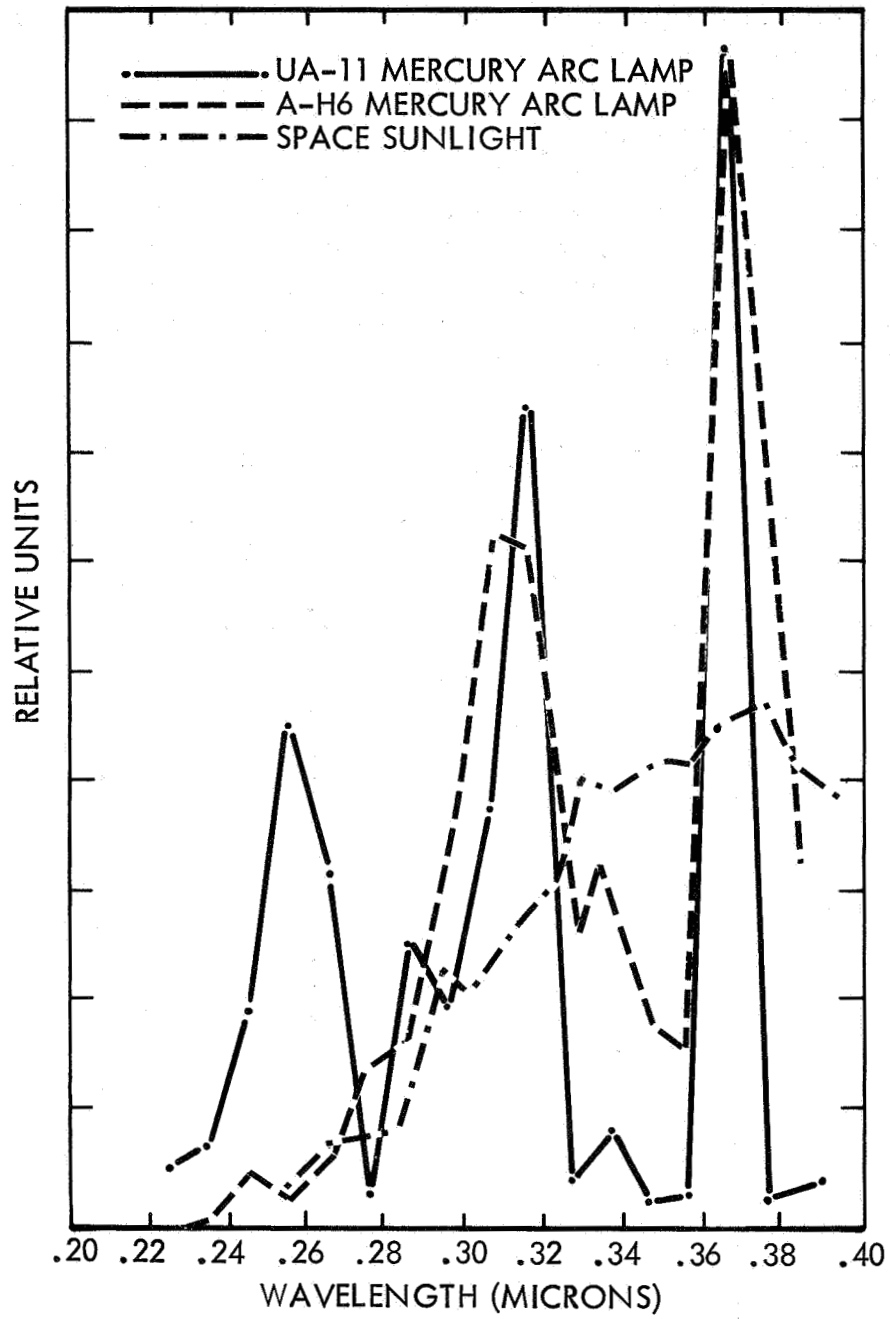


Figure 7: SPECTRAL DISTRIBUTION OF ULTRAVIOLET LAMPS

Recent experiments (Reference 5) in which the degradation of various spacecraft paints was determined for various ultraviolet wavelengths have indicated that the effectiveness for producing optical degradation increases as the wavelength decreases. In general, little or no damage was induced by photons of wavelength greater than 0.35 micron in the reference experiments. Thus, the UA-11 lamp emission lines in the 0.25 to 0.35 micron region should have been most effective. Considering the effectiveness and relative abundance of the shorter wavelength photons and the energy distribution in the solar spectrum, it is reasonable to assume that the exposure experienced in these tests is more severe than actual sunlight exposure.

Following the spectral and intensity measurements on the UA-11 lamp, a short test run was made to verify the operation of the facility and to check for contamination in the test chamber. The test samples were then installed on the four temperature-controlled sample holders. Reflectance measurements were made on the samples before, at various increments during, and after irradiation. For interim reflectance measurements, the samples had to be removed from the vacuum chamber and returned to ambient temperature.

The intensity of the ultraviolet lamp was checked after each test run. Since the amount of degradation in the wavelength region less than 0.4 micron was small (less than 20 percent) for even the longest run, the initial intensity of the lamp was used for estimating the total exposure.

5.3 Combined Proton-Ultraviolet Irradiation and Dosimetry

The procedure followed for conducting the combined proton-ultraviolet radiation experiments is given below. For these tests, a stainless steel section of beam tube in the shape of a cross was attached to the accelerator as shown in Figure 8. Prior to installation of any mirror samples, the ultraviolet lamp was operated for several days to thoroughly outgas the components in the immediate vicinity of the lamp. Ultraviolet intensity measurements were made at the position of the test sample. An equivalent space sun intensity of 10 was provided at the mirror sample surface. During lamp calibration measurements, a ratio was obtained between the outputs of the DR-2 radiometer (at the test sample position) and an Eppley thermopile viewing the lamp through a quartz window. The output of the lamp was then monitored during the test run with the Eppley thermopile.

The mirror sample was then installed on the sample holder, the system evacuated, and the temperature of the sample established at 0°C. A dosimetry measurement was then made on the proton beam to adjust the power supplies and to establish the proper flux. This proton dosimetry was done prior to turning on the ultraviolet lamp.

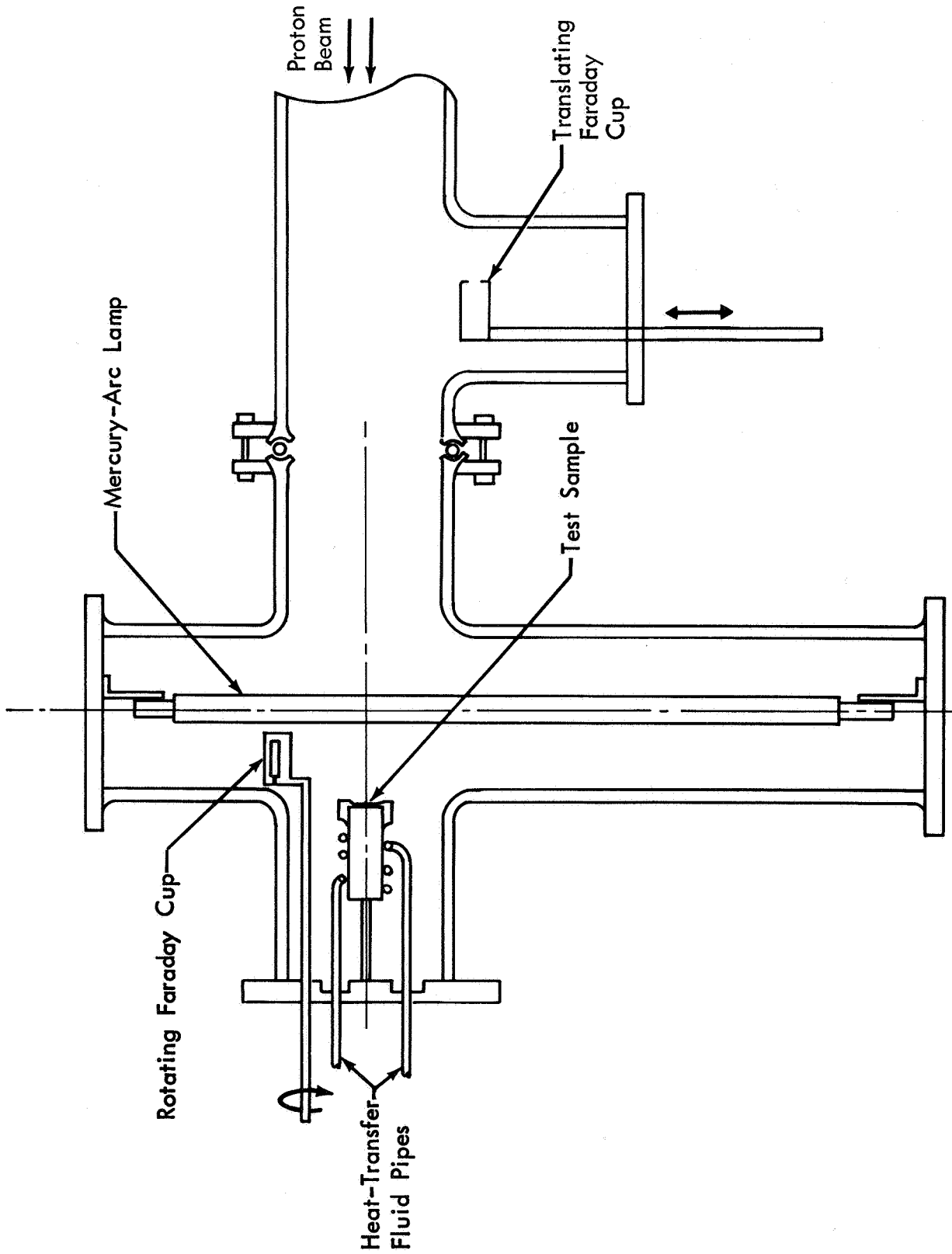


Figure 8: SCHEMATIC OF COMBINED PROTON/ULTRAVIOLET TEST SETUP

As noted in Figure 8 two Faraday cups were employed in the combined environment experiment, one of which was located at the test sample position and the other between the ultraviolet lamp and cold trap. It was discovered in preliminary check-out tests that erroneous current readings were obtained in the Faraday cup at the test sample position when the ultraviolet lamp was operating. This was believed to be due to photo-emission of electrons from the adjacent exposed metal surfaces. Because of this problem a second Faraday cup was installed upstream in the beam tube such that it was shielded from the ultraviolet radiation. However, since the proton beam was slightly divergent, the two Faraday cups read different flux values.

The procedure followed with the Faraday cups was to obtain the ratio of the current outputs before the ultraviolet lamp was turned on. Then, only the shielded, upstream cup was used during the test run. The flux distribution at the mirror sample position could then be calculated. A similar comparison of the outputs of the two Faraday cups was also made at the end of the run.

The proton flux was reduced from 1×10^{13} to 2.8×10^{11} protons-cm⁻²-sec⁻¹ for the combined environment tests. This flux provided an integrated flux of 5×10^{16} protons-cm⁻² in a 50-hour period. Since the output of the ultraviolet lamp was 10 ESS, 500 equivalent space sun hours (ESSH) was accumulated in the 50-hour test run. The 50-hour exposure was accumulated in successive periods of about 16 hours of irradiation and 8 hours of shut down. During the 8-hour shut down periods the cold trap was kept full of liquid nitrogen, the irradiation was stopped, mirror sample temperature was returned to ambient, and high vacuum was maintained.

5.4 In-Situ Reflectance Measurement Experiment

The procedure for performing the in-situ reflectance measurement experiment follows:

- 1) The mirror sample was installed on the water-cooled holder shown in Figure 4 and inserted into the vacuum system;
- 2) Specular-plus-diffuse reflectance measurements were then made before evacuation of the system over the wavelength region from 0.27 to 2.1 microns. The reflectance was measured at an angle of incidence of 10 degrees from normal;
- 3) The system was then evacuated to a pressure of about 2×10^{-7} torr and the reflectance was again measured in vacuum after a period of 1 to 2 hours;
- 4) The A-H6 mercury-arc lamp was then started and operated for a period of 68 to 115 hours. During the irradiation period the lamp output normally degraded by 2 to 10 percent. Intensities of the A-H6 lamps used in the runs varied from 6.7 to 7.5 ESS;

5) After irradiation the reflectance was measured in vacuum and again in air about one hour after backfilling. One of the samples was also measured about 12 hours after exposure to air to determine whether any long-term annealing occurred.

5.5 Electron Photomicrographs

Electron photomicrographs were prepared in the following manner:

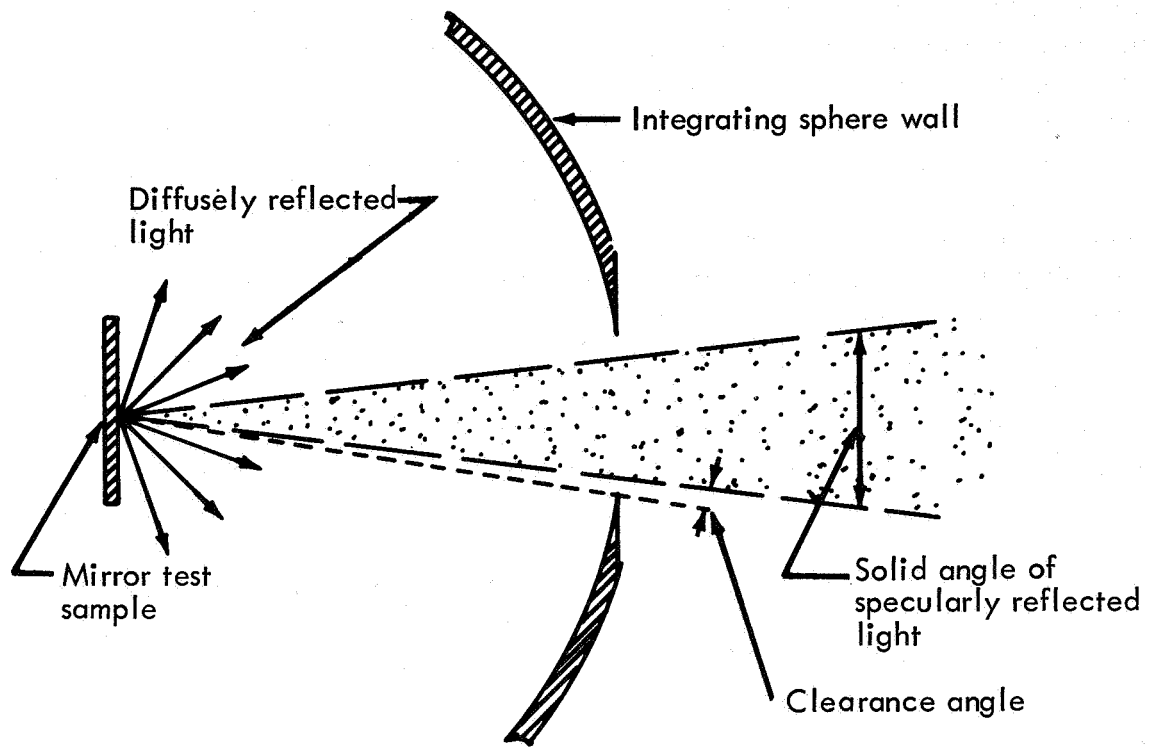
- 1) A polyvinyl alcohol (PVA) replica was taken of the aluminum surface;
- 2) The PVA replica was shadowed with vapor-deposited germanium at an angle of 65 degrees from normal;
- 3) A vapor-deposited film of carbon was applied to the germanium at normal incidence; and
- 4) The PVA was dissolved off of the vapor-deposited films and the films were mounted on a wire grid.

The photographs represent transmission of 60 keV electrons through the germanium-carbon films. A magnification of 10,000 X was used.

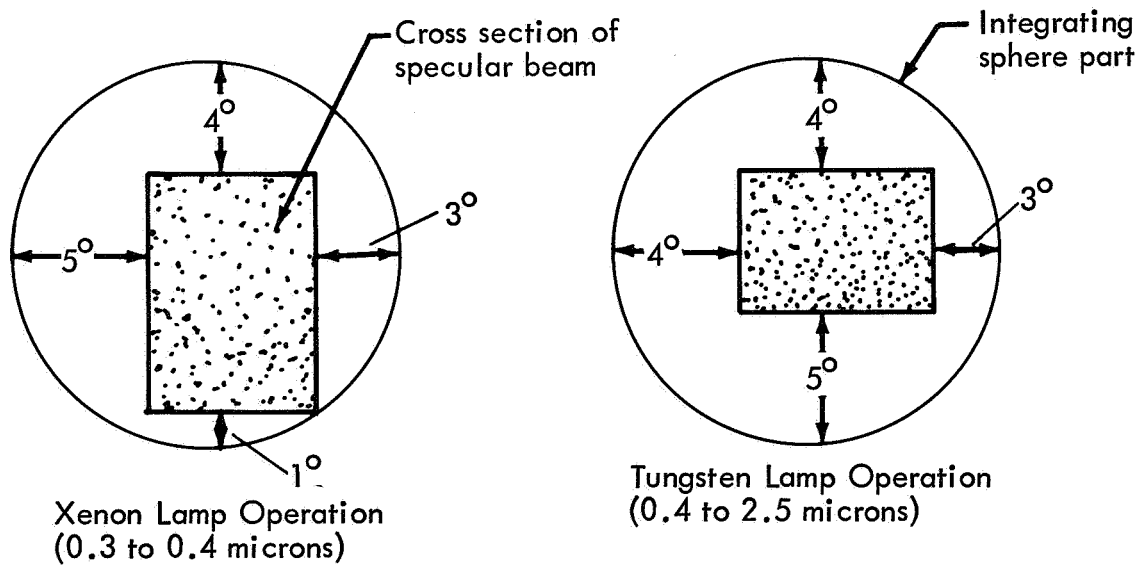
5.6 Reflectance Data Acquisition and Reduction Procedures

Reflectance measurements were made over the wavelength region from 0.30 to 2.5 microns in either 2- or 4-percent energy increments of the space solar spectrum (Reference 6). Two-percent increments were used on the mirrors employing thick Si_2O_3 and SiO_2 overcoatings, and 4-percent increments on all others. Both hemispherical (specular-plus-diffuse) and diffuse reflectance measurements were made on all mirror samples. The specular-plus-diffuse measurements were made at 10 degrees from normal and the diffuse measurement at normal incidence. Specular reflectance data were then obtained by subtracting diffuse from specular-plus-diffuse reflectance.

It is important that solar concentrator designers know the solid angle defining the specularly reflected light beam from the test samples, so that the effect of partially scattered light on the performance of a mirror can be predicted. In the Gier-Dunkle integrating sphere, light from the monochromator is focused onto the mirror sample surface as shown in Figure 9a. For normal orientation, the specularly reflected beam will then retrace its path out the sphere port. Roughness on the mirror surface causes a small portion of light to be hemispherically scattered. If the sphere port is considerably larger than the specular light beam, a portion of the diffusely reflected light will escape through the port. Also, the nature of the roughness on the mirror



a) SCHEMATIC OF INTEGRATING SPHERE



b) INTEGRATING SPHERE PORT

Figure 9: RELATIONSHIP OF SPECULARLY REFLECTED BEAM TO ENTRANCE PORT OF GIER-DUNKLE INTEGRATING SPHERE

surface may cause the specular component to merely broaden and have Gaussian shaped edges. Thus the amount of the specularly reflected beam which is clipped by the port may be significant. For the Gier-Dunkle integrating sphere, the solid angle of the specular reflectance measurement is established by the clearance between the specularly reflected beam and the entrance port when the diffuse measurement is being taken. Scale drawings showing the clearances between the specularly reflected beam and the entrance port for both tungsten and xenon lamp operation are shown in Figure 9b. Since the light beam is rectangular in shape and the entrance port is circular, it is obvious that no fixed clearance distance can be given. Nevertheless, maximum clearances can be given for the distance between the short and long sides of the rectangular beam and the entrance port. The clearances are given in angles, based on a distance of 10.2 cm from the reflecting surface to the port, for convenience of applicability to solar concentrator design. As noted in the sketch, the maximum clearance in both the vertical and horizontal directions was about 5 degrees.

A silicon oxide overcoated, nickel substrate mirror was chosen as a reflectance reference to check equipment each time a series of reflectance measurements was taken. This served as a check for equipment malfunction and also provided a means for determining the reproducibility that could be expected for any set of data. Data from the reference sample indicated a reproducibility within ± 1.5 percent.

6.0 RESULTS AND DISCUSSION

Included in this section are discussions of contamination problems experienced in preliminary radiation tests, radiation effects on the three types of solar mirrors evaluated in this program, and a discussion of anticipated effects in space. These various items are presented in respective order.

6.1 Contamination of Mirror Samples

The primary purpose of the program was to study the effects of protons and ultraviolet radiation on the reflectance of mirror surfaces; however, the contract specifically stated that special attention be given to contamination of test samples in the vacuum system. Since a considerable portion of the program was devoted to studying and minimizing contamination effects, a brief review of the contamination phenomena and problems encountered in this program is presented for the benefit of future experiments.

The reflectance of a mirror surface in the wavelength region shorter than about 5000\AA is both a sensitive indicator of contamination and a critical design parameter in many space-optical systems. Contaminant films which are strong absorbers in this wavelength region can be deposited either during environmental tests or actual space flight if suitable outgassing materials are located in the vicinity of the mirror surface. Since typical environmental vacuum chambers and spacecraft employ organic materials, special attention must be given to avoid contamination of optical surfaces.

The phenomena of radiation-induced contaminant film deposition has been observed for many years in vacuum systems. Early experimenters (References 7, 8, and 9) in vacuum coating work noted the formation of carbonaceous deposits on surfaces after both ionic or electron bombardment cleaning. These deposits were attributed to hydrocarbon vapors which were deposited on the surfaces and were subsequently polymerized or decomposed into a stable, low vapor pressure compound. This stable compound, which was normally brown or black in appearance, then remained on the surface.

In recent years the contaminant film problem has been encountered in space radiation testing of spacecraft materials, particularly in charged particle and ultraviolet radiation tests of spacecraft thermal control coatings and mirror surfaces (References 10, 11 and 12).

Although major improvements in vacuum system cleanliness have been made in recent years, the amount of time which surfaces are exposed to radiation in

vacuum has increased by 10^3 to 10^5 over that experienced in glow discharge cleaning in the early vacuum coating experiments. Thus, the effects of the cleaner vacuum systems containing a smaller fraction of organic contaminant vapors have been partially offset by the longer times of exposure to radiation.

At the present time no theory exists for relating the thickness of polymerized contaminant films to the variables of the phenomena. A complete theory of this type would no doubt have to include the partial pressure of the contaminant vapor, surface bond energies, surface temperature, and the interaction of the radiation with the adsorbed film. Numerous theories have been proposed for describing the adsorption process on clean surfaces in vacuum, including monolayer, multilayer, and capillary condensation on surfaces. A review of these theories is given in Reference 13 including: the Langmuir theory for monolayer adsorption; the Brunauer, Emmett, and Teller theory for multilayer adsorption; the potential theory; the polarization theory; and others. Despite the numerous theories, no completely rigorous or general treatment of the adsorption of gas molecules exists at the present time. Experimental observations have shown that in some instances only a monolayer forms; whereas, for other materials relatively thick films will form. In either case, a saturation effect is observed where the film thickness condensed on a clean surface increases very rapidly at first and then approaches a saturation value after a long period of time. The saturation thickness achieved is a function of the strength of the atomic forces from the underlying substrate surface, gas pressure, temperature, and the type of gas being adsorbed. After the saturation thickness value is reached, the rate of vapor atom condensation is equal to the evaporation rate. It is significant to note that even after a saturation thickness value has been achieved, the condensing vapor atoms or molecules are believed to spend a finite period of time on the surface of the adsorbed film before evaporating.

As discussed above, a variety of theories exist to explain the formation of adsorbed films without the presence of ionizing radiation. However, no known theories exist for predicting the influence of the radiation on the number of molecules that condense or remain bonded onto the surface. It can only be qualitatively predicted that the thickness of organic films will continue to increase indefinitely, assuming that an infinite source of outgassing contaminant molecules exists in the vacuum system. This prediction is based on the assumption that the ionization will cause alteration of the organic molecular bond structure such that molecules which would have re-evaporated now remain bonded to the surface. Experiments conducted in Reference 7 on contaminant film deposition during charged-particle irradiation have verified that the contaminant film thickness increases linearly with time indefinitely.

At the outset of this program contamination experiments were conducted in the low energy particle accelerator as it existed at that time. Optical sapphire windows were irradiated with 4 keV protons to various integrated flux levels and

under various conditions of operation and vacuum system cleanliness. The optical transmission, measured before and after irradiation, was used as an indication of the thickness of the contaminant film. To reduce the concentration of organic molecules in the system, the diffusion pumps were replaced with an ion pump and a turbo-molecular pump, the majority of the O-ring seals were replaced with indium wire and Viton-A seals, and a liquid nitrogen cold trap was installed in the beam tube. It was shown in the contamination experiments on the sapphire window that the level of contamination was substantially reduced by cleaning up the accelerator vacuum system. In fact, the degradation in spectral transmission was reduced to the point where the changes observed could have been due to proton radiation effects in the sapphire.

The stability of the contaminant films in this experiment was demonstrated in cleaning experiments on the coated sapphire windows. It was found that the films were not attacked at an appreciable rate by petroleum distillate solvents, ethyl alcohol, or by aqueous solutions of sodium hydroxide, nitric, sulphuric, and hydrochloric acid. Similar chemical stability was noted for diffusion pump oil contaminant films formed during ion bombardment experiments in References 10, 11, and 12. These films were apparently not removed by baking at temperatures up to 350° C since the transmission of the sapphire was not affected. The only successful cleaning techniques found in Boeing experiments were either scraping or abrading with aluminum oxide powder. However, a chemical cleaning technique described in Reference 12 also appears effective.

Various analysis techniques were used in an attempt to measure the thickness and composition of the contaminant films deposited on surfaces in the low energy particle accelerator. The only partially successful technique found for estimating the thickness was by observing changes in amplitude of interference minima on irradiated dielectric-coated metal surfaces as described in Reference 14. Using this technique, it was found that the contaminant film thickness accumulated during the longest irradiation period was in the order of 5 to 15Å. This rate of contaminant film deposition was very likely present during the proton and combined proton/ultraviolet radiation experiments. No satisfactory means for detecting or measuring the composition of such contaminant films could be found. Among the analysis techniques tried were X-ray and electron diffraction, infrared transmission of irradiated NaCl crystals, and mass spectrographic analysis of atoms sparked from irradiated high-purity aluminum surfaces and electroformed nickel mirrors.

In general, the contamination experiments in this program verify the need for carefully controlling the cleanliness of environmental test vacuum systems and the adjacent spacecraft surfaces when optical mirror surfaces are involved. The need for ultrapure vacuum environments will be especially important for irradiation of optical surfaces which must maintain high reflectance or transmission in the wavelength region as short as 1000Å.

6.2 Electroformed Nickel Mirrors

Included in this section of the report are typical reflectance data and discussions of results of proton, ultraviolet, combined proton/ultraviolet, and electron radiation experiments on electroformed nickel mirrors. Each of these general items will be presented in their respective order.

6.2.1 Typical Reflectance Data---Typical reflectance data for electroformed nickel mirrors having both bare aluminum and silicon oxide overcoated reflective surfaces are shown in Figure 10. Specifically, spectral reflectance curves are shown for an unprotected vacuum deposited aluminum surface and aluminum surfaces overcoated with about 1800\AA of Si_2O_3 , 8000\AA of Si_2O_3 and $17,000\text{\AA}$ of SiO_2 . As can be noted in the curves, the silicon oxide overcoatings caused a significant reduction in the specular reflectance, especially for the thicker films. Average solar specular reflectance values for the four types of surfaces were 0.891, 0.875, 0.762, and 0.754, respectively. A portion of the decrease in specular reflectance is due to the increase in diffuse reflectance; however, a major problem appears to exist in absorption in the oxide films. In theory, (Reference 15) when non-absorbing silicon oxide films are applied to aluminum the reflectance at interference maxima should equal, or slightly exceed, the reflectance of the bare aluminum surface. It can only be concluded from the reflectance data that the oxide films were not applied under the optimum conditions since non-absorbing films have been reported in the literature.

In regard to absorption in the oxide films, the first two batches of nickel mirror samples which were overcoated with 1800\AA of Si_2O_3 were extremely non-uniform in reflectance. Sample-to-sample variations were as large as ± 9 percent at a 5000\AA wavelength, and even larger variations were apparent throughout the near infrared wavelengths. This non-uniformity cannot be explained because 66 samples were coated in each batch in a rotating array. All other silicon oxide overcoated mirrors prepared in the program showed good uniformity. It should be noted that the silicon oxide overcoated mirrors which had non-uniform reflectances were used primarily for proton-only radiation experiments. The effects of protons were, however, checked on a series of silicon oxide overcoated mirrors which had uniform reflectances.

Prior experiments on silicon oxide overcoatings have shown that the absorption in freshly prepared films can be eliminated by exposure to ultraviolet radiation in air for a period of about 5 hours (Reference 16). It is recommended for future experiments on oxide overcoated mirrors that the surfaces be treated with ultraviolet radiation prior to their use. This will both increase the solar reflectance and provide good uniformity of reflectance from sample to sample.

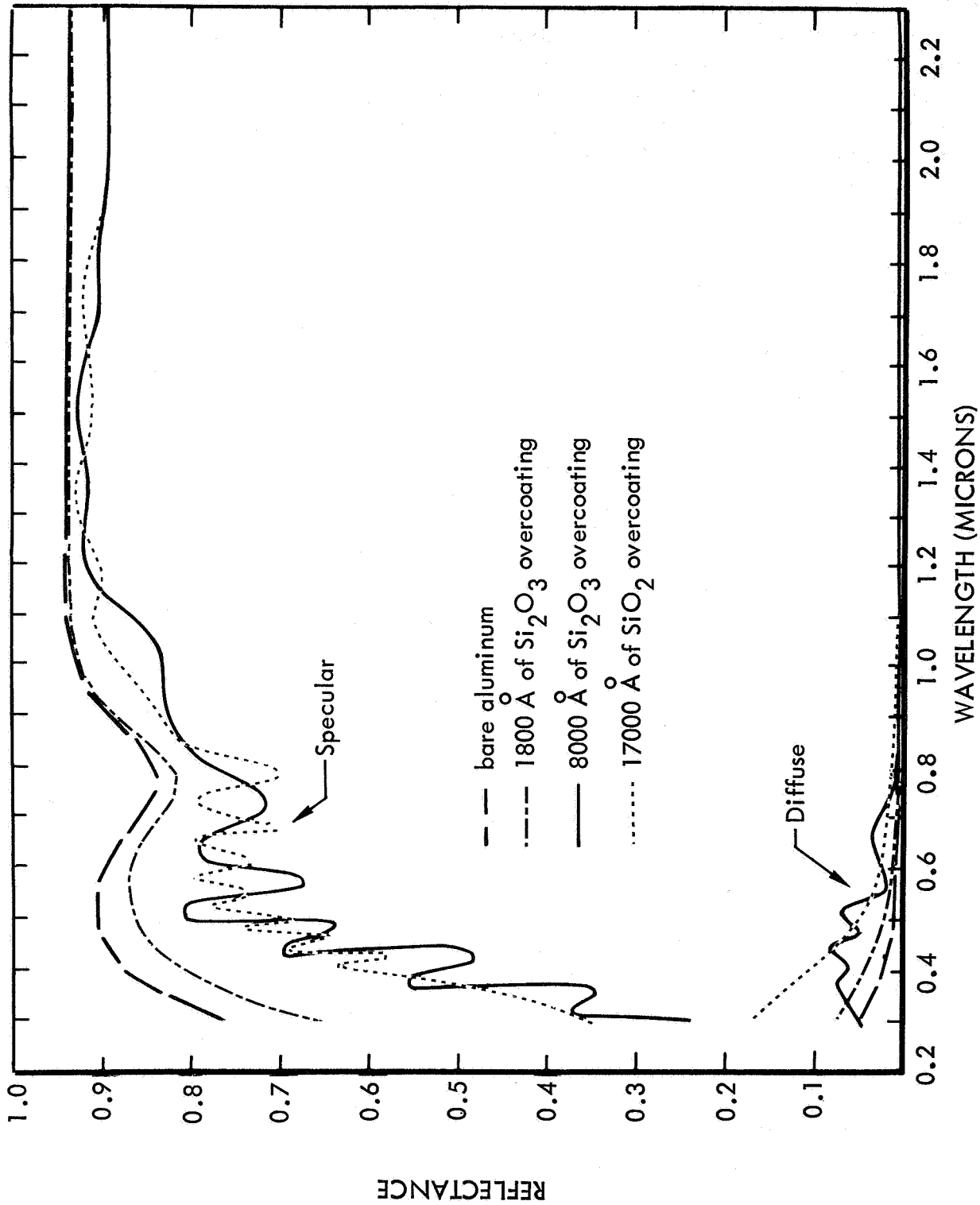


Figure 10: SPECTRAL REFLECTANCE OF TYPICAL ELECTROFORMED NICKEL MIRROR SAMPLES

6.2.2 Proton Radiation Effects---In the proton radiation effects studies on nickel-substrate mirrors the effects of proton energy, angle of incidence, integrated flux, and mirror temperature were investigated. Specifically, energies in the range of 2 to 30 keV, angles of incidence from 0 to 60 degrees, integrated fluxes from 1×10^{15} to 2×10^{17} protons-cm⁻², and mirror temperatures from -195° to 200°C were evaluated. A general summary of the proton test conditions experienced by the various types of electroformed nickel mirrors is given in Table II and a complete tabulation of proton test data is given in Appendix C. Included in the appendix are a tabulation of temperature, energy, angle of incidence, integrated flux, and reflectance data. The results of varying each of the above parameters are discussed below in respective order.

Energy Dependence Experiments:

In the energy dependence experiments electroformed nickel mirrors having bare aluminum and 1800Å thick silicon oxide overcoatings were irradiated with protons at energies of 2, 4, 8, 16, and 30 keV at a mirror temperature of 0°C. An initial series of tests was performed at integrated fluxes of 1×10^{15} , 5×10^{15} and 5×10^{16} protons-cm⁻² for the purpose of establishing a measurable damage threshold at the various proton energies. A proton flux of about 1×10^{13} protons-cm⁻² sec⁻¹ was used in all experiments to avoid differences due to rate-effects, since it was not known whether the rate of exposure had any effect on optical damage. These tests showed that integrated flux values up to 5×10^{16} protons-cm⁻² produced negligible reflectance changes. The variations in reflectance due to possible energy-dependence effects were not significantly larger than experimental error or other effects. Therefore, it was decided to irradiate a set of silicon oxide overcoated mirrors with an integrated flux of 1×10^{17} protons-cm⁻² and energies varying from 2 to 30 keV. These particular samples were selected because they appeared to be more radiation sensitive and thus would show larger reflectance changes.

The results of this experiment on the silicon-oxide overcoated mirrors are shown in Figure 11 which is a plot of the change in specular reflectance in percent against wavelength in microns. The limits of possible error due to non-reproducibility of reflectance measurements from day to day are shown on the 16 keV curve, although the same limits are also applicable to the other curves. An examination of the curves in the 0.4 to 0.6 micron wavelength region reveals that the maximum reflectance change was produced by the 16 keV protons. Both the 16 and 30 keV protons produced significantly higher damage than the 2, 4, and 8 keV protons.

The resulting change in solar specular reflectance (ΔR_s) for the 16 keV curve was $\Delta R_s = -(0.773 - 0.715) = -0.058^*$, and for the 4 keV case was $\Delta R_s = -(0.755 -$

* A decrease in absolute solar specular reflectance will be indicated with a minus sign on the ΔR_s value.

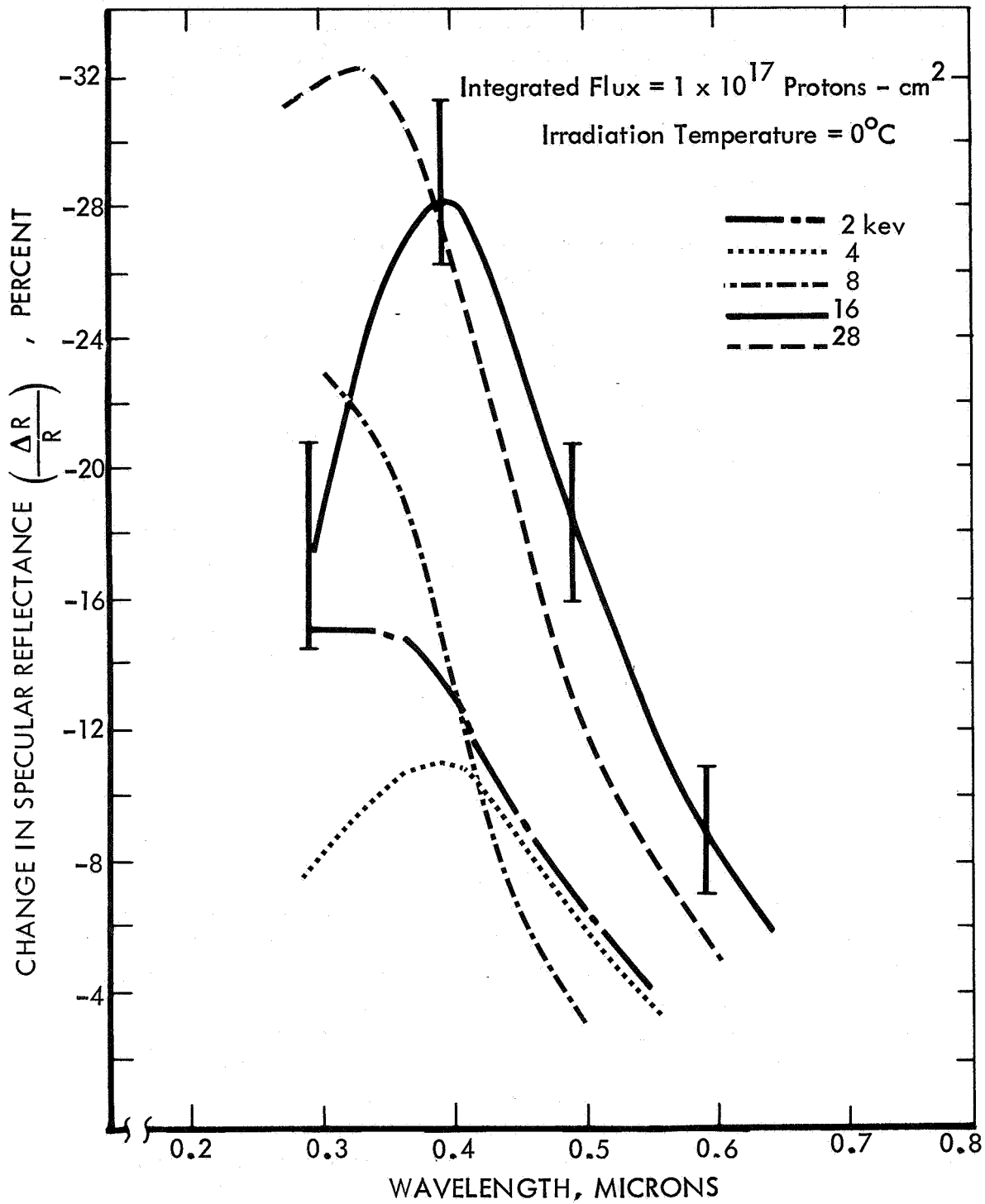


Figure 11: EFFECT OF PROTON ENERGY ON SILICON-OXIDE OVERCOATED, NICKEL SUBSTRATE MIRRORS

0.734) = -0.021. These two values represent the upper and lower limits of solar specular reflectance changes produced by all proton energies in these test samples.

At the conclusion of the energy-dependence experiment it was decided to use 16 keV protons for subsequent tests because: (1) maximum damage was produced in the silicon oxide coatings at that energy; and (2) sputtering efficiencies for most materials peak out in the 5 to 20 keV energy range (References 17, 18 and 19).

Angle of Incidence Experiments:

Proton angle of incidence experiments were conducted on the nickel mirror samples having bare aluminum and 1800Å thick silicon oxide overcoatings. The objective of this study was to determine the effect of irradiation at various proton incidence angles on reflectance changes. Mirror samples were irradiated with 1×10^{17} proton-cm⁻² of 16 keV protons at angles of incidence of 0, 30 and 60 degrees from normal. Detailed data from these tests are given in Appendix C. It should be noted that the integrated fluxes of particles reported in the table were measured in a plane that was normal to the axis of the beam. Therefore, the actual integrated flux on the surface of the mirror samples is reduced proportionally to the cosine of the angle of incidence. This irradiation technique was chosen because it is similar to the condition existing during irradiation in space.

The data on the electroformed nickel mirrors showed that a variation in the angle of incidence had only a small effect on the amount of degradation. No conclusions could be made because of the small changes observed and the insufficient number of irradiated samples.

Integrated Flux and Mirror Temperature Experiments:

To evaluate the effects of proton integrated flux and mirror temperature, tests were run at temperatures of -195°, 0°, 100°, and 200°C at integrated fluxes varying from 1×10^{15} to 2×10^{17} protons-cm⁻². Data is presented in respective order for mirrors with bare aluminum and overcoatings of thin Si₂O₃, 8000Å thick Si₂O₃, and 17,000Å thick SiO₂ coatings. Typical data for the bare aluminum reflective surface showing the effect of protons on specular and diffuse spectral reflectances are shown in Figure 12. Three different integrated flux levels are shown indicating the progression of degradation in specular reflectance with increased proton dosage. A negligible change in diffuse reflectance was observed on these mirrors which is evidence that negligible sputtering or roughening of the surface occurred. The decrease in specular reflectance must then be due to increased absorption. An increase in absorption could be due to: (1) color center formation in the natural aluminum-oxide film, (2) conversion of a thin layer on

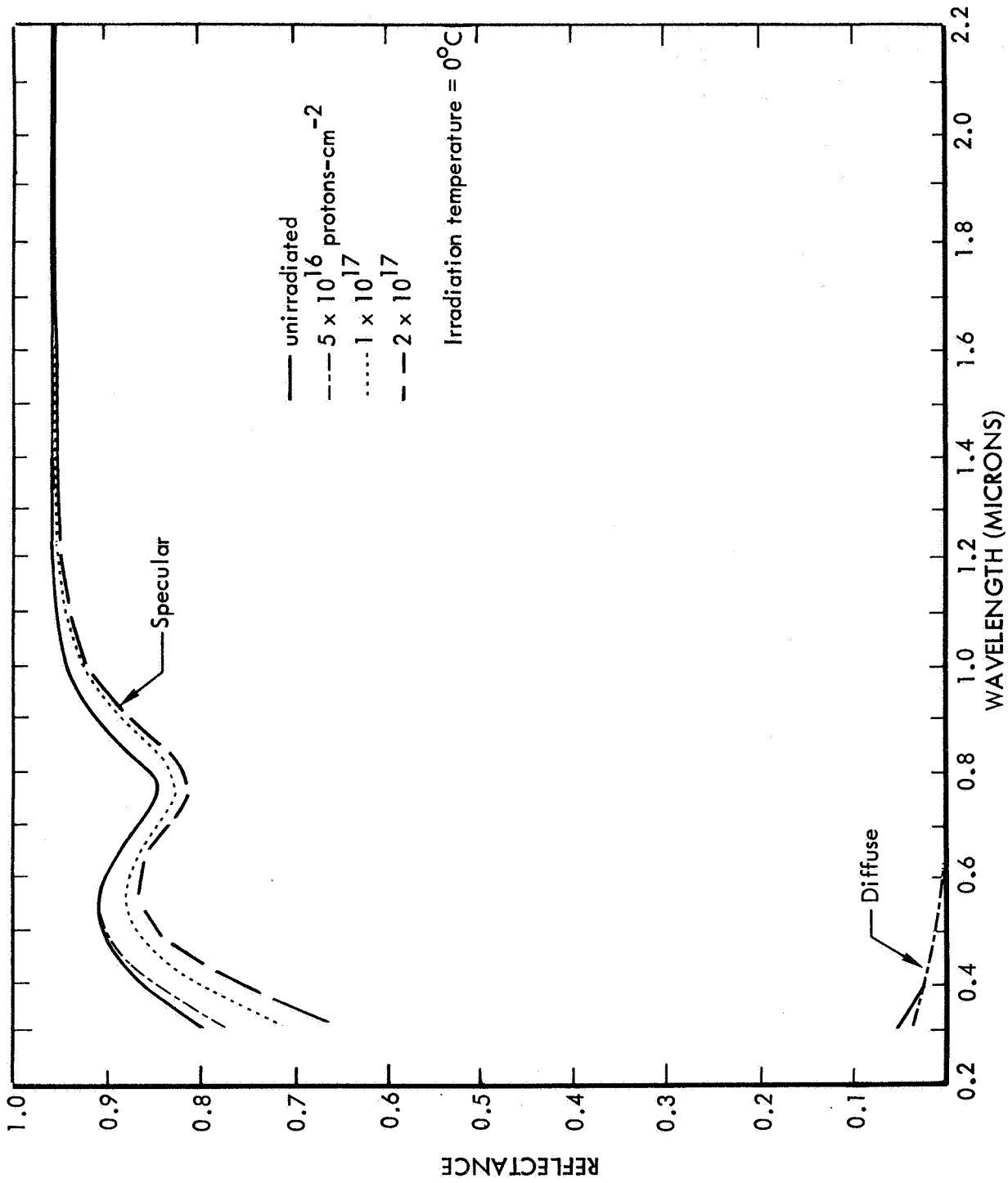


Figure 12: EFFECT OF PROTONS ON SPECTRAL REFLECTANCE OF BARE ALUMINUM COATED, NICKEL SUBSTRATE MIRRORS

the aluminum reflective surface to a compound such as an aluminum hydroxide, or (3) deposition of a thin contaminant film on the surface.

The effects of both proton integrated flux and mirror temperature on the solar specular reflectance of electroformed nickel mirrors are shown in Figure 13. The plot shows the change in solar specular reflectance (ΔR_s) vs. proton integrated flux with mirror temperature as a parameter. The negative change in reflectance (ordinate scale) on the graph actually represents a decrease in the absolute reflectance. All data given were obtained using 16 keV protons at a flux of about 1×10^{13} protons-cm⁻² sec.⁻¹. Three mirror samples were irradiated for each data point to obtain better statistical data. The vertical bars on the curves represent the spread in data between the three identical mirror samples and the circles are located at the numerical average of the three ΔR_s values. As noted in the Figure, the reflectance changes produced in these mirrors at the highest integrated flux levels were barely larger than the instrumentation reproducibility.

It is significant to note that the maximum degradation occurred for the mirrors irradiated at -195°C, which suggests that the changes in reflectance observed may be a result of contamination. However, since the spread in the -195°C data was so large, as indicated by the data spread bars, no conclusions regarding contamination can be made. Prior work by Ennos (Reference 9) on electron-induced contamination in kinetic vacuum systems showed that the rate of deposition of decomposed hydrocarbon films increases very rapidly as the condensing surface temperature decreases. Thus, in our work, a large change in solar specular reflectance would have been observed on the -195°C mirrors if contaminant film deposition had occurred.

The spectral reflectance degradation (Figure 14) of mirrors employing a 1800Å thick Si₂O₃ overcoating was similar to that experienced on the bare aluminum surface, except larger. It should be noted, however, that the diffuse reflectance of the silicon-oxide overcoated mirrors decreased slightly as a result of the irradiation. This phenomena is discussed in more detail later in the report.

The effects of protons on the solar specular reflectance of the nickel mirrors overcoated with 1800Å of silicon oxide are shown in Figure 15. A relatively large variation occurred between identically irradiated samples as noted by the bars on some of the data points. No explanation for this variation can be given at this time. To determine whether highly absorbing Si₂O₃ films degraded more than slightly absorbing films, (see Sec. 6.2.1) three mirror samples from batch D17A to D34A (Appendix A) were irradiated at 0°C. Data points for these samples, shown in Figure 15, indicate comparable degradation between mirror samples from the two coating batches.

In contrast to results obtained on the majority of the silicon-oxide overcoated nickel substrate mirrors, the three samples from batch D17A to D34A exhibited a

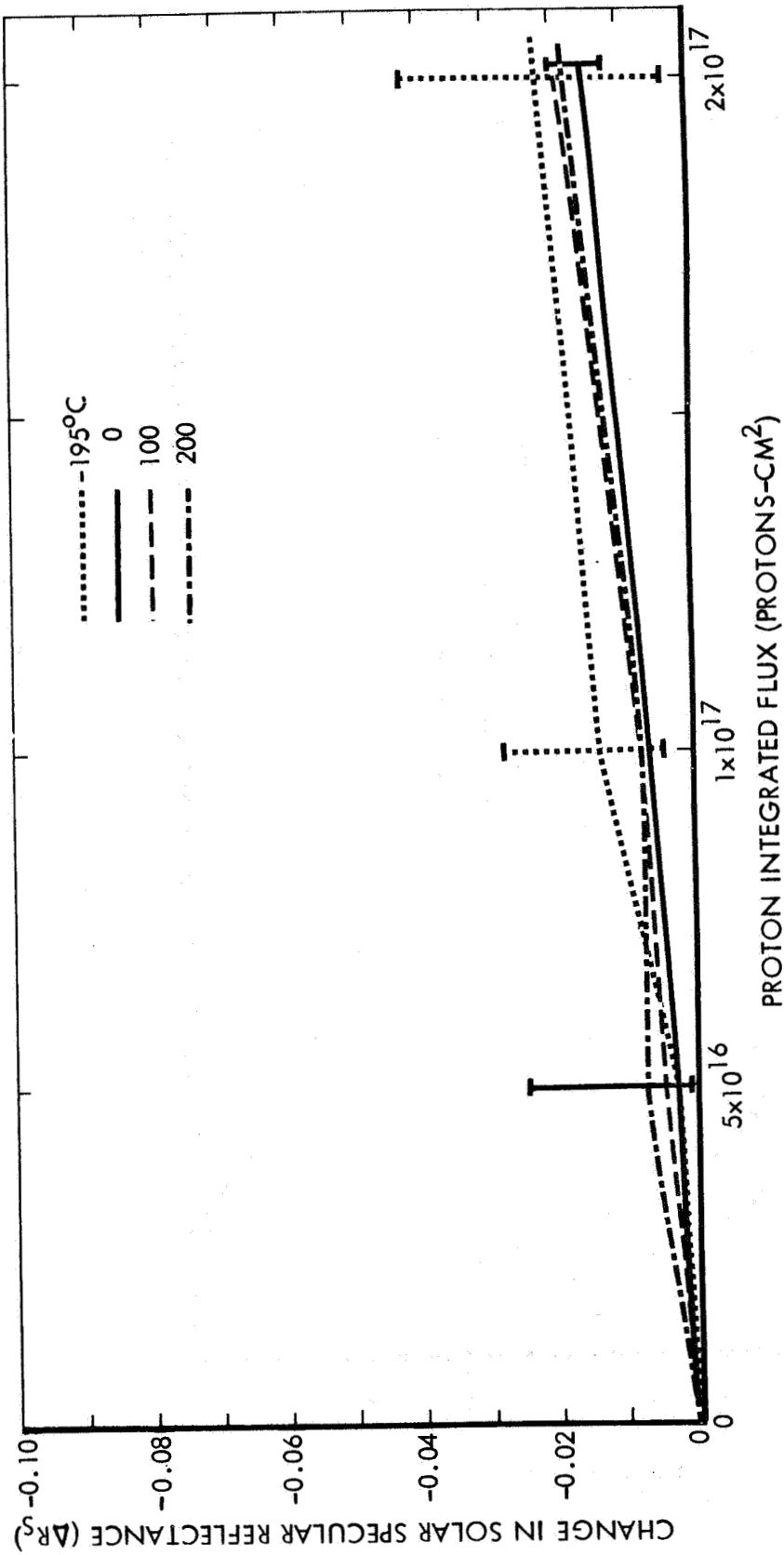


Figure 13: EFFECT OF PROTONS ON SOLAR SPECULAR REFLECTANCE OF ALUMINUM COATED, NICKEL SUBSTRATE MIRRORS

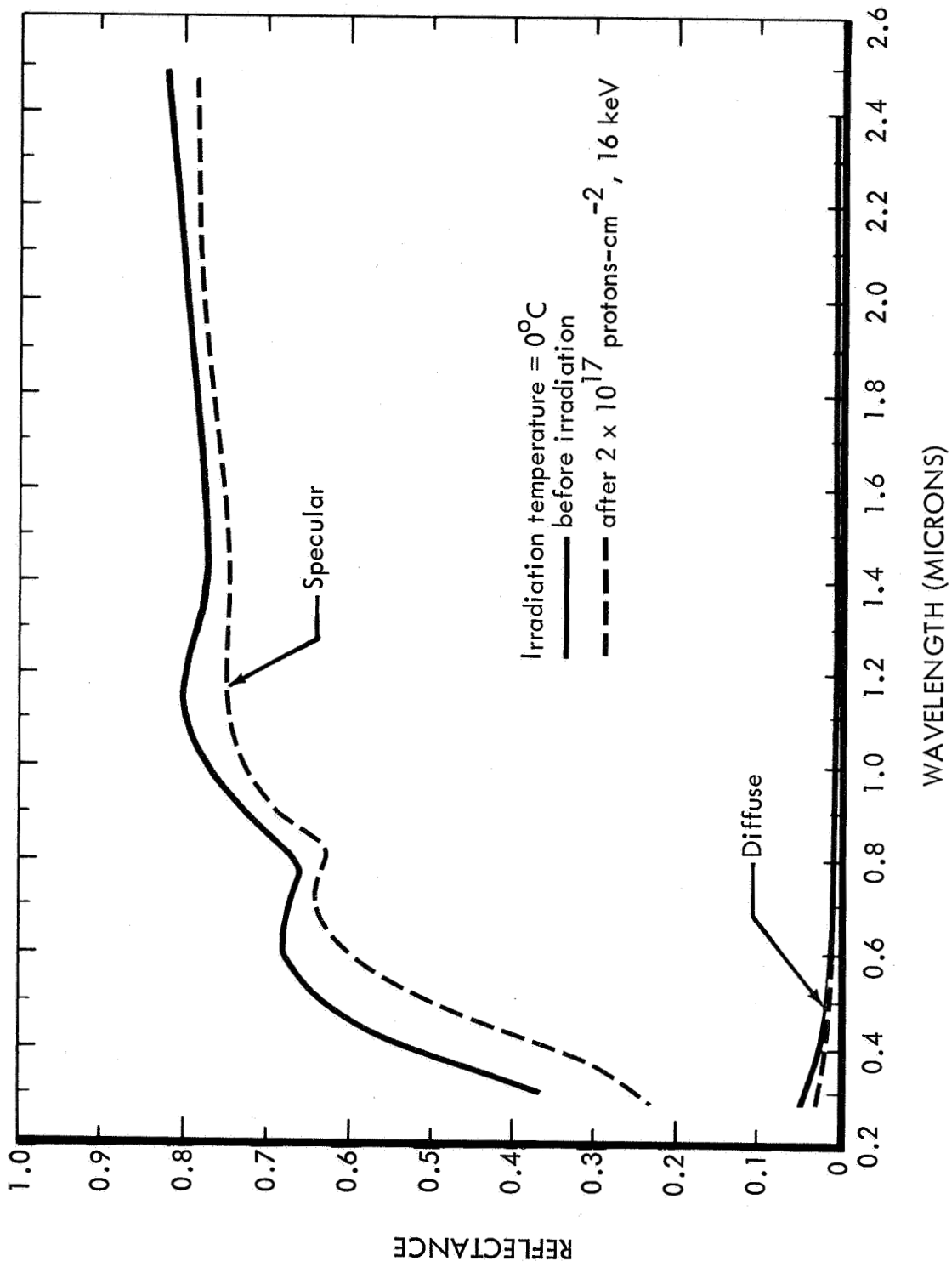


Figure 14: EFFECT OF PROTONS ON SPECTRAL REFLECTANCE OF Si₂O₃ OVERCOATED, NICKEL SUBSTRATE MIRRORS

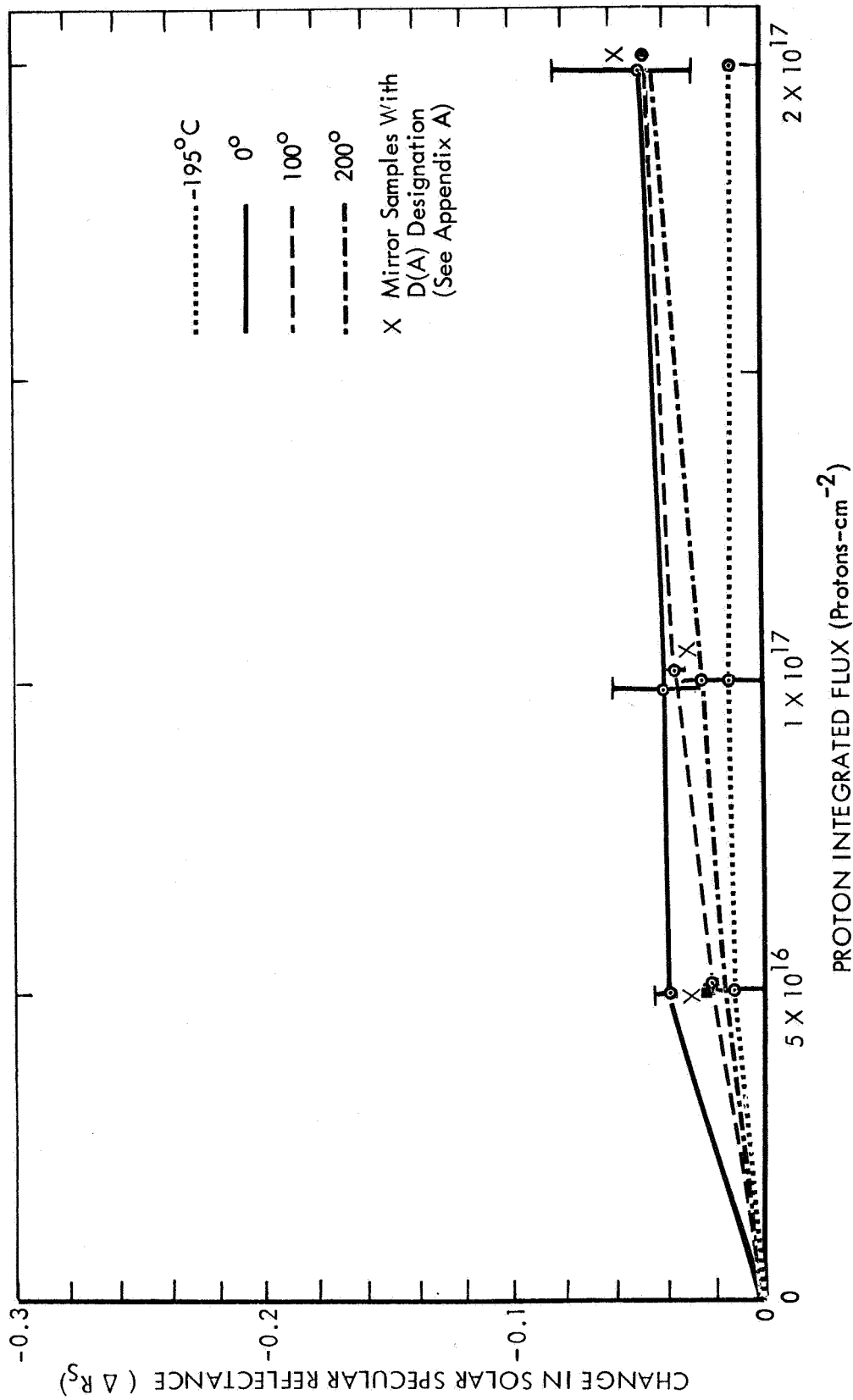


Figure 15: EFFECT OF PROTONS ON SOLAR SPECULAR REFLECTANCE OF Si_2O_3 OVERCOATED, NICKEL SUBSTRATE MIRRORS

delamination of vacuum deposited films at random locations. Relatively large patches of the aluminum and Si_2O_3 films separated from the SiO interface. The mirror sample irradiated at 1×10^{17} protons- cm^{-2} exhibited only one patch about 3mm in diameter; however, the samples irradiated at 2×10^{17} protons- cm^{-2} had lost about one-half of their reflective surface. The reflectance measurements on those mirrors which were irradiated with 5×10^{16} and 1×10^{17} protons- cm^{-2} were made in the areas where no delamination occurred. However, the data point (Figure 15) given for the mirror sample exposed to 2×10^{17} protons- cm^{-2} is of questionable significance because so much of the aluminum film was missing.

In an attempt to explain why the one batch of nickel-substrate mirrors delaminated during irradiation, a review was made of the vacuum coating data (Appendix A). A comparison between the coating conditions for samples numbered 1 to 66 vs. 17A to 34A indicates that the only significant difference was the temperature of the substrates during coating. The coatings which delaminated were applied at 80°C vs. 100°C for the coatings which neither blistered nor delaminated. This temperature difference may be significant because, as will be discussed later, coatings applied at ambient temperature blistered severely. The results obtained here suggest that additional work be done to evaluate the effect of vacuum coating procedures on the blistering or delamination of mirror surfaces.

From a radiation-effect standpoint, it is of interest to determine whether proton-induced radiation damage continues to increase with increasing integrated flux or saturates at some maximum value of degradation. A continuous increase in ΔR_s would indicate the formation of new color centers by proton-induced dislocations, whereas, a saturation of radiation damage would indicate that the protons are only energizing the color centers which are inherent in the oxide prior to irradiation. It would appear from the data of ΔR_s vs. integrated flux that the change in reflectance reaches a saturation value. In general, very little or no additional damage occurred above 5×10^{16} protons- cm^{-2} . No data were taken between 0 and 5×10^{16} protons- cm^{-2} with 16 keV protons; however, tests at integrated flux levels of 1×10^{15} and 5×10^{15} protons- cm^{-2} using 2 keV protons and a mirror temperature of 0°C showed that the threshold of significant damage ($\Delta R_s > 0.01$) was between 5×10^{15} and 5×10^{16} protons- cm^{-2} .

As noted in the figure, at an integrated flux level of 2×10^{17} protons- cm^{-2} , the -195°C samples showed less damage than the 0° , 100° , and 200°C samples which were all equivalent. This result is an indication of the cleanliness of the vacuum system. The change in reflectance of the latter three is comparable to the ΔR_s obtained for the 0° and 50°C silicon-oxide overcoated aluminum-substrate mirrors discussed later. This agreement is expected if the change in reflectance is due to increased absorption in the silicon-oxide overcoatings.

In addition to the increase in absorption in the silicon-oxide coatings, other proton effects were found in these mirrors. A series of electron photomicrographs were prepared from replicas of silicon-oxide surfaces irradiated at 0°C. It was noted from these photomicrographs (Figures 16, 17, 18, and 19) that the surfaces became much smoother when the integrated flux was increased from 5×10^{16} to 1×10^{17} protons-cm⁻². A surface irradiated with 5×10^{16} protons-cm⁻² showed no change from an unirradiated surface. Similarly, a surface irradiated with 2×10^{17} protons-cm⁻² showed little change from the surface which was exposed to 1×10^{17} protons-cm⁻². Based on the photomicrographs, it was concluded that silicon oxide was removed from the surface by either a sputtering or spallation process. The amount of silicon oxide that could be removed by sputtering after 2×10^{17} protons-cm⁻² was calculated to be only about 6Å, based on a sputtering yield given in Reference 19. Thus, it is most likely that the surfaces were made smoother by a blistering or spallation process. The improvement in surface finish noted here has been previously observed in References 20 and 21. In a recent report on studies of proton-induced blistering of metal surfaces (Reference 22) it was shown that anodic aluminum-oxide films on aluminum spall off as a result of irradiation with 30-50 keV protons.

As noted earlier, diffuse reflectances of silicon-oxide overcoated surfaces decreased as a result of the proton irradiation. It was also pointed out earlier that the diffuse reflectance of the oxide overcoated surfaces was larger than that of the bare aluminum surfaces. Assuming that the higher diffuse reflectance on the unirradiated oxide-coated mirrors was due to light scattering from the non-specular surface of the oxide, the smoothing of the surface during irradiation could account for the decrease in diffuse reflectance.

Results of proton experiments on nickel mirrors overcoated with 8000Å of Si₂O₃ will now be discussed. These mirror samples were irradiated at integrated flux levels of 5×10^{16} , 1×10^{17} , and 2×10^{17} protons-cm⁻² at a temperature of 0°C. Typical spectral reflectance data for a mirror of this type before and after irradiation is given in Figure 20. The irradiation with 2×10^{17} protons-cm⁻² resulted primarily in a decrease in specular reflectance in the wavelength region from 0.3 to 0.5 micron. A slight shift in interference maxima and minima to shorter wavelength was also experienced although precise amounts could not be determined from the point-by-point reflectance data. Since the diffuse reflectance showed nearly a negligible change, the decrease in specular reflectance can probably be attributed to increased absorption in the silicon oxide film. The integrated values of solar specular reflectance before and after irradiation were $R_s = 0.756$ and $R_s = 0.738$, respectively.

Infrared reflectance data were also measured before and after irradiation with protons. The purpose of this measurement was to determine whether the protons caused any change in the lattice structure or stoichiometry of the silicon oxide. Any change in the composition of the oxide should result in a change in

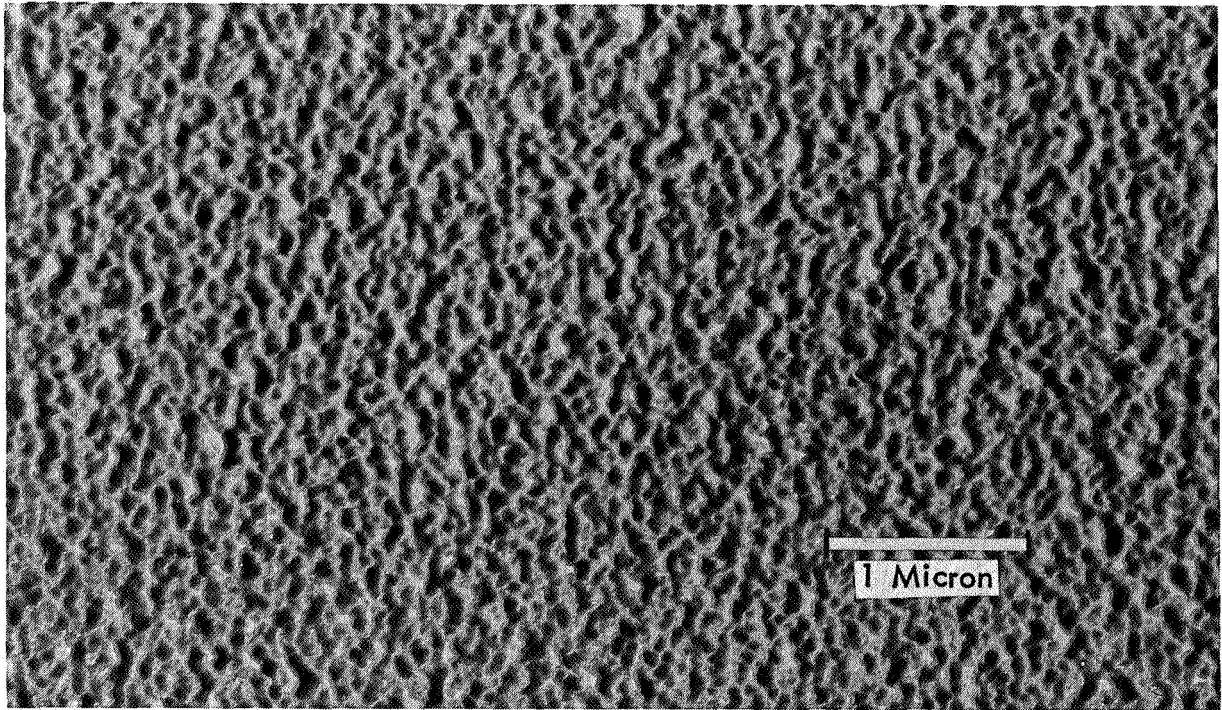


Figure 16: PHOTOMICROGRAPH OF UNIRRADIATED SILICON-
OXIDE SURFACE

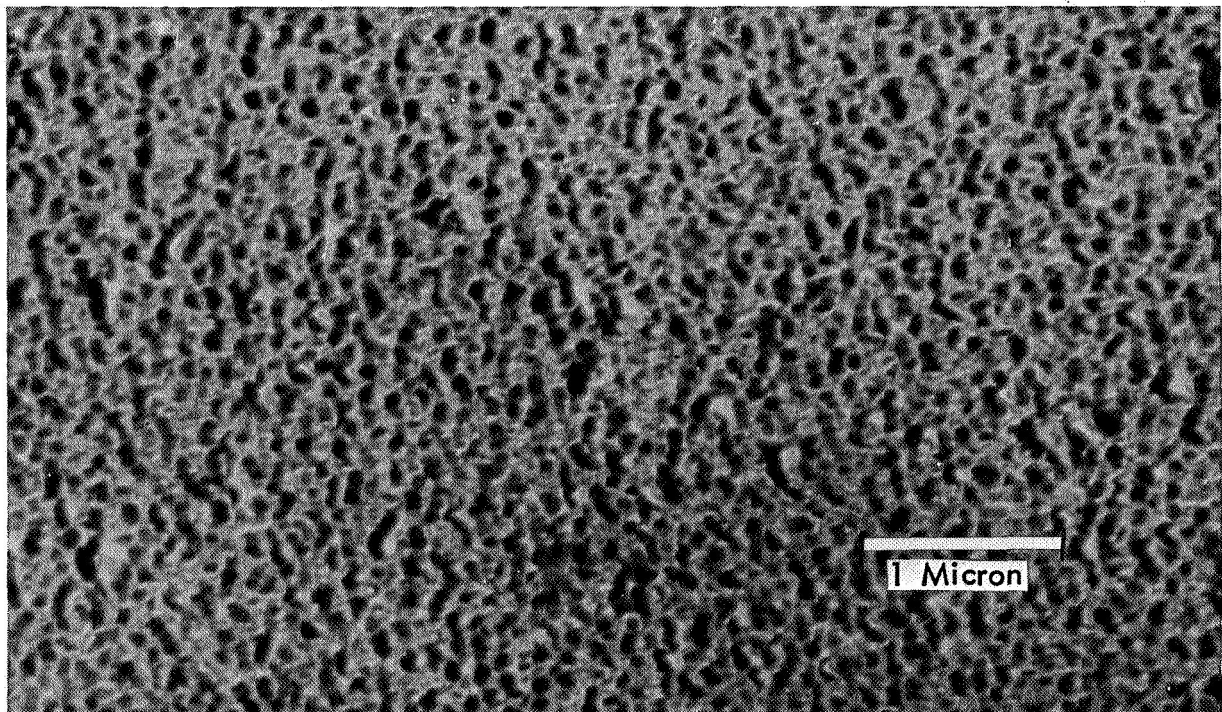


Figure 17: PHOTOMICROGRAPH OF SILICON-OXIDE SURFACE
IRRADIATED WITH 4.7×10^{16} PROTONS-CM⁻²
(16 keV, 0° C)

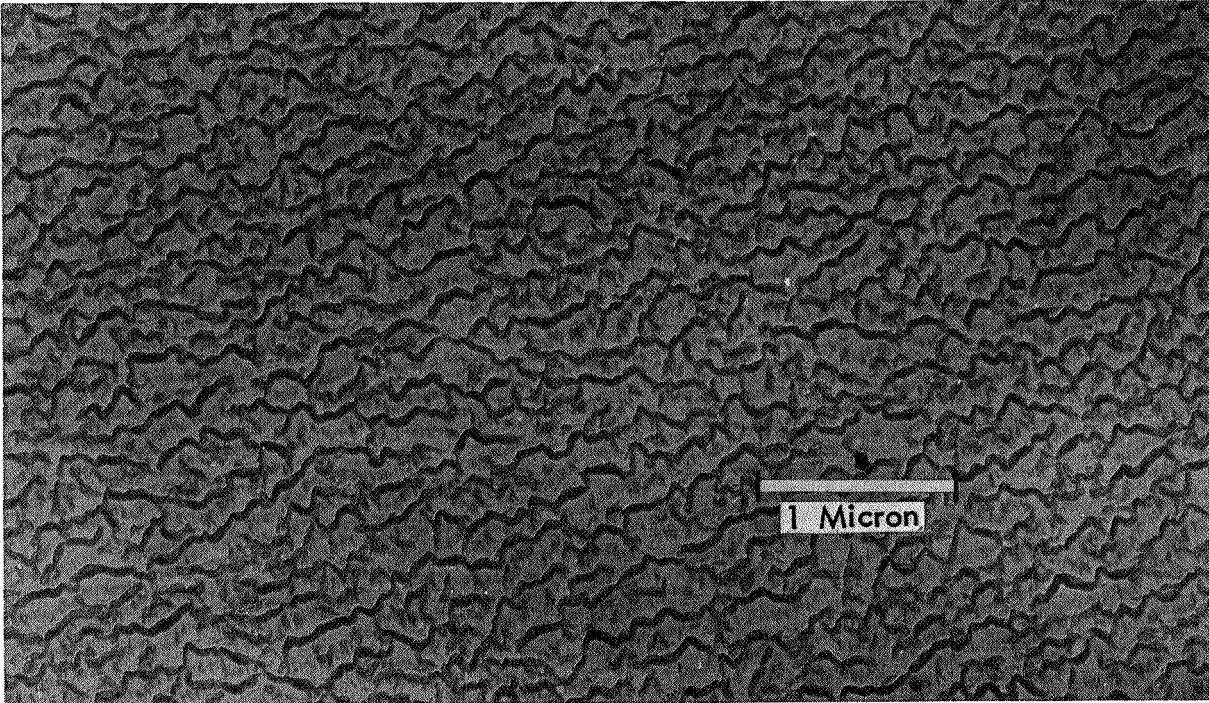


Figure 18: PHOTOMICROGRAPH OF SILICON-OXIDE SURFACE
IRRADIATED WITH 1×10^{17} PROTONS-CM⁻²
(16 keV, 0^o C)

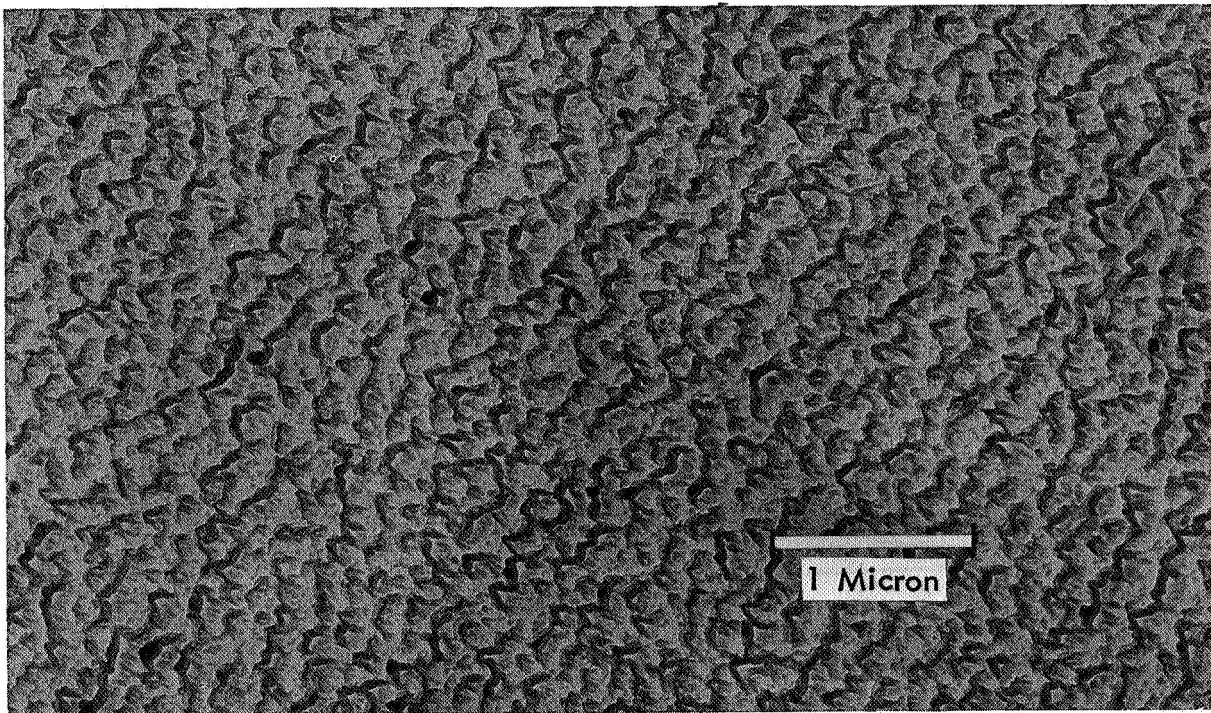


Figure 19: PHOTOMICROGRAPH OF SILICON-OXIDE SURFACE
IRRADIATED WITH 2×10^{17} PROTONS-CM⁻²
(16 keV, 0^o C)

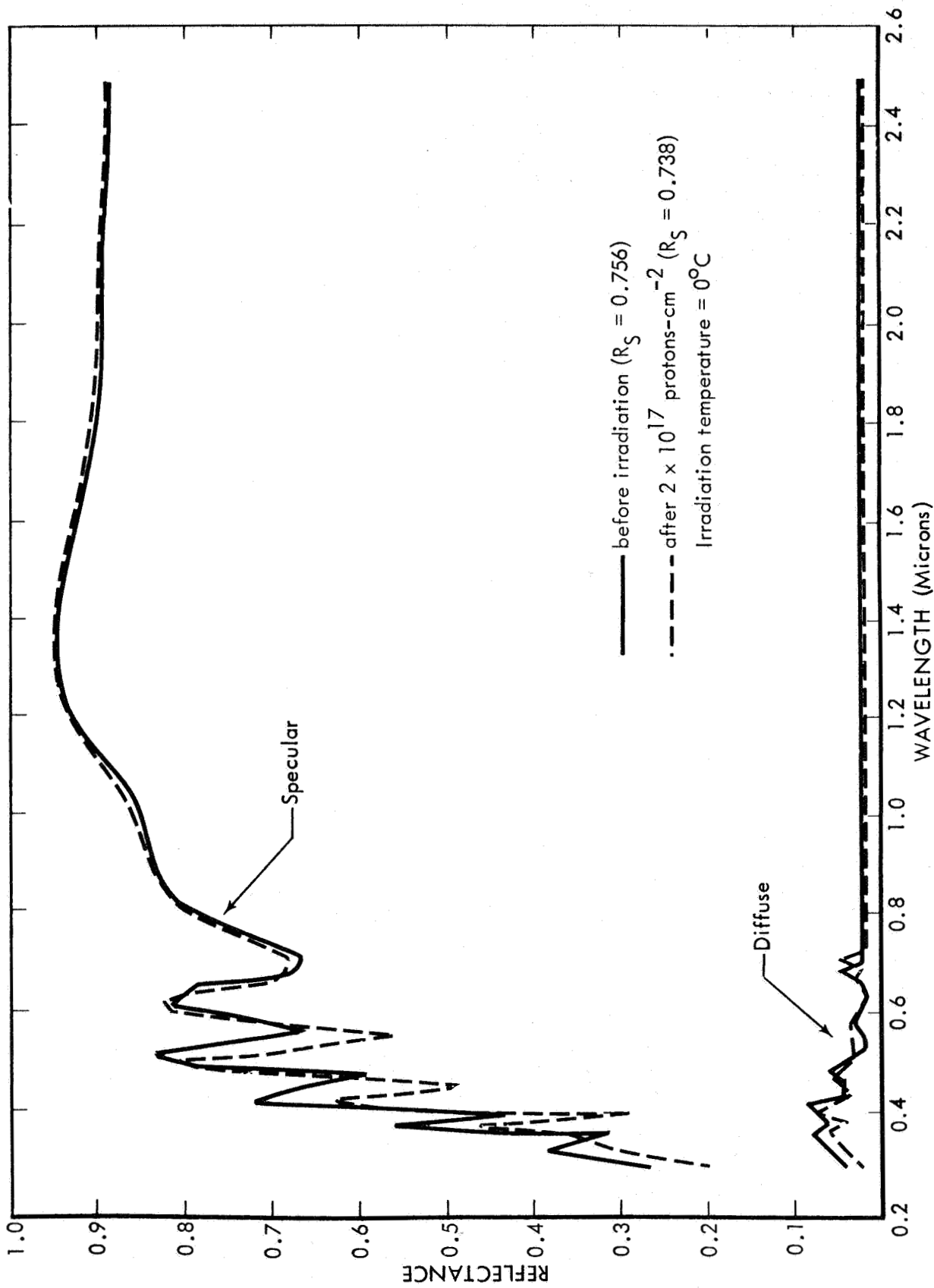


Figure 20: EFFECT OF PROTONS ON SPECTRAL REFLECTANCE OF 8000 Å Si_2O_3 OVERCOATED, NICKEL SUBSTRATE MIRRORS

either the magnitude or wavelength position of the infrared absorption peaks. The effect of the protons on the infrared spectra of the Si₂O₃ coating was small as noted in Figure 21. The 11.4 micron absorption peak was eliminated and it appears that a peak started to form at about 12.5 microns. Insufficient reflectance changes occurred to conclude that any significant chemical compound changes occurred.

It is interesting to compare the wavelengths of the various rotational, vibrational and infrared interference peaks obtained here with those obtained in Reference 16. According to the reference, the chemical compound of Si₂O₃ should exhibit absorption peaks at a wavelength of 9.6 to 9.8 microns and at 11.5 microns. The reflectance data on the unirradiated surface shows a very strong absorption peak at 9.85 microns and a very weak peak at 11.4 microns, which is in good agreement with the reference data. Thus, the labeling of the silicon oxide coatings as Si₂O₃ is apparently justified.

A summary of the effects of protons on the solar specular reflectance of mirrors coated with 8000Å thick Si₂O₃ films is given in Figure 22. As noted in the figure, the change in reflectance below an integrated flux level of 5×10^{16} protons-cm⁻² was assumed to be negligible. At 2×10^{17} protons-cm⁻² the average decrease in specular reflectance was only $\Delta R_s = -0.022$. Comparing this data to that obtained with the 1800Å thick Si₂O₃ coatings, it can be seen that the thicker coatings degraded less for some unknown reason.

Results of proton experiments on nickel substrate mirrors overcoated with 1700Å thick SiO₂ coatings will now be discussed. Reflectance data showing typical proton effects is given in Figure 23. The irradiation produced both a slight increase in the amplitude of oscillation of interference maxima and minima and a shift of their positions to shorter wavelength. Based on optical interference theory, an increase in amplitude is indicative of an increase in the refractive index of the silicon oxide, and the shift in wavelength indicates either a decrease in refractive index or thickness of the oxide film. The proton irradiation also produced a small decrease in the diffuse reflectance in the wavelength region less than 0.6 micron. Solar specular reflectances of the mirror sample shown in Figure 23 before and after irradiation were $R_s = 0.762$ and $R_s = 0.740$, respectively.

Infrared reflectance data, measured before and after irradiation with 2×10^{17} protons-cm⁻², are shown in Figure 24. As noted in the figure, protons had an insignificant effect on the infrared reflectance spectra. The relatively small changes in absorption peak amplitudes are not conclusive of any crystalline or chemical changes and may well be due to instrumentation problems.

A comparison was made between the wavelength positions of absorption peaks observed on SiO₂ overcoated mirror samples and those given in References 16 and 23 for quartz. The data given in Reference 16 indicates that quartz should show

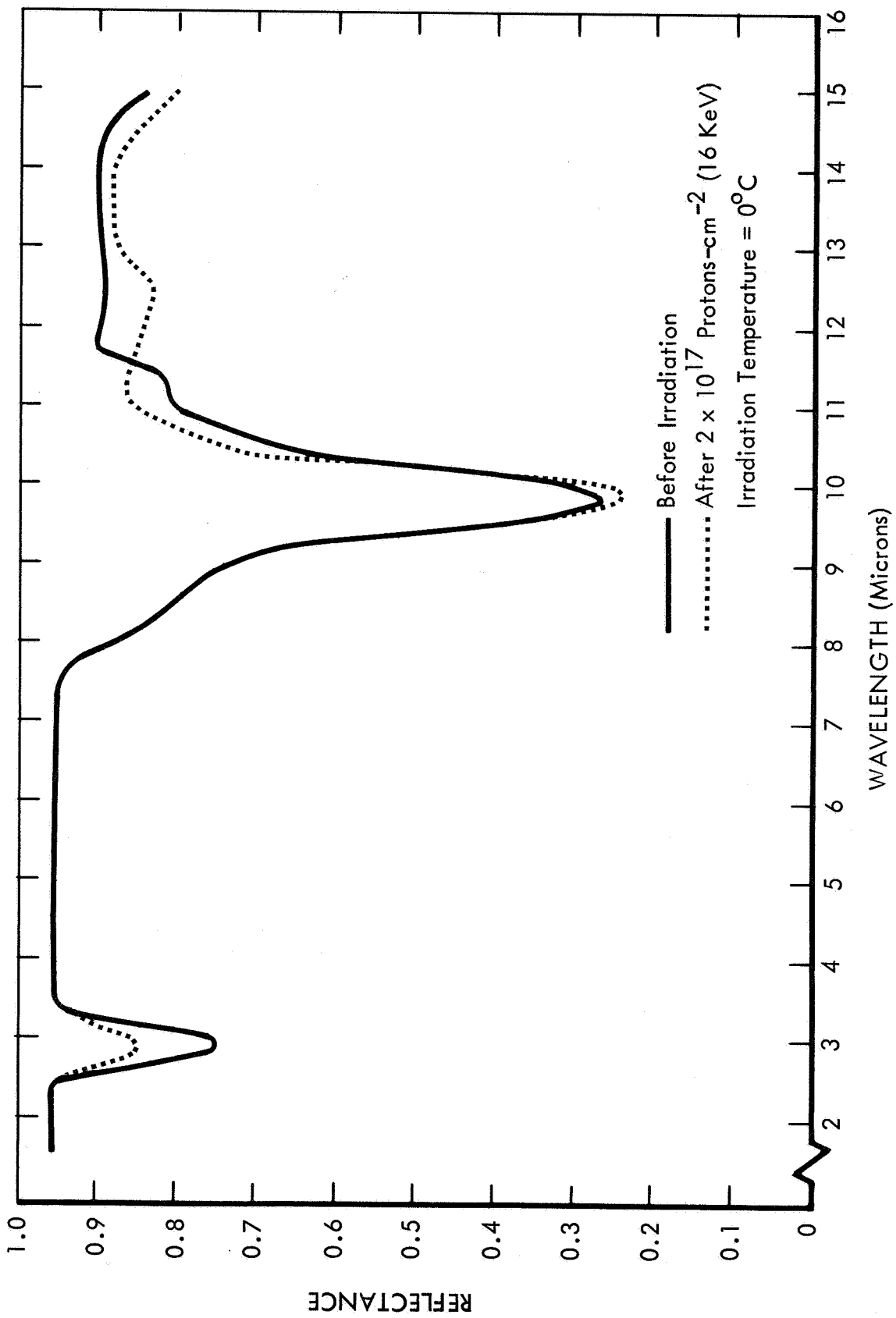


Figure 21: EFFECT OF PROTONS ON THE INFRARED REFLECTANCE OF Si₂O₃ OVERCOATED, NICKEL SUBSTRATE MIRRORS

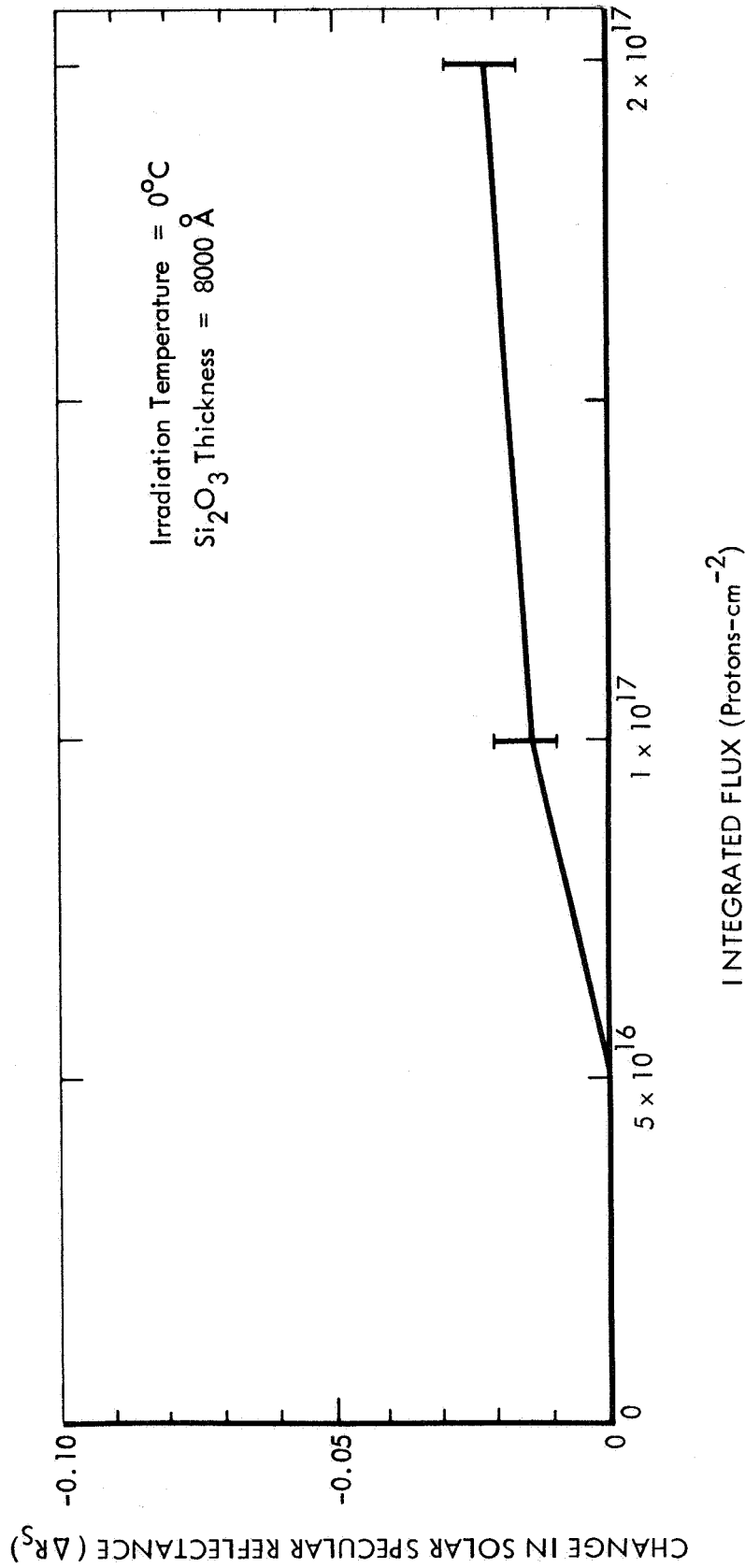


Figure 22: EFFECT OF PROTONS ON SOLAR SPECULAR REFLECTANCE OF 8000 Å Si₂O₃ OVERCOATED, NICKEL SUBSTRATE MIRRORS

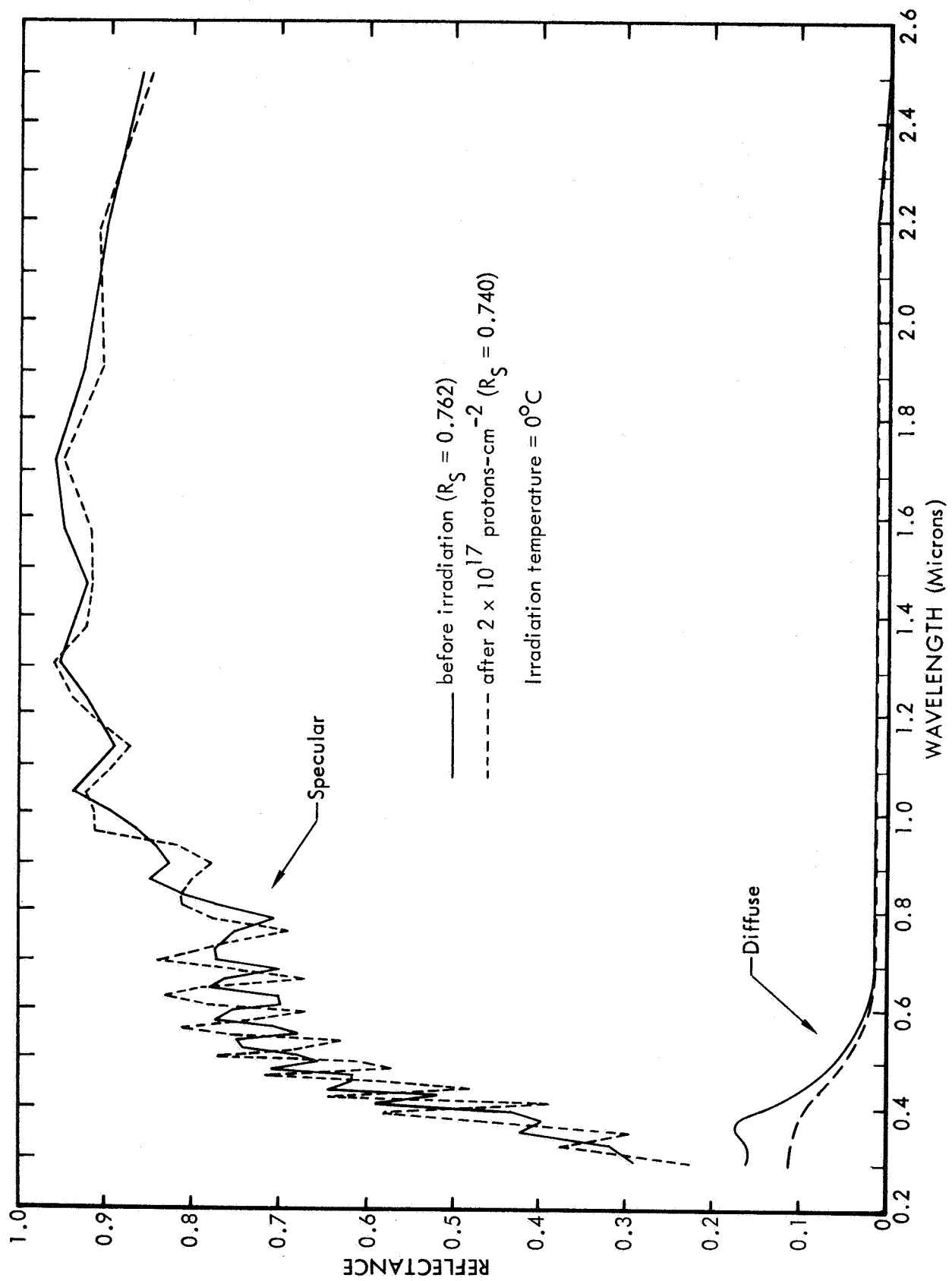


Figure 23; EFFECT OF PROTONS ON SPECTRAL REFLECTANCE OF 17,000 Å SiO₂ OVERCOATED, NICKEL SUBSTRATE MIRRORS

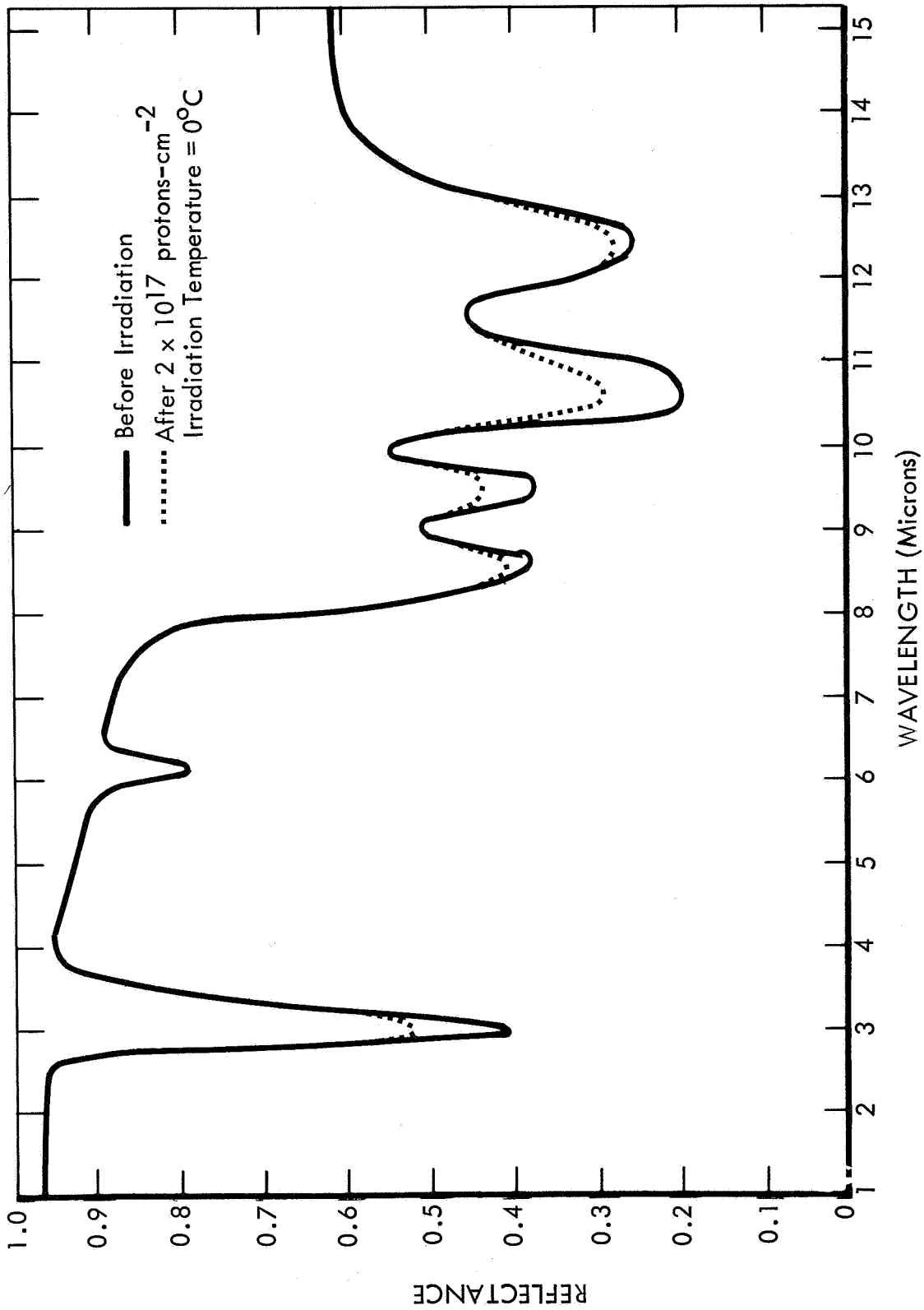


Figure 24: EFFECT OF PROTONS ON THE INFRARED REFLECTANCE OF SiO₂ OVERCOATED, NICKEL SUBSTRATE MIRRORS

characteristic peaks at 9.5 and 12.5 microns. In Reference 23, absorption peaks are shown at 3.1, 9.1, 12.5, 12.8, and 14.4 microns. The vacuum-deposited fused silica shows comparative peaks at 3, 9.5, and 12.5 microns; however, additional peaks are shown which cannot be explained at this time. It is possible that the additional peaks are due to infrared interference phenomena associated with refractive index changes near vibrational and rotational peaks (Reference 24). Based on the infrared spectra, it cannot be definitely concluded that the vacuum deposited overcoatings are identical to quartz.

A summary of the effects of protons on the solar specular reflectance of SiO₂ overcoated nickel mirrors is shown in Figure 25. As noted in the figure, the solar specular reflectance of the SiO₂ overcoated mirrors actually increased at integrated fluxes of 5×10^{16} and 1×10^{17} protons-cm⁻². At 2×10^{17} protons-cm⁻², however, a slight decrease in reflectance was obtained. A comparison between the Si₂O₃ coating data (Figure 22) and the SiO₂ data (Figure 25) indicates a slightly higher stability for the latter coating. In general, the effects of 16 keV protons on both types of oxide was small.

6.2.3 Ultraviolet Radiation Effects---A general summary of ultraviolet test conditions experienced by the various types of electroformed-nickel mirrors was given earlier in Table III, and a complete tabulation of ultraviolet test data is given in the Appendix B. Included in the appendix are a complete tabulation of test hour increments, ultraviolet intensities, total equivalent exposures, mirror temperatures, solar specular reflectances before and after irradiation, and the changes in solar specular reflectance.

Data for the various combinations of overcoatings on electroformed-nickel mirrors which were irradiated at different temperatures are given in Figures 26, 27, 28, and 29. Curves showing the change in solar specular reflectance vs. equivalent space sun hours (ESSH) are given for bare aluminum reflective surfaces, and data points are shown for the oxide overcoated surfaces. Each figure represents a different irradiation temperature. It will be noted in examining the figures that three curves have been plotted for each temperature, representing data from the three assumed identical mirrors. This particular way of showing the data was chosen because it illustrates the significant difference between mirrors prepared in different batches. The results of ultraviolet radiation tests on the bare aluminum surfaces will be discussed first.

A comparison of the degradation obtained with the bare aluminum surfaces at different temperatures shows that the amount of degradation obtained does not vary by a conclusive amount with temperature. It should also be noted that a saturation effect was found where, in general, little or no additional degradation occurred after a 2000-4000 ESSH exposure. Similar saturation characteristics

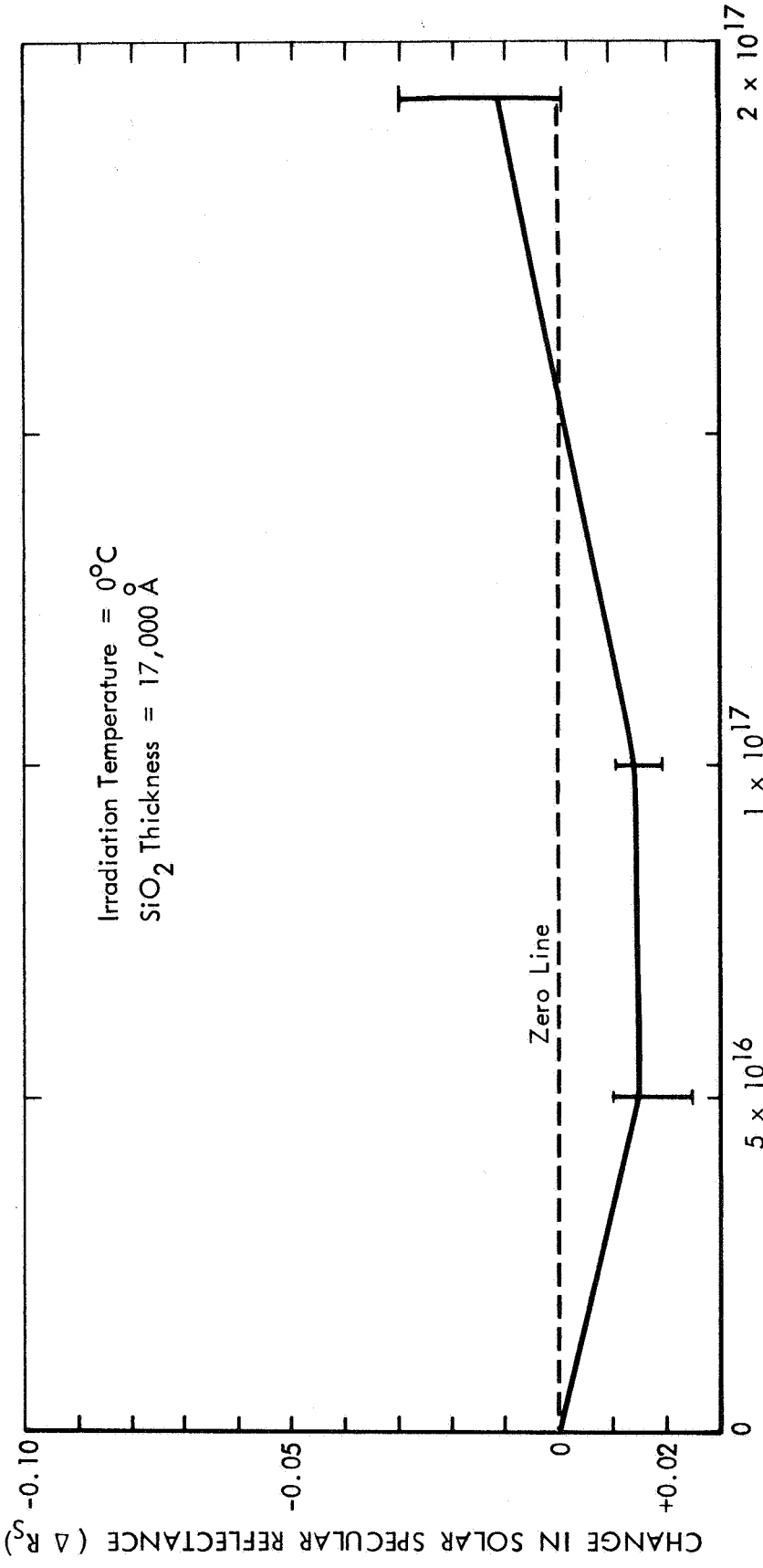


Figure 25: EFFECT OF PROTONS ON SOLAR SPECULAR REFLECTANCE OF SiO₂ OVERCOATED, NICKEL SUBSTRATE MIRRORS

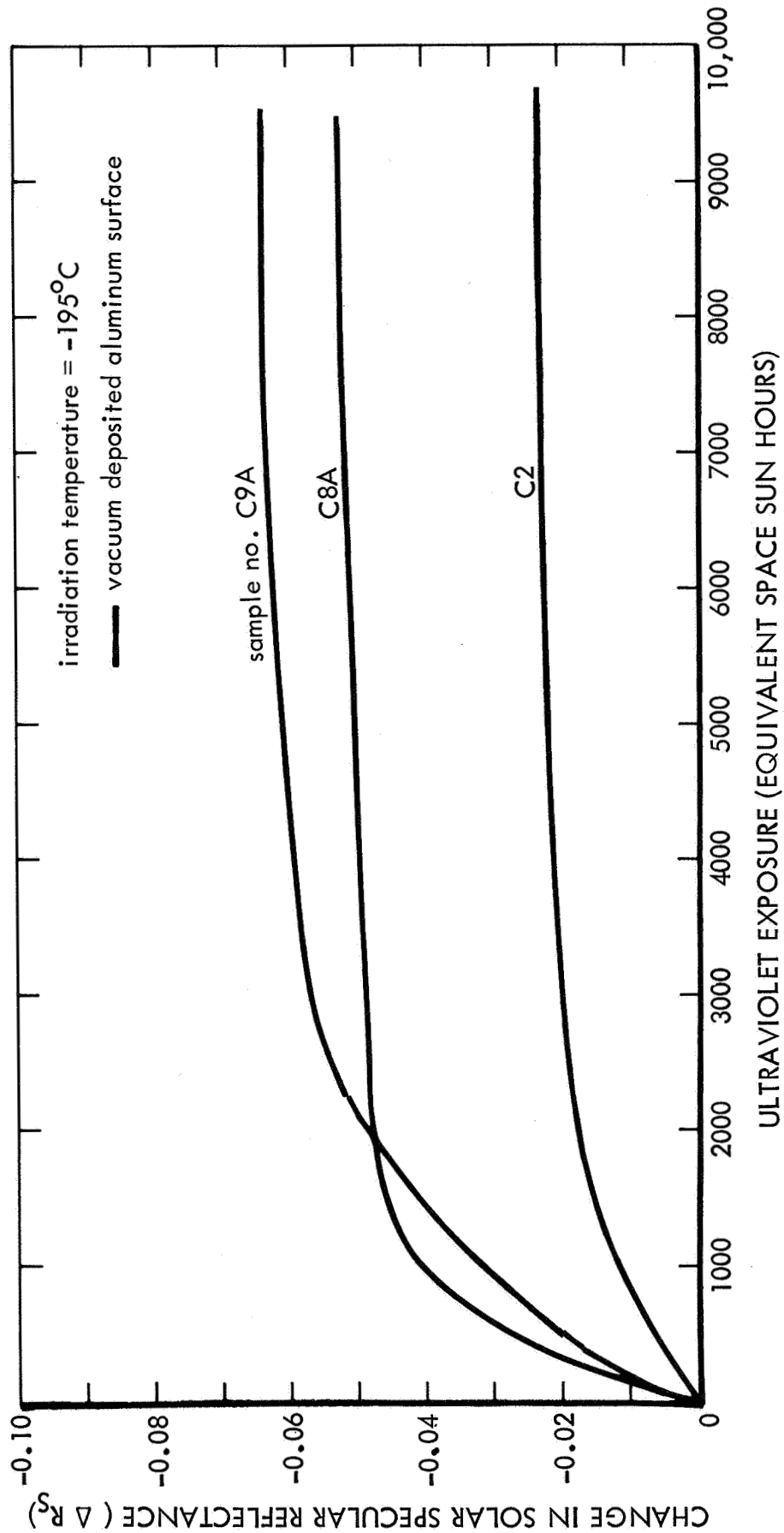


Figure 26: EFFECT OF ULTRAVIOLET RADIATION ON SOLAR SPECULAR REFLECTANCE OF NICKEL SUBSTRATE MIRRORS

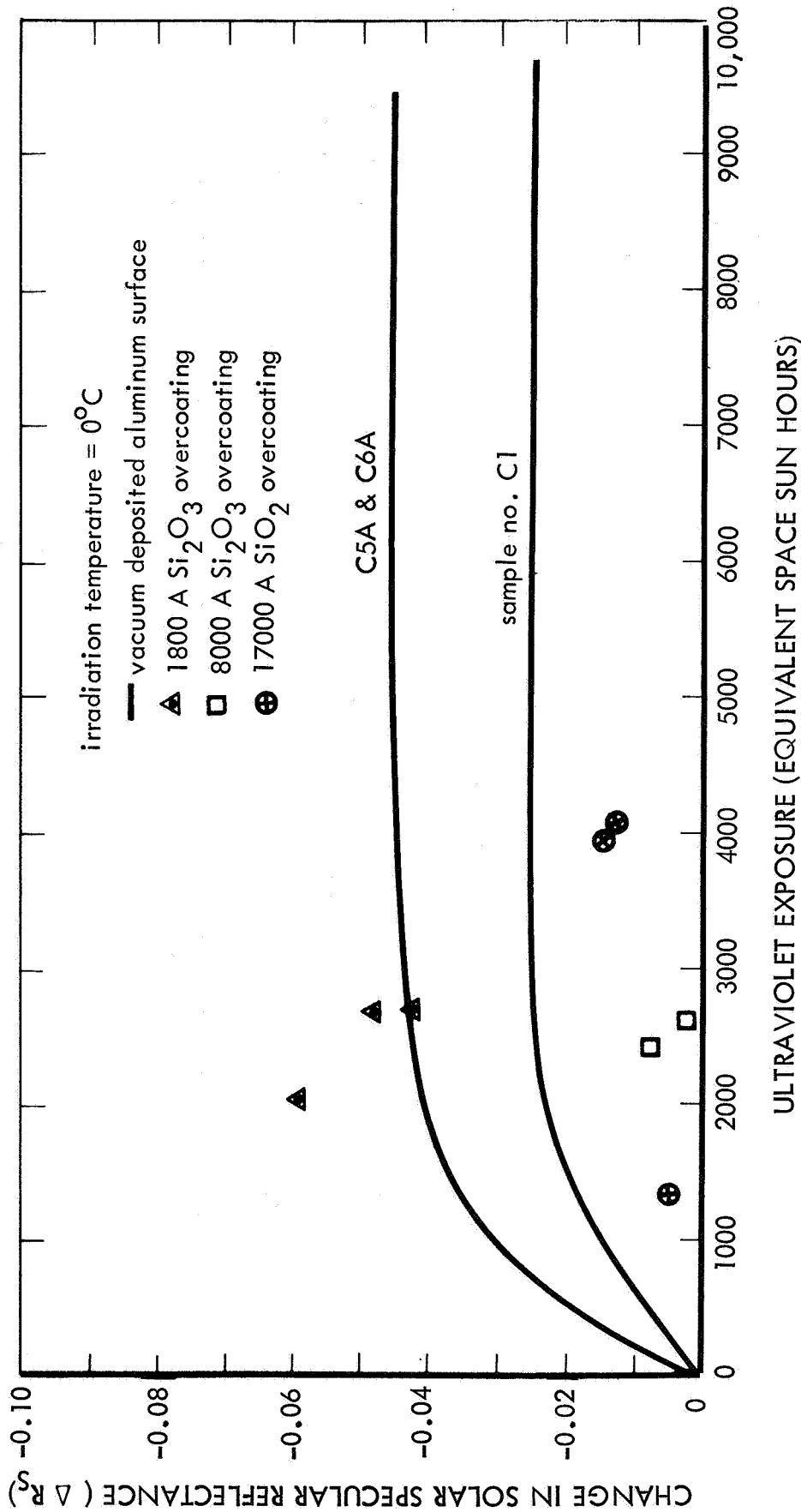


Figure 27: EFFECT OF ULTRAVIOLET RADIATION ON SOLAR SPECULAR REFLECTANCE OF NICKEL SUBSTRATE MIRRORS

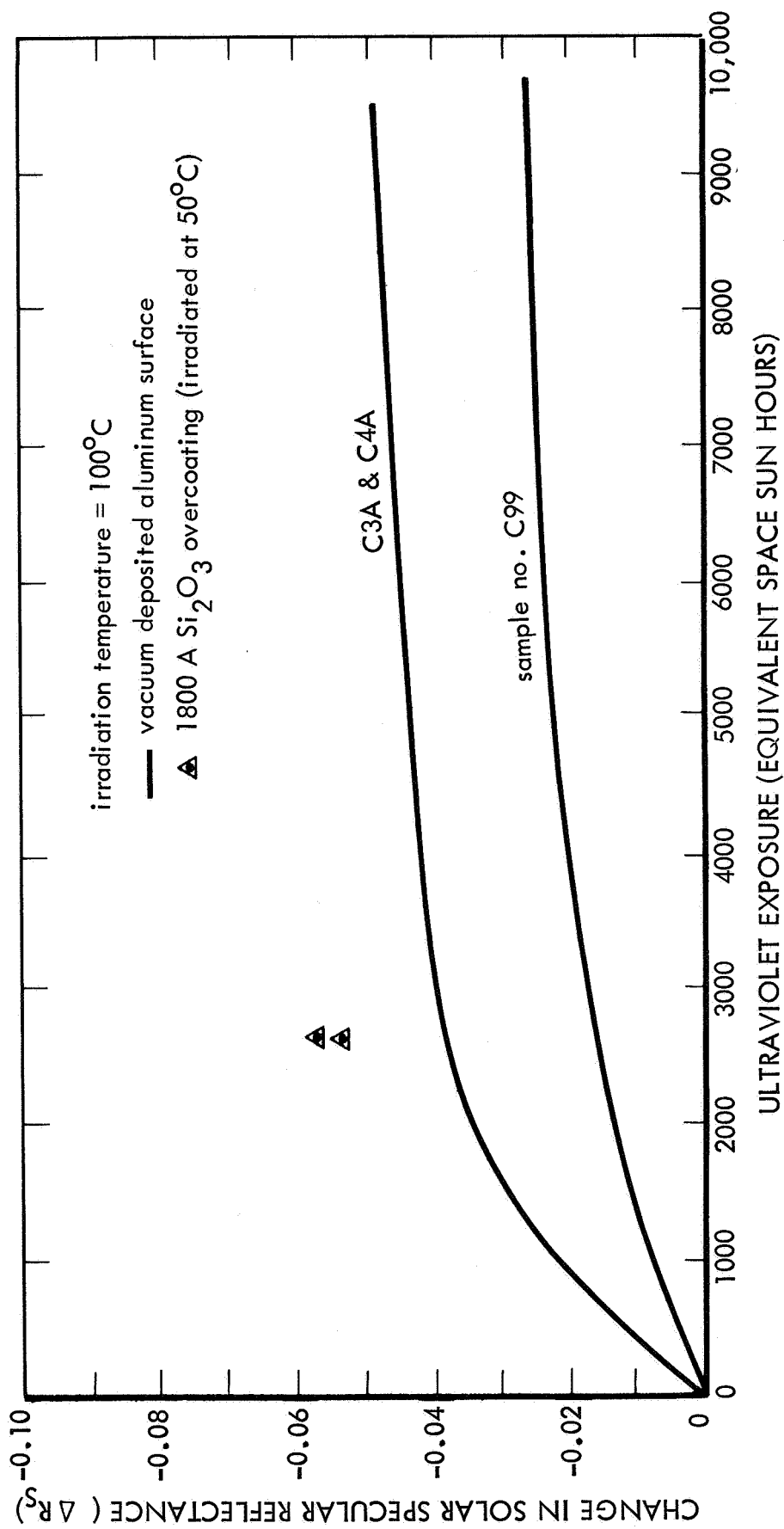


Figure 28: EFFECT OF ULTRAVIOLET RADIATION ON SOLAR SPECULAR REFLECTANCE OF NICKEL SUBSTRATE MIRRORS

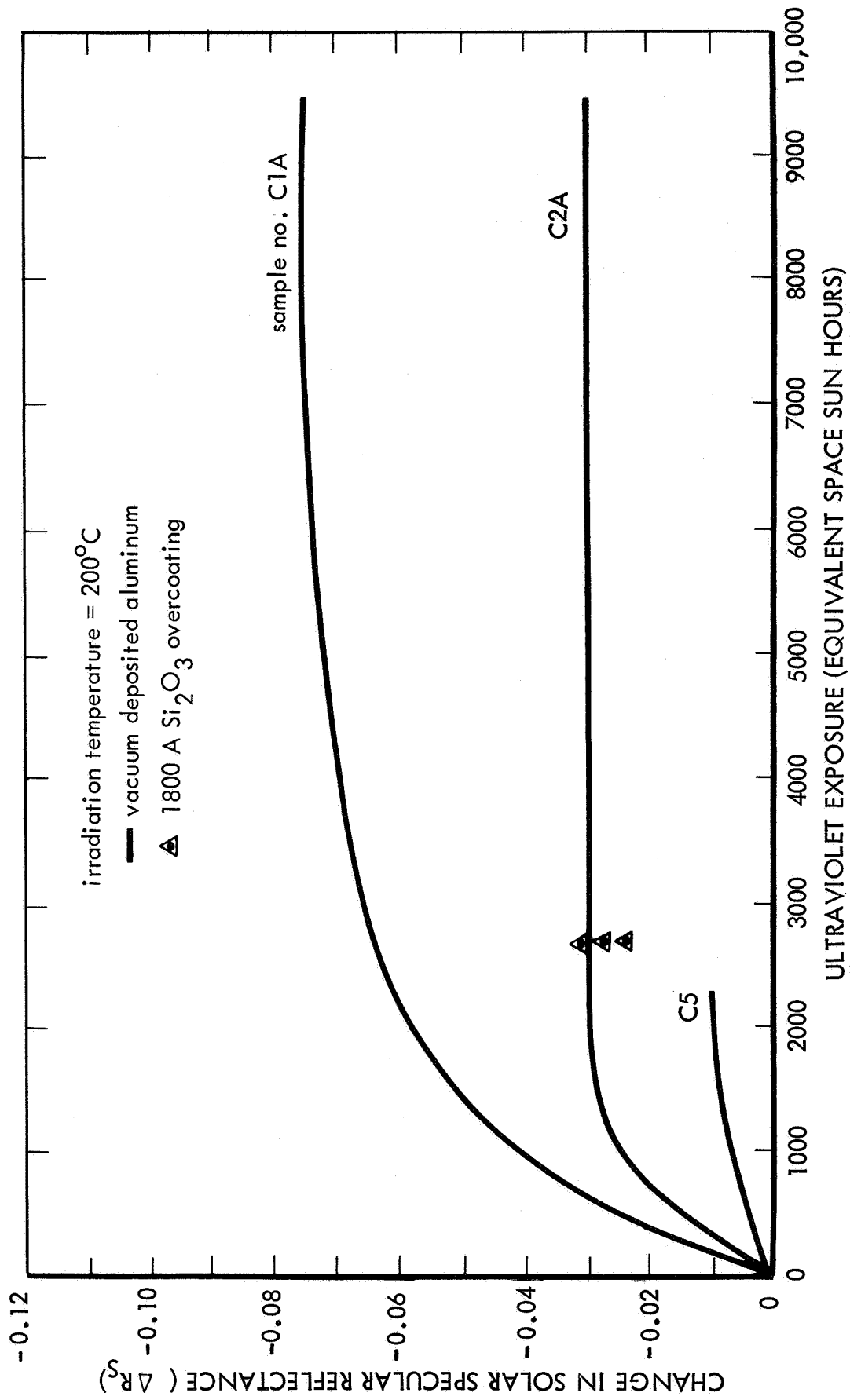


Figure 29: EFFECT OF ULTRAVIOLET RADIATION ON SOLAR SPECULAR REFLECTANCE OF NICKEL SUBSTRATE MIRRORS

are normally observed in ultraviolet irradiation of paints and anodic oxide coatings, where the principle mechanism of damage is the formation of color centers. The saturation value is established by the number of lattice defects available for forming color centers. The difference in degradation between the aluminum-coated samples prepared in different batches, for example C2 vs. C8A in Figure 26, may suggest a mechanism of damage for the aluminum surfaces. An examination of the differences between the vacuum coating data in the two batches shows that the mirrors with an "A" following the sample number (C8A) were coated at a pressure of 1×10^{-5} torr vs. 5×10^{-6} torr for the other batch. Prior experiments reported in Reference 25 have shown that more aluminum oxide is present in vacuum deposited aluminum films prepared at higher pressures than in those prepared at lower pressures. The fact that the films prepared at higher pressure both degrade more and contain more aluminum oxide suggests that color centers in the oxide may account for the degradation observed. In general, the amount of degradation obtained on the aluminum coated surfaces at the saturation value was small, $\Delta R_s = -0.01$ to -0.03 for one batch and -0.04 to -0.07 for the other batch. It is significant, however, that a small amount of degradation does occur and that it is probably dependent on coating conditions. The effects of ultraviolet radiation on the mirror samples overcoated with silicon oxide films will now be discussed.

Results of ultraviolet experiments on the 1800\AA thick Si_2O_3 overcoated mirrors are shown by data points in Figures 27, 28, and 29. Although mirrors of this type were irradiated at -195°C , it appeared that they had become contaminated during the test and thus the data have not been included. The amount of degradation experienced on these mirrors was in the order of $\Delta R_s = -0.04$ to -0.06 at the 2700 ESSH increment for temperatures of 0° and 50°C . At a temperature of 200°C , however, the degradation dropped to $\Delta R_s = -0.02$ to -0.03 .

Data for the 8000\AA thick Si_2O_3 and $17,000\text{\AA}$ thick SiO_2 overcoatings, shown in Figure 27, surprisingly shows nearly negligible degradation for those two coatings after about 2500 to 4000 ESSH exposures. Since this amount of degradation was significantly less than that noted above for the 1800\AA thick Si_2O_3 overcoatings, an attempt was made to explain this difference. The possibility of contamination was eliminated because all of these mirror samples were irradiated in the same test. An examination of the vacuum coating data revealed that the thicker coatings had been applied at both a higher pressure and temperature (1×10^{-4} torr and 100°C vs. 8×10^{-5} torr and 80°C). It is not presently known whether these relatively small differences in vacuum coating conditions would affect the ultraviolet stability of the coatings. Results of an ultraviolet irradiation experiment in which in-situ reflectance measurements were made will be discussed next.

An in-situ reflectance measurement experiment was conducted on electroformed nickel substrate mirrors to determine whether annealing of radiation-induced

optical absorption occurred when mirror surfaces irradiated in vacuum were exposed to ambient atmospheric conditions. Thus, the validity of "in-air" reflectance measurements which were performed on the majority of the ultraviolet irradiated mirror surfaces in the program, could be established. A complete set of reflectance measurements were made in air and vacuum both before and after irradiation on nickel mirrors which were overcoated with 1800Å Si₂O₃, 8000Å Si₂O₃ and 17,000Å SiO₂ coatings. Bare aluminum surfaces were not evaluated because an earlier experiment had shown no change in reflectance during pump-down and only a negligible change during irradiation. It should be noted that only the hemispherical (specular-plus-diffuse) reflectance was measured in these tests.

Results of the in-situ reflectance experiment in general showed that no significant change in solar reflectance occurred in either the transition from air-to-vacuum or vacuum-to-air. Furthermore, the amount of degradation measured in vacuum was in the order of the amounts measured on other mirror samples in air. Therefore, it is concluded that in-air reflectance measurements performed on the majority of the mirrors in this program appear to be valid. However, an interesting effect was observed in the tests which should be discussed because of its significance to space optical systems employing interference filters. It was found that the wavelength position of reflectance maxima and minima shifted during either evacuation, readmission of air, or irradiation. The vacuum deposited SiO₂ film was a particularly good example of this effect. A plot of the relative spectral reflectance* of this type of mirror, as measured with the in-situ reflectometer, is shown in Figure 30. Curves are given for conditions of in-air and in-vacuum both before and after irradiation with ultraviolet. As noted in the figure the positions of maxima and minima shifted to shorter wavelengths during irradiation, and shifted to longer wavelengths when air was readmitted to the chamber. It is interesting that the permanent shift in wavelength observed here is comparable and in the same direction as the shift observed during other proton and ultraviolet tests. No explanation for the shift in wavelength of interference maxima and minima can be given at this time. It is recommended that additional experiments be performed on dielectric interference coatings to study this effect and to assess its significance to space optical systems employing interference coatings.

The results of in-situ reflectance experiments on the 8000Å thick Si₂O₃ coating are shown in Figure 31. In contrast to results obtained on the SiO₂ coating, the Si₂O₃ only shifted in wavelength during irradiation. Also, the reflectance in the wavelength region of less than about 0.32 micron increased during irradiation, indicating a decrease in absorption in the oxide film.

* Absolute spectral reflectances could not be obtained with the in-situ reflectometer.

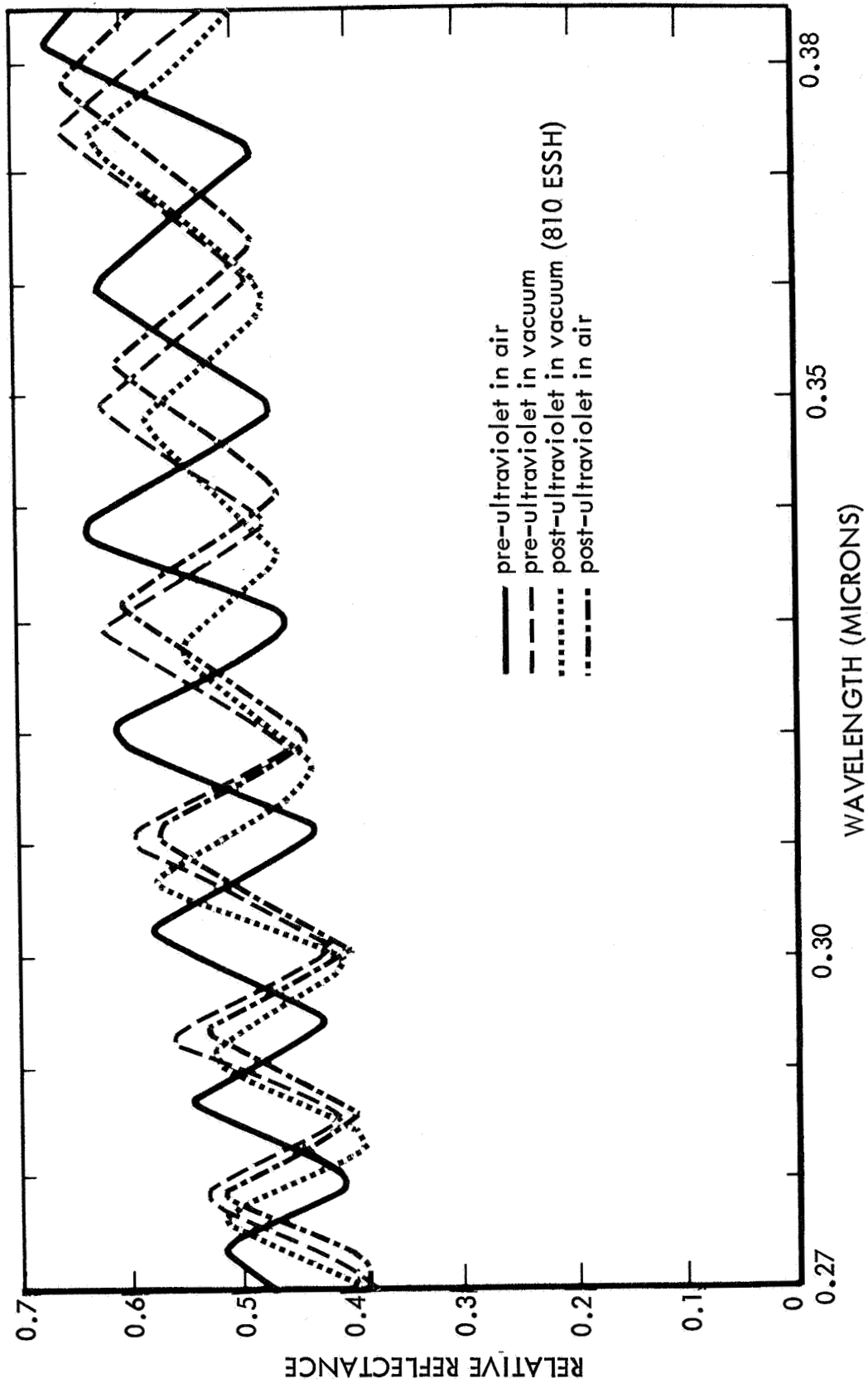


Figure 30: IN-SITU REFLECTANCE DATA ON SiO_2 OVERCOATED, NICKEL SUBSTRATE MIRROR

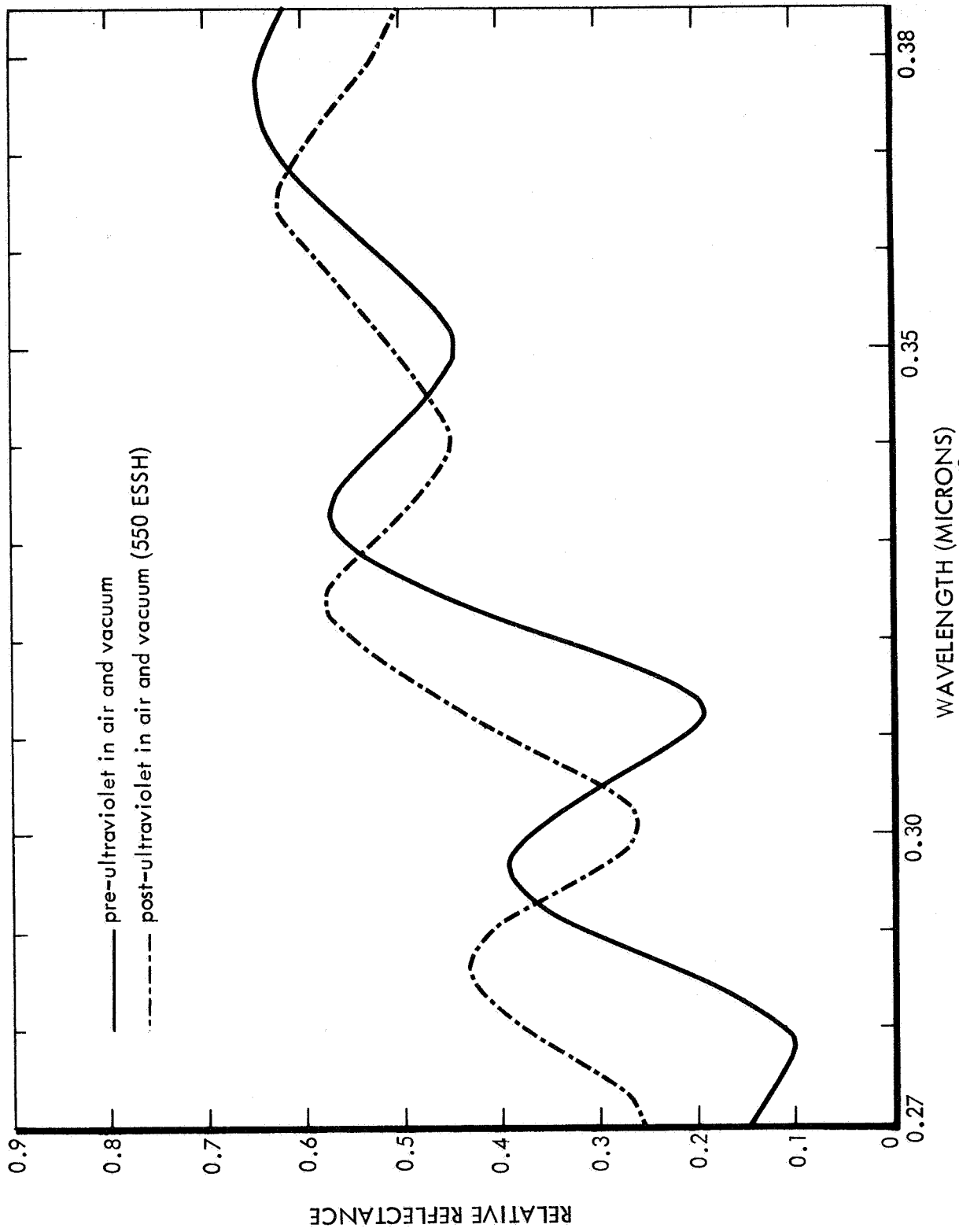


Figure 31: IN-SITU REFLECTANCE DATA ON 8000 Å -THICK Si₂O₃ OVERCOATED, NICKEL SUBSTRATE MIRRORS

6.2.4 Combined Proton-Ultraviolet Radiation Effects---An experiment was performed to determine whether any synergistic effects occur when mirrors are irradiated with both proton and ultraviolet radiation simultaneously. This experiment was of interest because prior tests by others and the bulk of the tests in this program were run with only one component of the space environment present. To ascertain whether synergistic effects occur, mirrors were irradiated at 0°C with a simultaneous exposure of 5×10^{16} protons-cm⁻² and 500 ESSH of ultraviolet radiation. In addition, mirrors which had been irradiated with 5×10^{16} protons-cm⁻² were subsequently exposed to 500 ESSH of ultraviolet radiation. Results of the simultaneous and sequential irradiation tests are given in Figures 32, 33, 34, and 35, which are plots of the change in spectral, specular reflectance (ΔR_{λ}). Figures 32 and 33 show results for bare aluminum coated electro-formed nickel mirrors and Figures 34 and 35 show data for these mirrors overcoated with 1800Å of Si₂O₃.

Results of the simultaneous irradiation experiments on the bare aluminum reflective surfaces (Figure 32) show that a small synergistic effect may have occurred. The change in spectral reflectance for the simultaneously irradiated mirror was slightly larger than the sum of the changes for the individual mirrors. However, additional tests should be run at higher exposures to definitely conclude whether a synergistic effect occurred because of the deviations between like-samples, possible instrumentation errors, and the relatively small changes in specular reflectance that occurred. Deviation bars on the proton-only curve represent the spread in data between three identically irradiated samples. No deviation bars are shown on the combined environment or ultraviolet-only curves since only one mirror sample was irradiated in each of the tests. The changes in solar specular reflectance (ΔR_s) for the proton-only and ultraviolet-only tests were negligible and the change in the combined-environment test was only $\Delta R_s = -0.016$.

In the experiment in which a bare aluminum coated mirror was irradiated with ultraviolet radiation after proton irradiation (Figure 33), results showed that more ultraviolet-induced damage was produced when the surface had been pre-irradiated with protons. No explanation for this increased degradation can be given at this time. Solar specular reflectance changes for the mirrors irradiated with ultraviolet-after-protons and ultraviolet-only were $\Delta R_s = -0.042$, and -0.019 , respectively.

The simultaneous irradiation of Si₂O₃ overcoated mirrors (Figure 34) resulted in a larger-than-additive effect in the wavelength region less than 0.45 micron and a less-than-additive effect in the region from 0.45 to about 0.8 micron. Changes in solar specular reflectances for the proton-only, ultraviolet-only, and proton + ultraviolet curves were $\Delta R_s = -0.024$, -0.015 , and -0.078 , respectively.

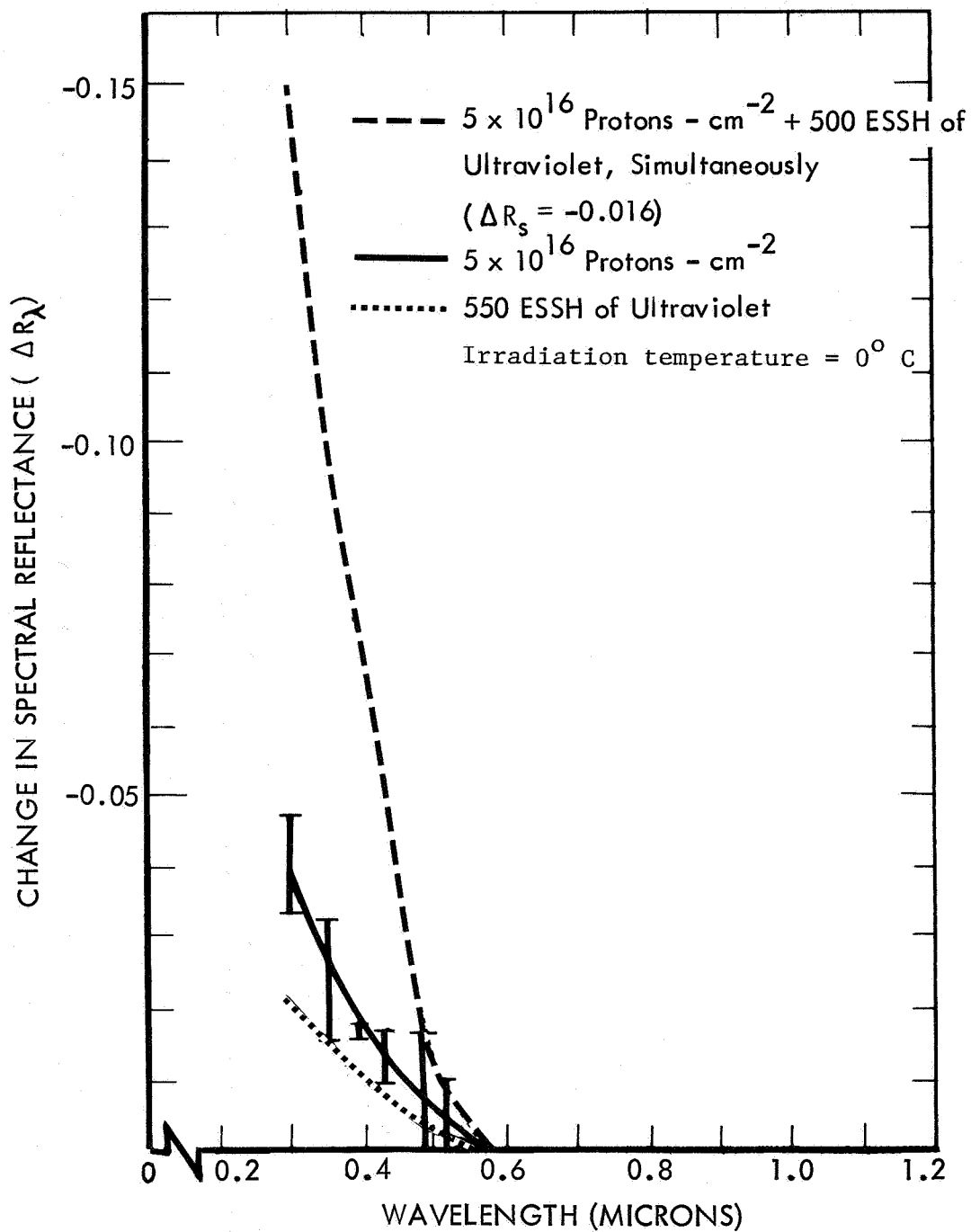


Figure 32: EFFECT OF COMBINED PROTON-ULTRAVIOLET RADIATION ENVIRONMENT ON ALUMINUM COATED, ELECTROFORMED NICKEL MIRRORS.

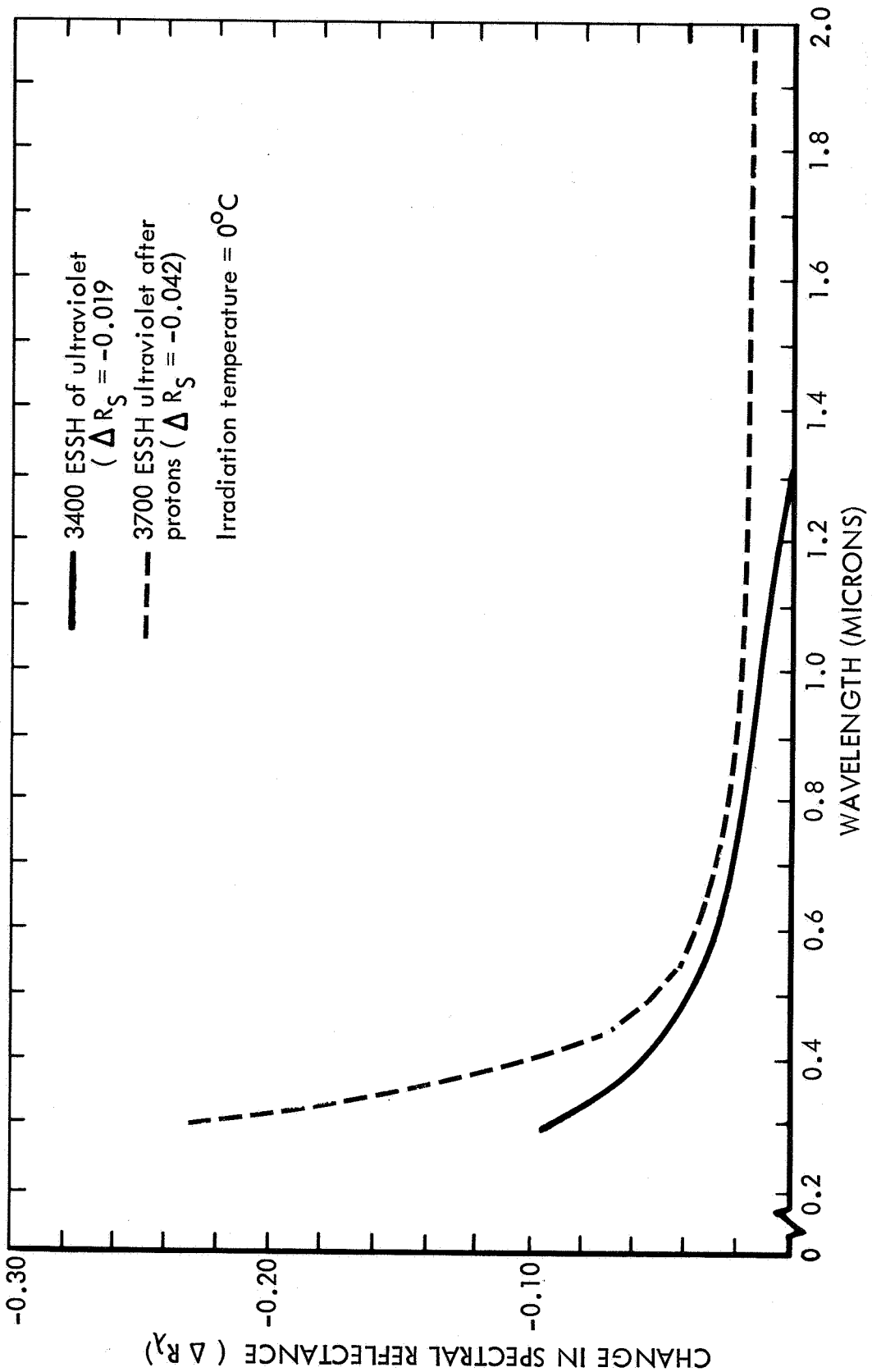


Figure 33: EFFECT OF PROTON IRRADIATION ON ULTRAVIOLET DEGRADATION OF ALUMINUM COATED, NICKEL SUBSTRATE MIRRORS

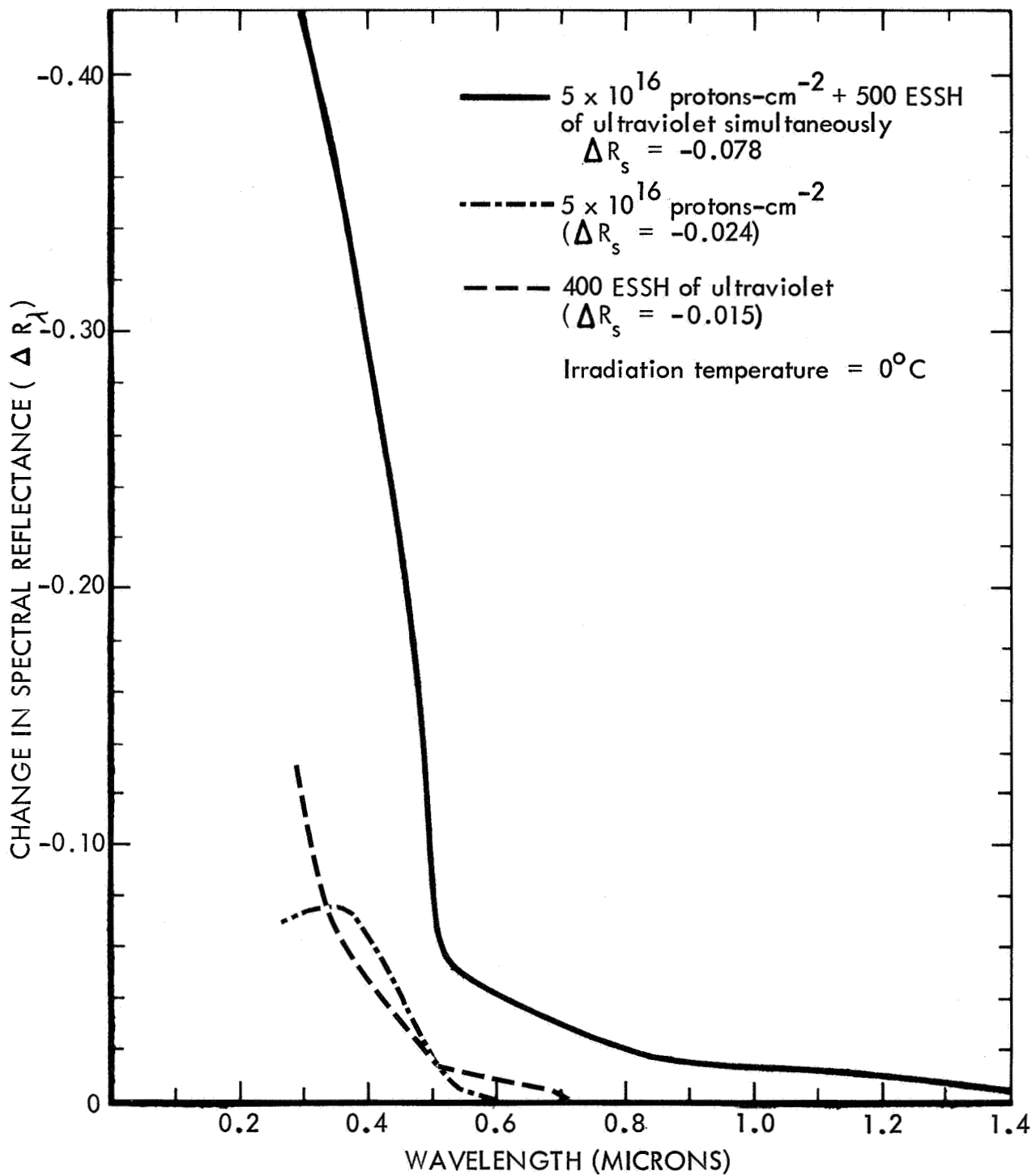


Figure 34: EFFECT OF COMBINED PROTON-ULTRAVIOLET RADIATION ENVIRONMENT ON Si_2O_3 OVERCOATED, NICKEL SUBSTRATE MIRRORS

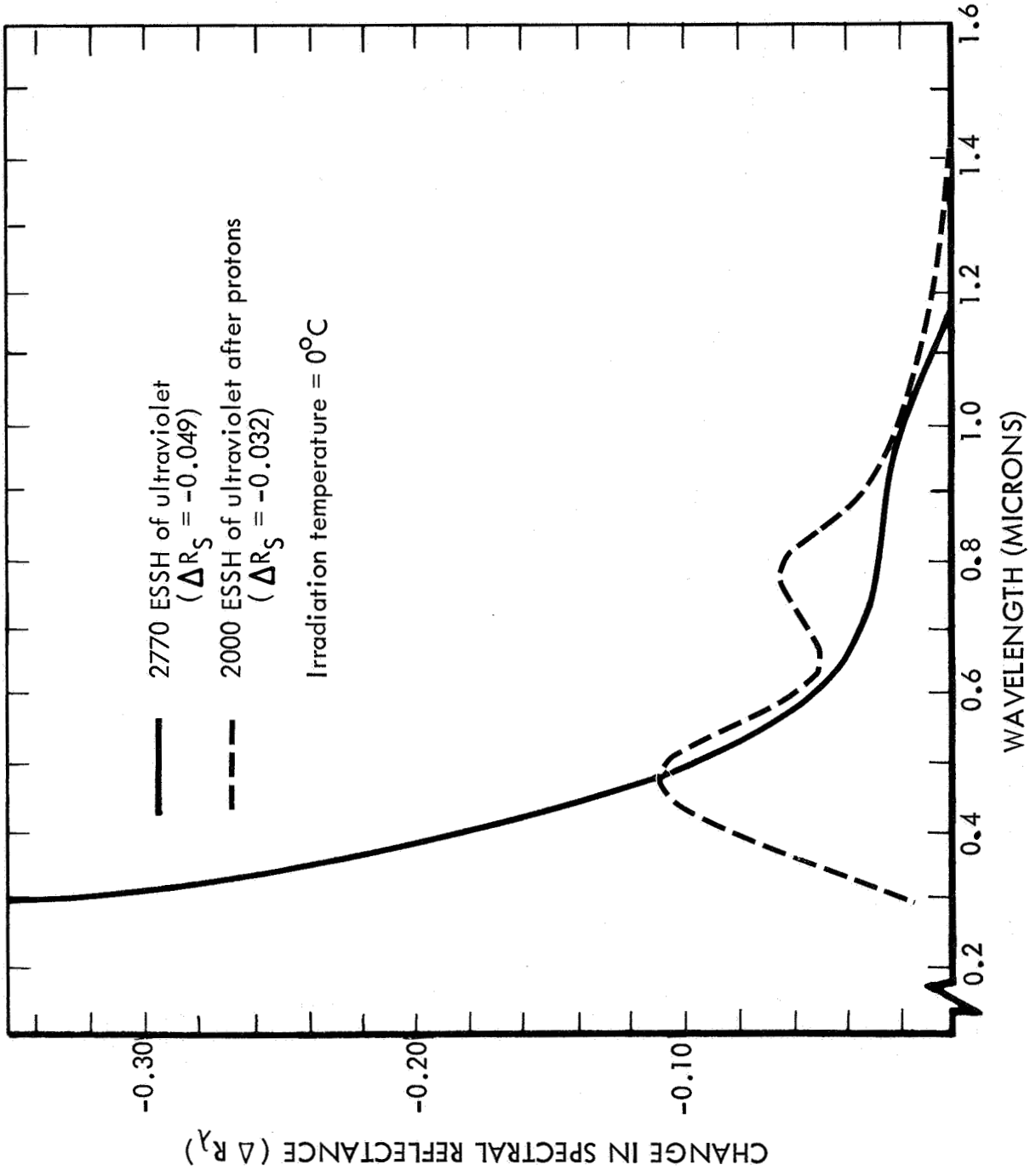


Figure 35: EFFECT OF PROTON IRRADIATION ON ULTRAVIOLET DEGRADATION OF Si_2O_3 OVERCOATED, NICKEL SUBSTRATE MIRRORS

It was concluded for the oxide-coated mirror that a complicated synergistic effect may have occurred, although more tests should be conducted to verify the results.

The effect of prior irradiation with protons on the ultraviolet-induced degradation of oxide-overcoated mirrors is shown in Figure 35. As noted from the curves, the mirror sample which had been pre-irradiated with protons showed less degradation. Changes in solar specular reflectances for the pre-proton irradiated and ultraviolet-only curves were $\Delta R_s = -0.032$ and -0.049 , respectively. In contrast to results obtained on aluminum surfaces, the silicon-oxide films exhibited a double-peak absorption spectra for the mirror sample which had been pre-irradiated with protons. This is indicative of color center formation.

A general review of the data from the synergistic-effects tests indicates that synergistic radiation effects probably occurred, but that additional experiments need to be conducted before definite conclusions can be made. In future experiments of this type it is recommended that: (1) more than one identical sample be exposed at each test condition; (2) higher radiation doses be used to provide larger reflectance changes for analysis; and (3) all tests should be run in the same vacuum system to eliminate the possibility of contamination occurring in one of the systems.

6.2.5 Electron Radiation Effects---Electroformed nickel mirrors with overcoatings of Si_2O_3 (8000 Å) and SiO_2 were irradiated with nominal integrated fluxes of 5×10^{16} , 1×10^{17} , and 2×10^{17} electrons-cm⁻² at 16 keV energy. Mirror temperatures were controlled at 0°C during this experiment. The primary purpose of the electron experiments was to obtain reflectance degradation data which could be compared with data from proton and ultraviolet experiments. It was hoped that equivalence factors could be developed for the three different types of radiation.

A summary of the results of electron radiation experiments is given in Table V. As noted in the table, the Si_2O_3 overcoated mirrors showed more optical degradation than SiO_2 overcoated mirrors. A slight increase in reflectance was obtained with SiO_2 overcoatings as was encountered in proton experiments. In general, the degradation in reflectance produced by any type of radiation in these coatings was too small to permit the calculation of equivalence factors.

TABLE V. SUMMARY OF ELECTRON IRRADIATION DATA

Sample No.	Integrated Flux (electrons-cm ⁻²)	Solar Specular Reflectance		Change in Reflectance, ΔR _S
		Before	After	
E8	4.6 x 10 ¹⁶	0.776	0.782	0.006
E9	9.8 x 10 ¹⁶	0.781	0.765	-0.016
E16	1.8 x 10 ¹⁷	0.807	0.768	-0.039
F20	5.1 x 10 ¹⁶	0.764	0.776	0.012
F15	9.7 x 10 ¹⁶	0.762	0.759	-0.003
F16	2.0 x 10 ¹⁷	0.760	0.769	0.009

The effect of electrons on the spectral reflectance of Si₂O₃ and SiO₂ coatings was a small shift in wavelength to shorter values of interference maxima and minima. The shift of the interference peaks was indicative of either a decrease in oxide film thickness or refractive index. A slight increase in absorption was noted in the data for the Si₂O₃ overcoated mirrors in the wavelength region less than 0.5 micron. The SiO₂ overcoated mirror did not show a similar increase in absorption, thus indicating its greater stability.

6.3 Stretch-Formed Aluminum Mirrors

Included in this section of the report are typical reflectance data and discussions of results of proton, ultraviolet, and combined proton/ultraviolet radiation experiments on stretch-formed aluminum mirrors. Each of these general items will be discussed in respective order.

6.3.1 Typical Reflectance Data---Typical reflectance data for stretch-formed aluminum mirrors having both bare aluminum and silicon oxide overcoated reflective surfaces are shown in Figure 36. As noted in the figure, the Si_2O_3 overcoating causes a significant reduction in reflectance. Average solar specular reflectances of the bare and protected aluminum surfaces were $R_s = 0.890$ and 0.865 , respectively.

6.3.2 Proton Radiation Effects---In the proton radiation studies the effects of angle of incidence, energy, integrated flux and mirror temperature were investigated. These various items are discussed below in respective order. A general summary of proton test conditions was given in Table II and a detailed tabulation of proton test data is given in Appendix C.

Angle of Incidence Experiment:

In the angle-of-incidence experiment mirror samples were irradiated at angles of 0, 30 and 60 degrees from normal, an integrated flux of 1×10^{17} protons- cm^{-2} (16 keV), and a temperature of 0°C . A significant angle-of-incidence effect was observed on samples having bare aluminum coatings as shown in Figure 37. It was found that the degradation in reflectance became progressively larger as the angle of incidence from normal was increased. Solar specular reflectance (R_s) values shown in the figure for the various curves ranged from $R_s = 0.876$, for a sample irradiated normally, to $R_s = 0.828$ for the 60-degree case. It is interesting to note that the change in specular reflectance is much larger than the change in diffuse reflectance at any given wavelength. The fact that the two values of change are not equivalent indicates an increase in absorption on the reflective surface.

An electron microscope examination of the surfaces revealed that the primary cause of reflectance changes from the proton irradiation was blister formation. A series of photomicrographs of the reflective surfaces represented in Figure 37 is shown in Figures 38, 39, 40 and 41. The technique used to prepare the photomicrographs was described earlier in the report. An analysis of blister sizes was performed on the photomicrographs to determine the change in size distribution as the angle of incidence was varied. A plot showing the effect of irradiation angle of incidence on the size distribution is shown in Figure 42. Note that the ordinate represents the integral number of blisters, $N(>D)$. Two significant

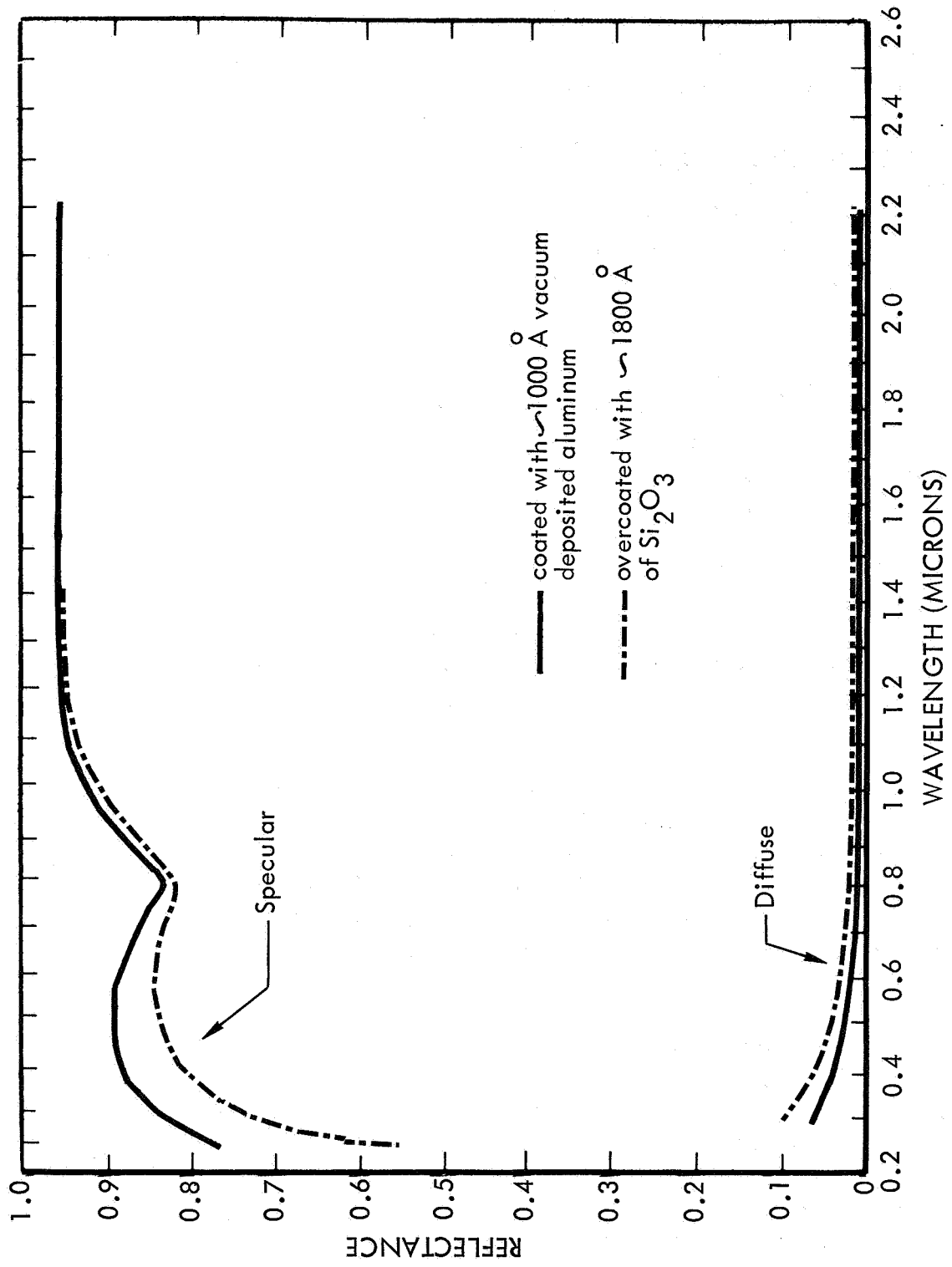


Figure 36: SPECTRAL REFLECTANCE OF TYPICAL STRETCH-FORMED ALUMINUM MIRROR SAMPLES

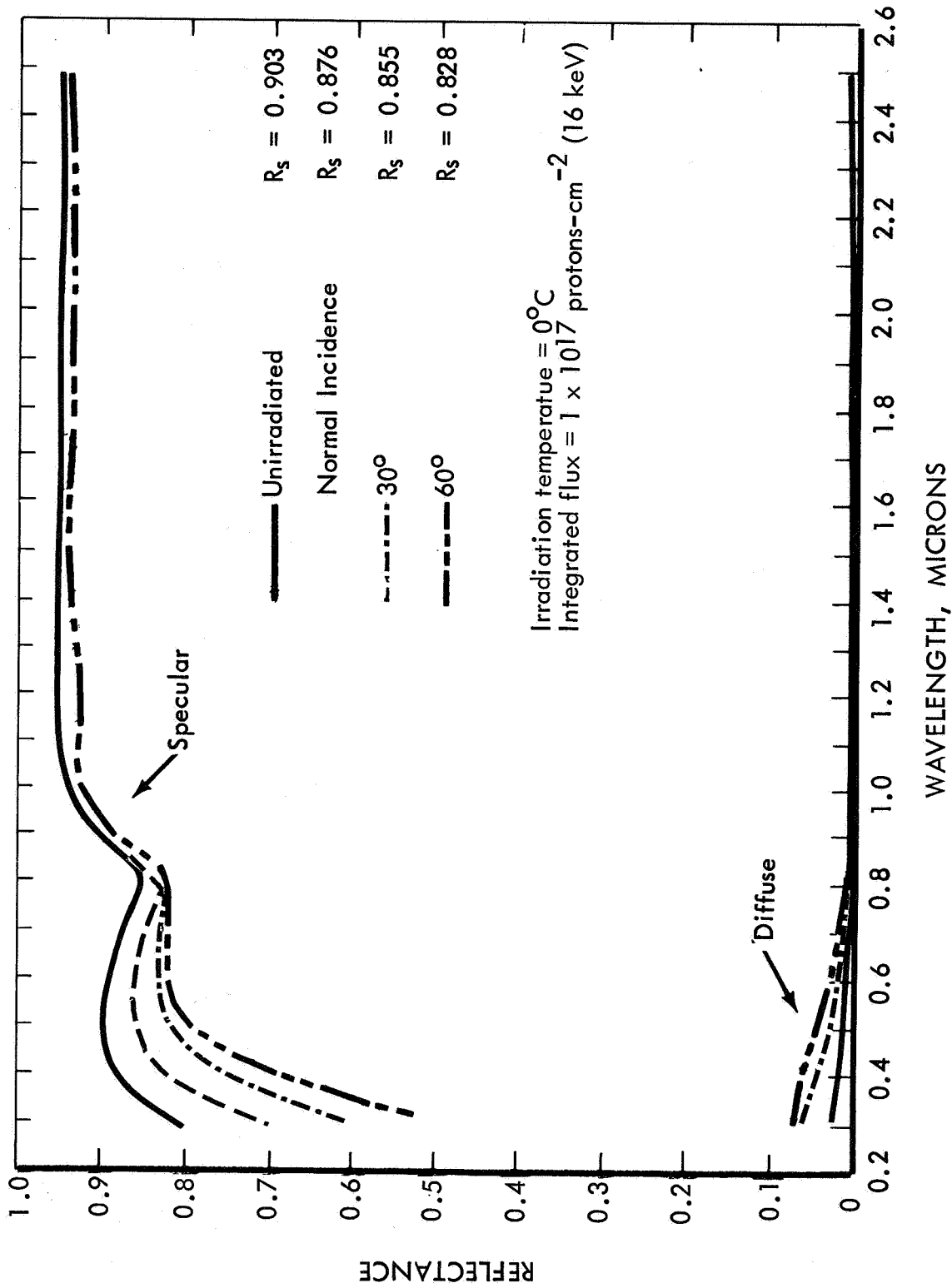


Figure 37: EFFECT OF PROTON ANGLE OF INCIDENCE ON BARE ALUMINUM COATED, ALUMINUM SUBSTRATE MIRRORS

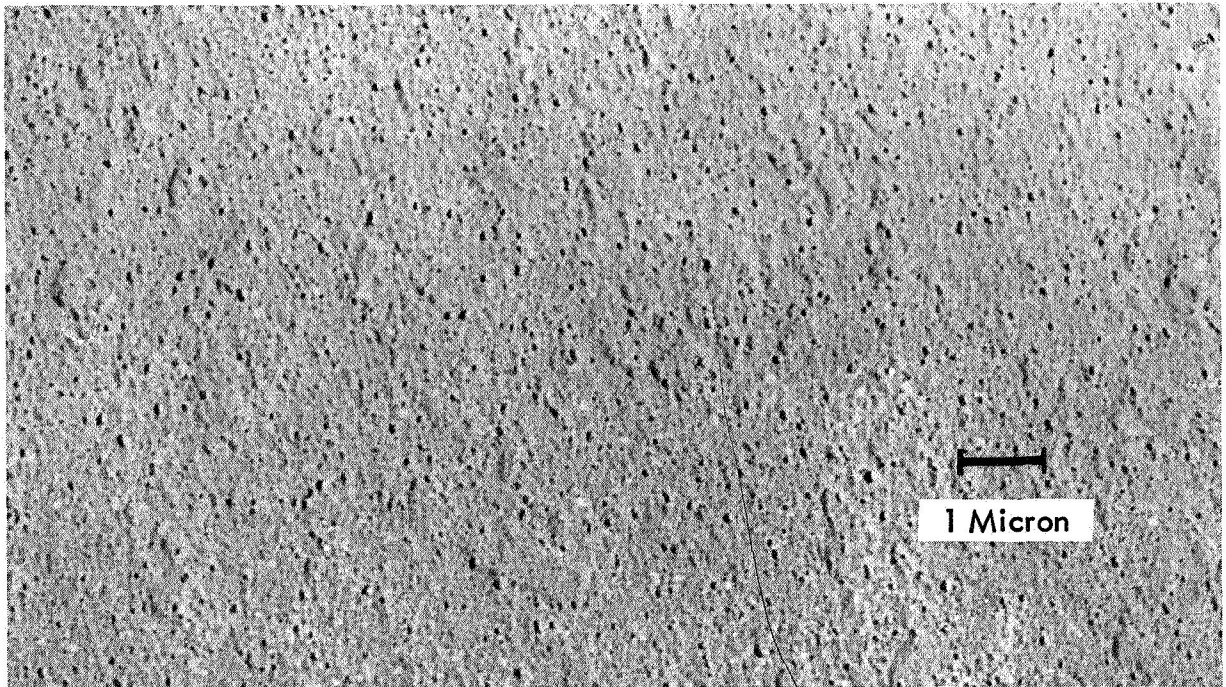


Figure 38: PHOTOMICROGRAPH OF UNIRRADIATED BARE ALUMINUM COATED, ALUMINUM SUBSTRATE MIRROR

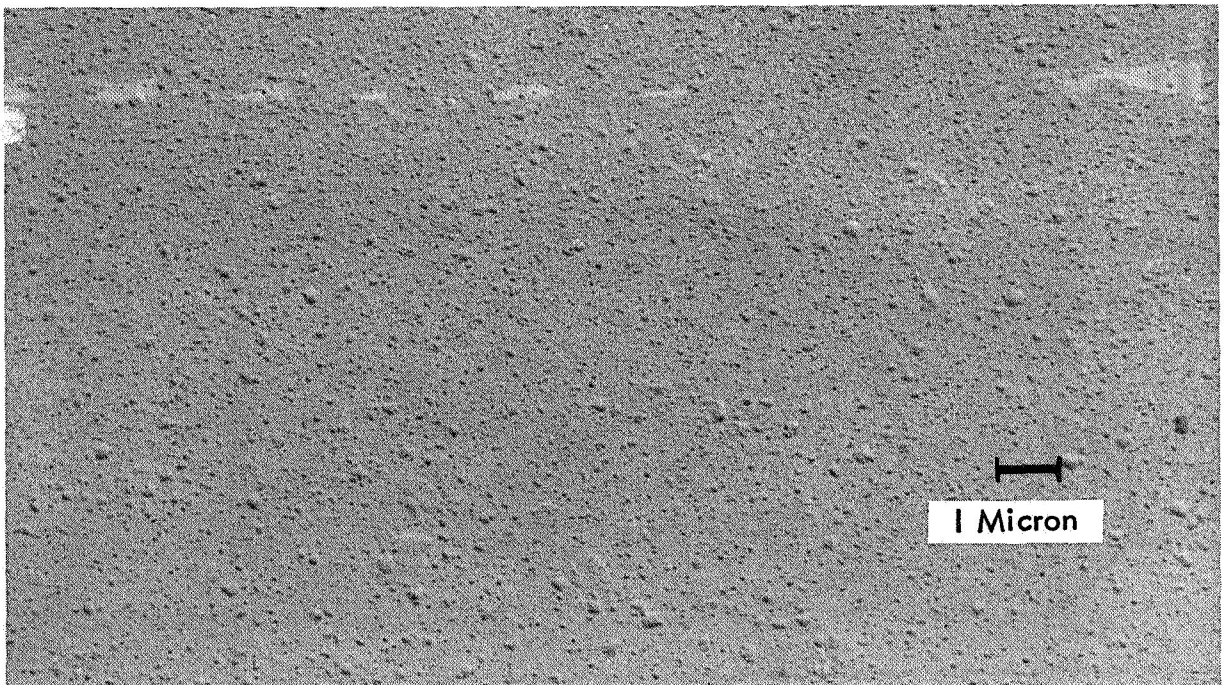


Figure 39: PHOTOMICROGRAPH OF BARE ALUMINUM COATED, ALUMINUM SUBSTRATE MIRROR IRRADIATED AT NORMAL INCIDENCE (1×10^{17} protons-cm⁻², 0° C, 16 keV)

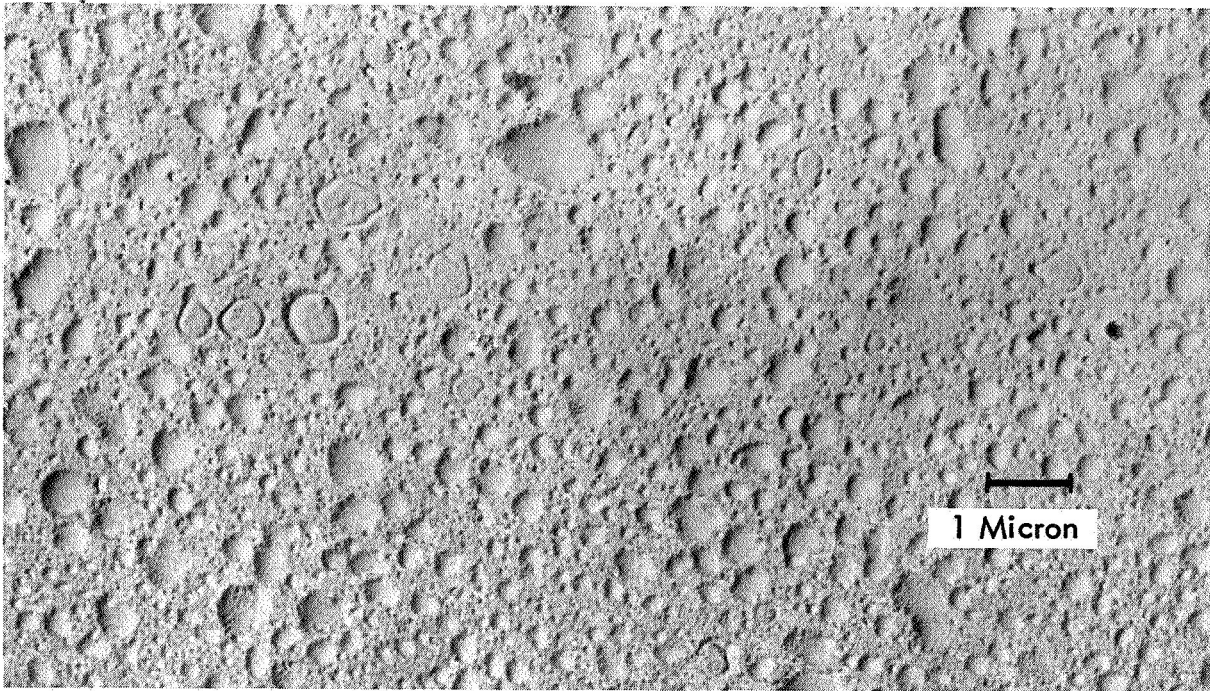


Figure 40: PHOTOMICROGRAPH OF BARE ALUMINUM COATED, ALUMINUM SUBSTRATE MIRROR IRRADIATED AT 30° FROM NORMAL (1×10^{17} protons- cm^{-2} , 0° C, 16 keV)

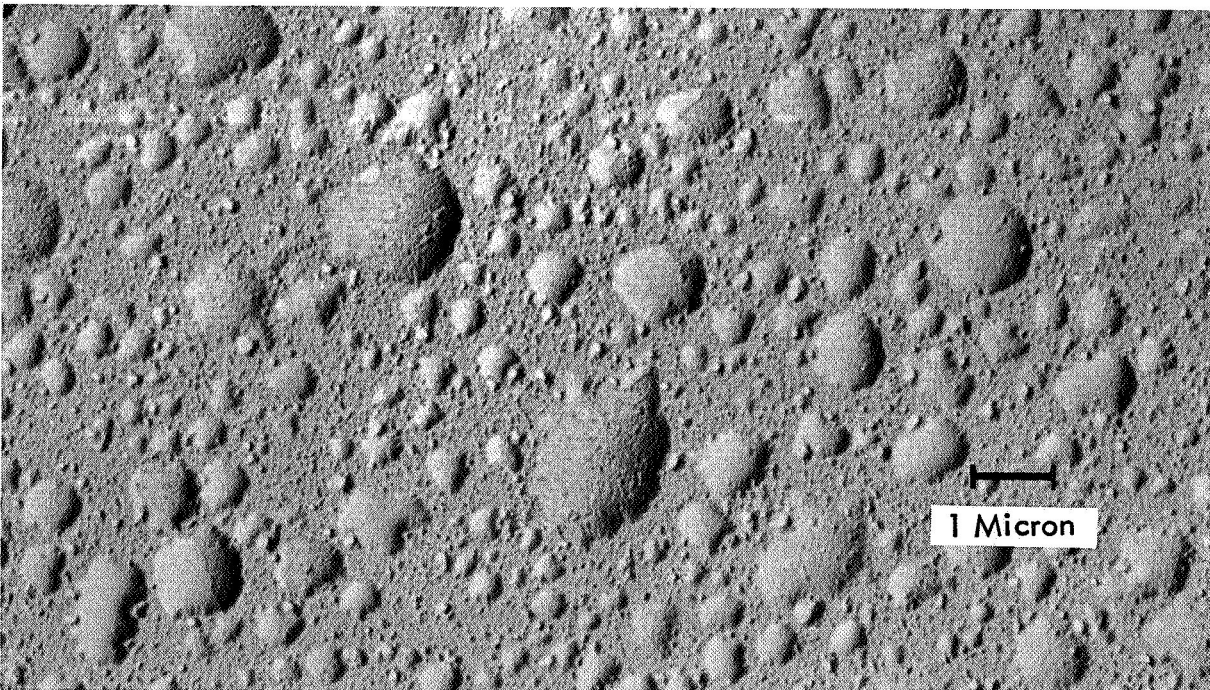


Figure 41: PHOTOMICROGRAPH OF BARE ALUMINUM COATED, ALUMINUM SUBSTRATE MIRROR IRRADIATED AT 60° FROM NORMAL (1×10^{17} protons- cm^{-2} , 0° C, 16 keV)

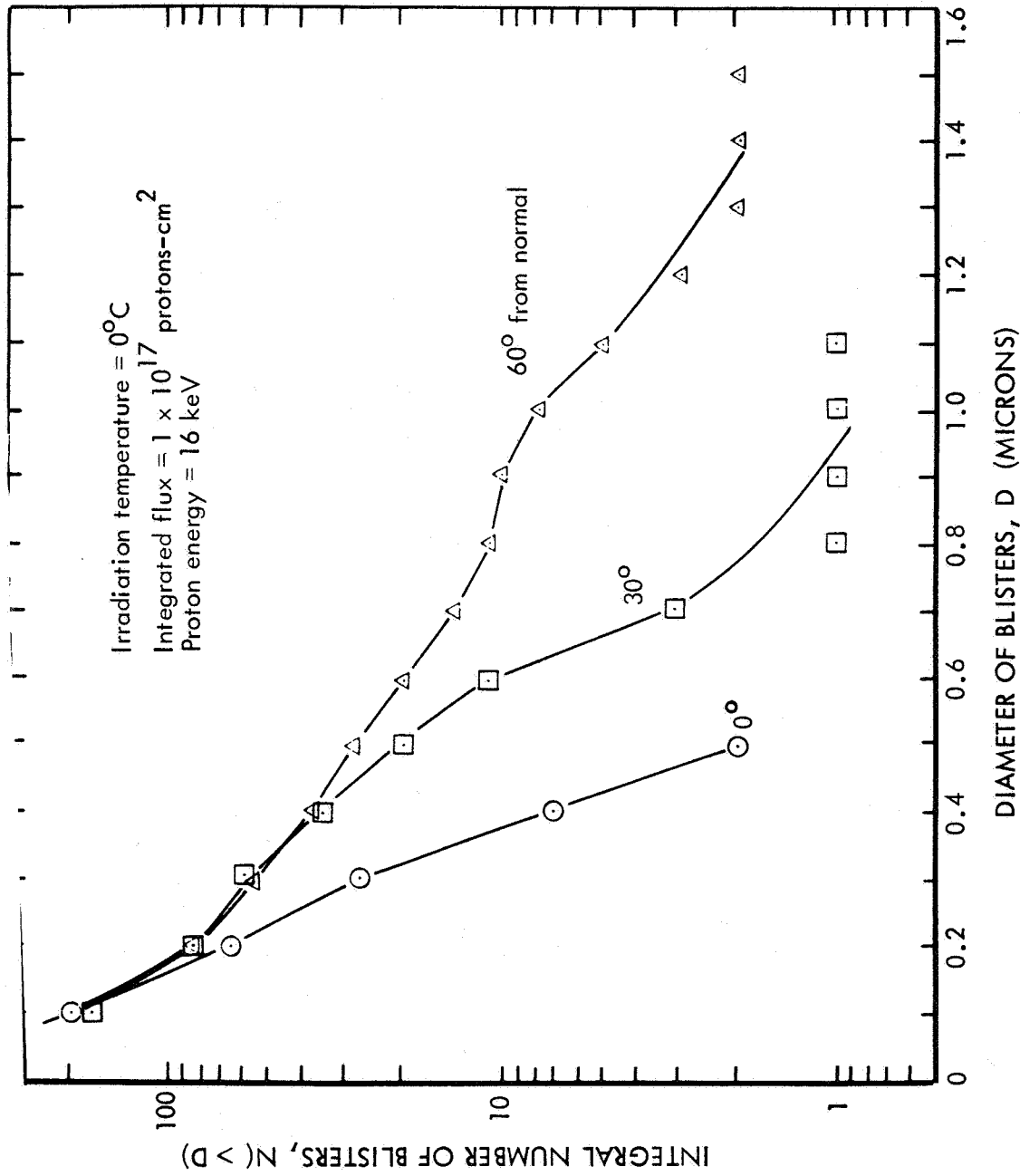


Figure 42: EFFECT OF PROTON ANGLE OF INCIDENCE ON BLISTER SIZE DISTRIBUTION ON BARE ALUMINUM COATED, ALUMINUM SUBSTRATE MIRRORS

observations can be made from the data: (1) the total number of blisters within a given area remained about constant for all three angles of incidence (~ 180); and (2) the size distribution changed from predominantly small blisters (less than 0.5 micron diameter) to a mixture of small and large blisters which vary up to about 2 microns in diameter.

The formation of blisters on metallic surfaces has been attributed to the agglomeration of hydrogen gas at lattice imperfections, grain boundaries, and vacuum-deposited film interfaces (References 12, 21, 22, and 26). Anderson (Reference 26) has noted that the size and density (number/cm²) of blisters observed on gold-coated aluminum are a function of the gold-film thickness. Other known variables in the blistering process are the substrate and film material, the rate of bombardment, and the incident-ion energy and species. In addition, as will be discussed later, it was discovered in this program that the blistering is highly temperature dependent.

It has been observed in this program that the blister formation represents a separation of the vacuum-deposited films. Irradiation of samples at 50°C produced large blisters that ruptured, thus revealing the underlying silicon monoxide film. Assuming that all blisters formed at this depth, it is of interest to correlate the variation in blister size and density at various angles of incidence to the theoretical mean penetration depth* of protons in the material. For purposes of this discussion the mean penetration depth was found to be about 3000 Å in quartz (see Sec. 6.5.3 of this report). Considering the uncertainties in both theory and experiments and the similar stopping power for aluminum, silicon oxide (Si₂O₃), and quartz, the same value will be assumed for all three coatings. A schematic cross section of a typical bare aluminum coated, aluminum substrate mirror indicating the range of 16 keV protons is shown in Figure 43. The two extreme cases, 0- and 60-degree incident angles, are shown. If the assumption is made that the stopped protons or hydrogen atoms are scattered uniformly throughout the depth of the path length, it can be shown by calculation that the density of hydrogen atoms in the material is the same for both the 0- and 60-degree cases. Thus, the density of hydrogen atoms in the vicinity of the aluminum/SiO interface is the same for both cases, and no difference in the character of the blisters should occur. Since the electron photomicrographs showed a significant difference between the two cases, it is apparent that the assumption of uniform distribution of hydrogen atoms is not valid. A better assumption to make based on energy dependence experiments, theoretical considerations for proton diffusion or scatter in the material as discussed later and data from Reference 27, is that the majority of the protons stop near the predicted mean penetration depth. Thus, as the plane at the mean penetration depth moves toward the aluminum/SiO interface, due to an increase in the angle of incidence, blistering becomes more severe.

*The "mean penetration depth" is defined as the depth at which the number of incident particles has been reduced to 50 percent.

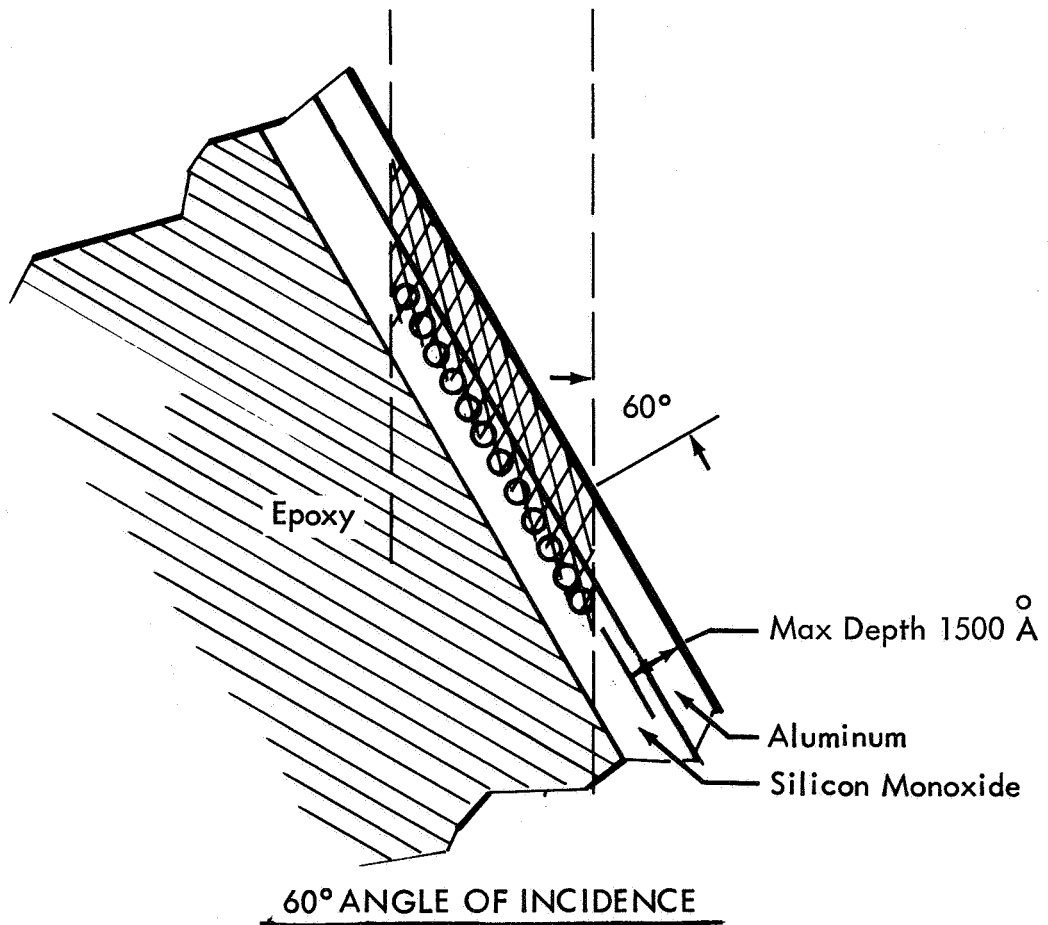
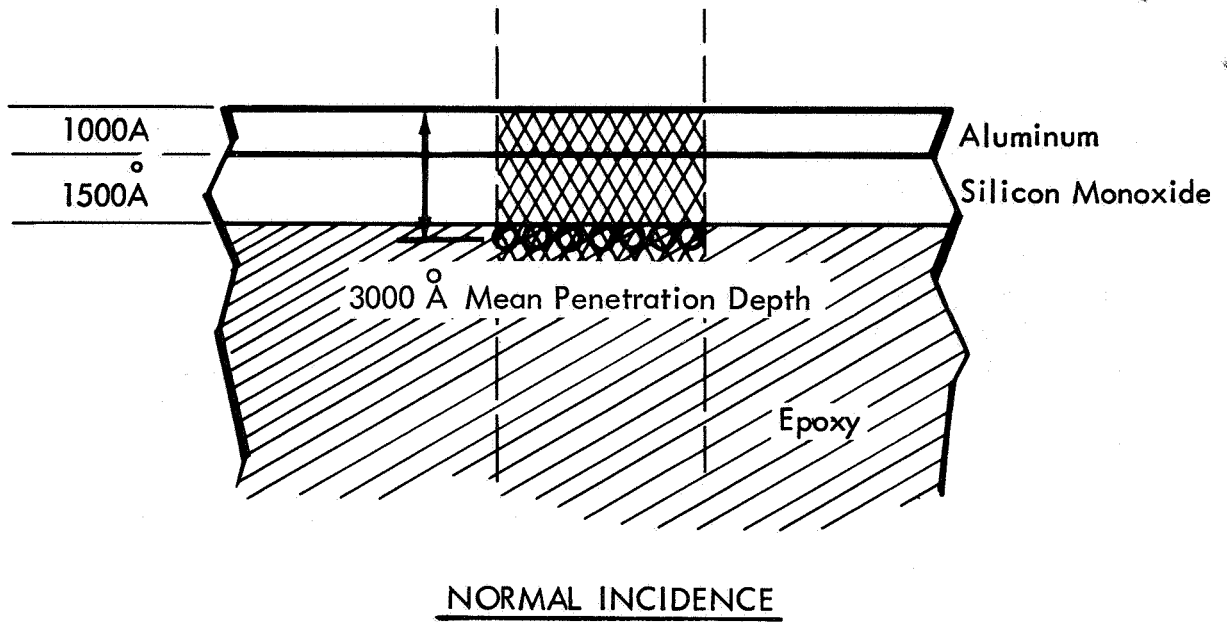


Figure 43: PROTON PENETRATION IN A BARE ALUMINUM COATED, ALUMINUM SUBSTRATE MIRROR

It was concluded from the above observations that there is a significant angle-of-incidence effect when blistering occurs. In general, the variation in blistering with angle of incidence is believed to be due to the non-uniformity of particle deposition in the material and hydrogen agglomeration at a given vacuum-deposited film interface. Similar effects have been obtained in the energy dependence experiments as will be discussed next.

Energy Dependence Experiment:

An energy dependence study was made early in the program wherein energies of 2, 4, 8, and 16 keV were evaluated. However, since integrated flux values in the range of 1×10^{15} to 5×10^{16} protons-cm⁻² were used in this study, no significant degradation occurred. Later in the program when the angle-of-incidence blistering effect was discovered it was decided to re-run a few energy dependence tests on bare aluminum surfaces at an integrated flux level of 1×10^{17} protons-cm⁻² (0°C). The primary purposes of this later experiment were to determine whether the results obtained by varying the angle of incidence could be duplicated by varying the proton energy, and to obtain quantitative data on blister sizes, heights, and densities. It was theorized that if the blisters were all occurring at the aluminum/SiO interface, then there should be an optimum energy for producing blisters. In other words, the energy which deposits the maximum number of protons near the sensitive interface would be optimum. Energies above or below this should produce a lower density of smaller blisters or no blisters.

Energies of 4, 6.4, 13.3, 21.3 and 27 keV were used in addition to the prior data obtained using 16 keV protons. These energies were chosen to obtain maximum penetration depths of 1230, 1700, 2700, 3540, and 4000 Å, respectively, in the vacuum deposited films.

It was anticipated that the blistering produced with protons having a mean penetration depth of about 1500 Å should be comparable to results obtained with 16 keV protons at a 60-degree angle of incidence. The effects of varying proton energy on the spectral, specular and diffuse reflectances are shown in Figure 44. As noted in the figure, maximum degradation was obtained with the 6.4 keV protons which have a mean penetration range of about 1700 Å. Comparing data in Figure 44 for the 6.4 keV protons to that given in Figure 37 for the 60-degree angle of incidence case, it can be seen that the spectral degradation in specular reflectance is roughly comparable. Data for the mirror sample irradiated with 13.3 keV protons are not shown in Figure 44 because it was suspected that erroneous reflectance values had been obtained.

Photomicrographs made of the irradiated surfaces are shown in Figures 45, 46, 47, 48 and 49. Several significant observations can be made from the series of photomicrographs: (1) the surface irradiated with 13.3 keV protons exhibited comparable blistering to the 6.4 keV sample and thus it probably would have shown

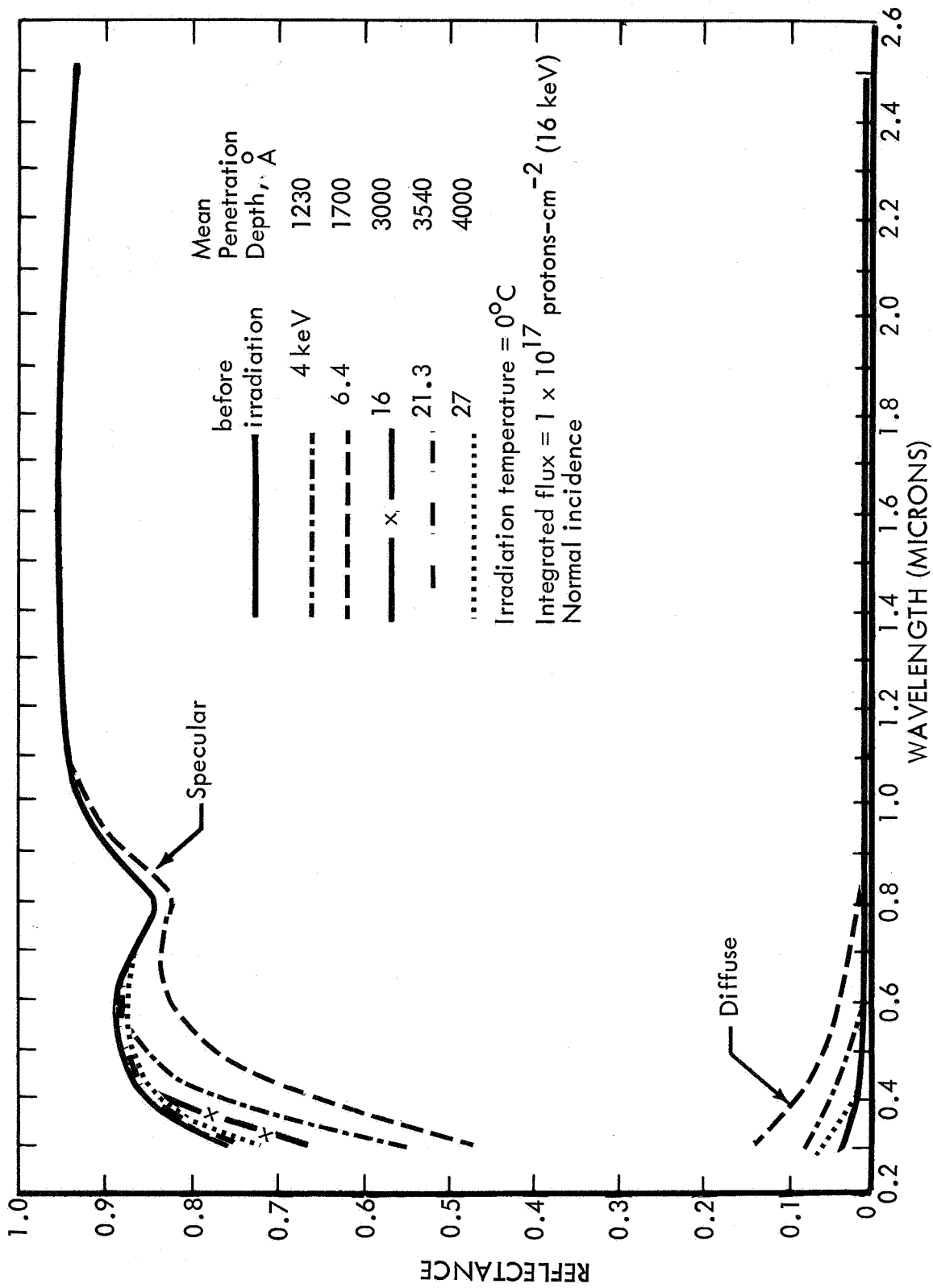


Figure 44: EFFECT OF PROTON ENERGY ON BLISTER FORMATION IN BARE ALUMINUM COATED, ALUMINUM SUBSTRATE MIRRORS

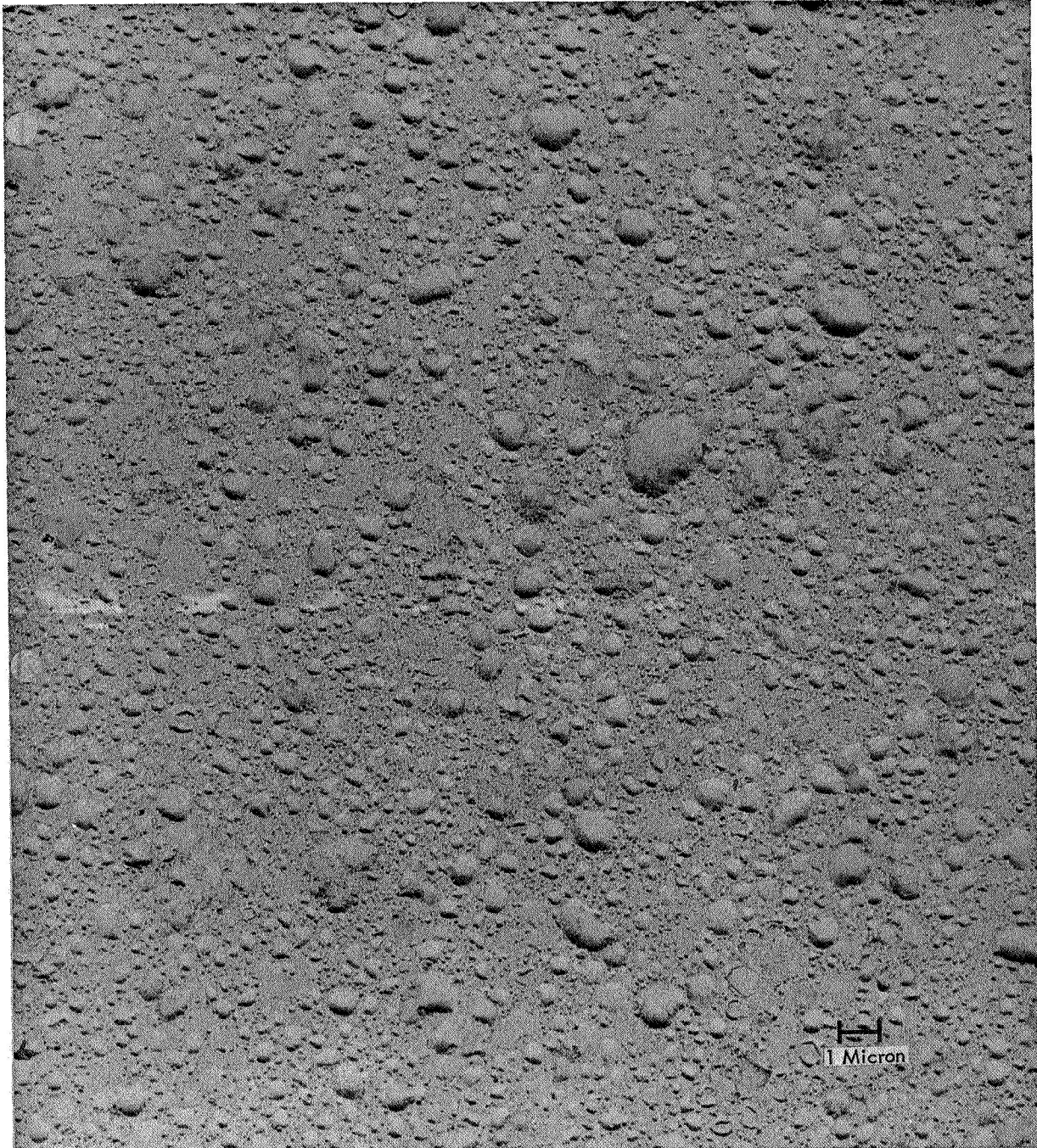


Figure 45: PHOTOMICROGRAPH OF BARE ALUMINUM COATED, ALUMINUM SUBSTRATE MIRROR IRRADIATED WITH 4 keV PROTONS, (1×10^{17} protons- cm^{-2})

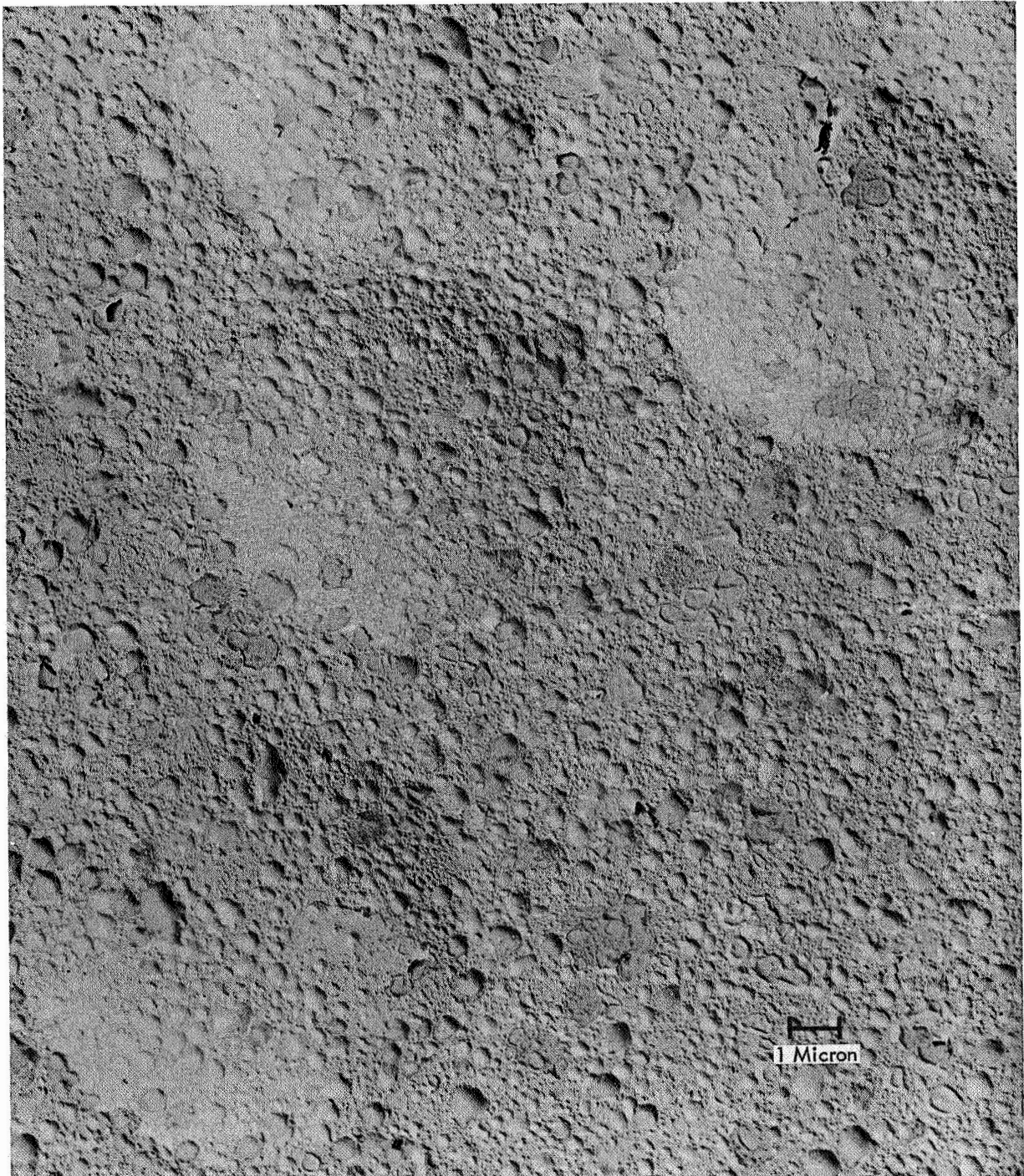


Figure 46: PHOTOMICROGRAPH OF BARE ALUMINUM COATED, ALUMINUM SUBSTRATE MIRROR IRRADIATED WITH 6.4 keV PROTONS (1×10^{17} protons - cm^{-2})

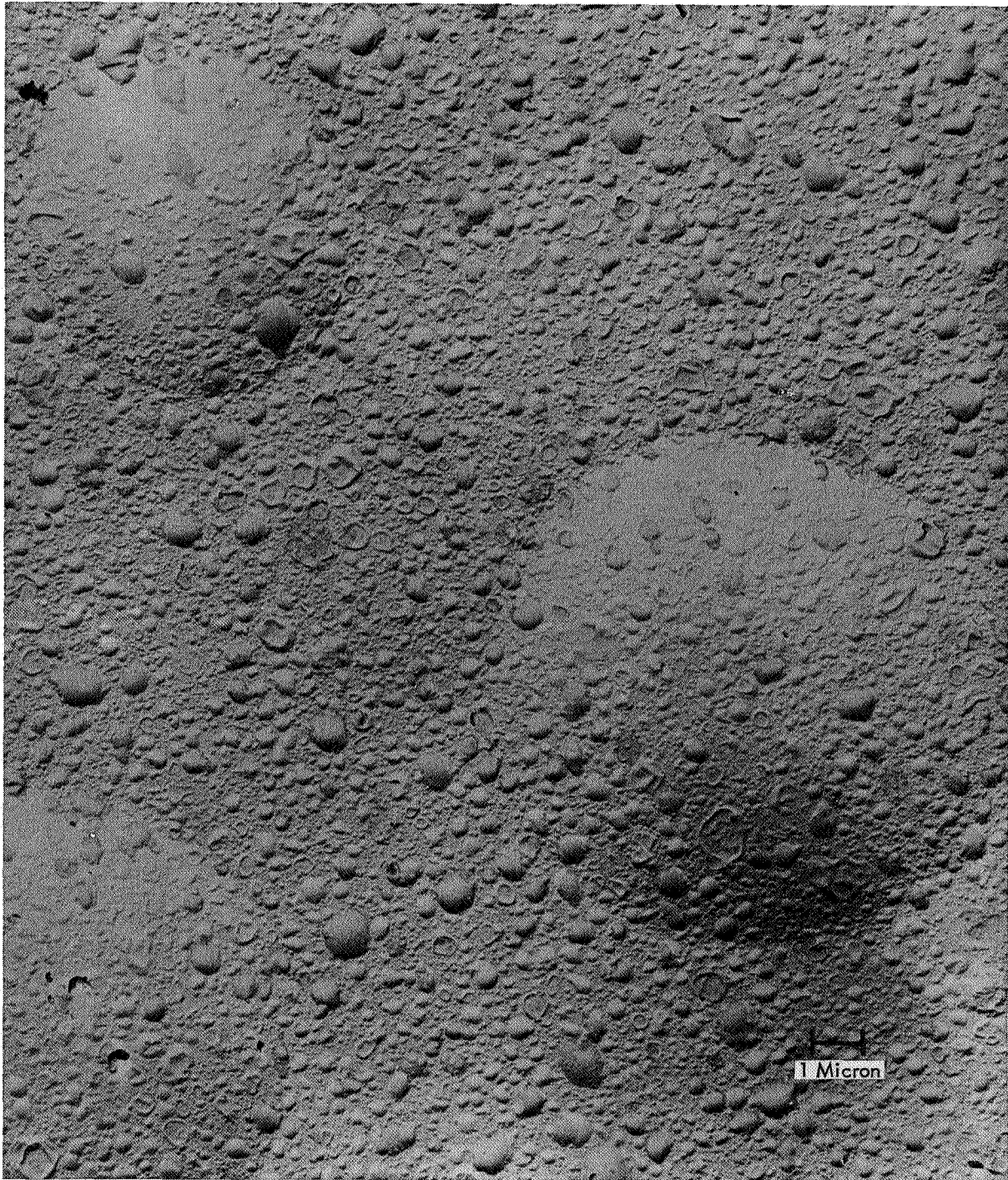


Figure 47: **PHOTOMICROGRAPH OF BARE ALUMINUM COATED, ALUMINUM SUBSTRATE MIRROR IRRADIATED WITH 13.3 keV PROTONS (1×10^{17} protons - cm^{-2})**

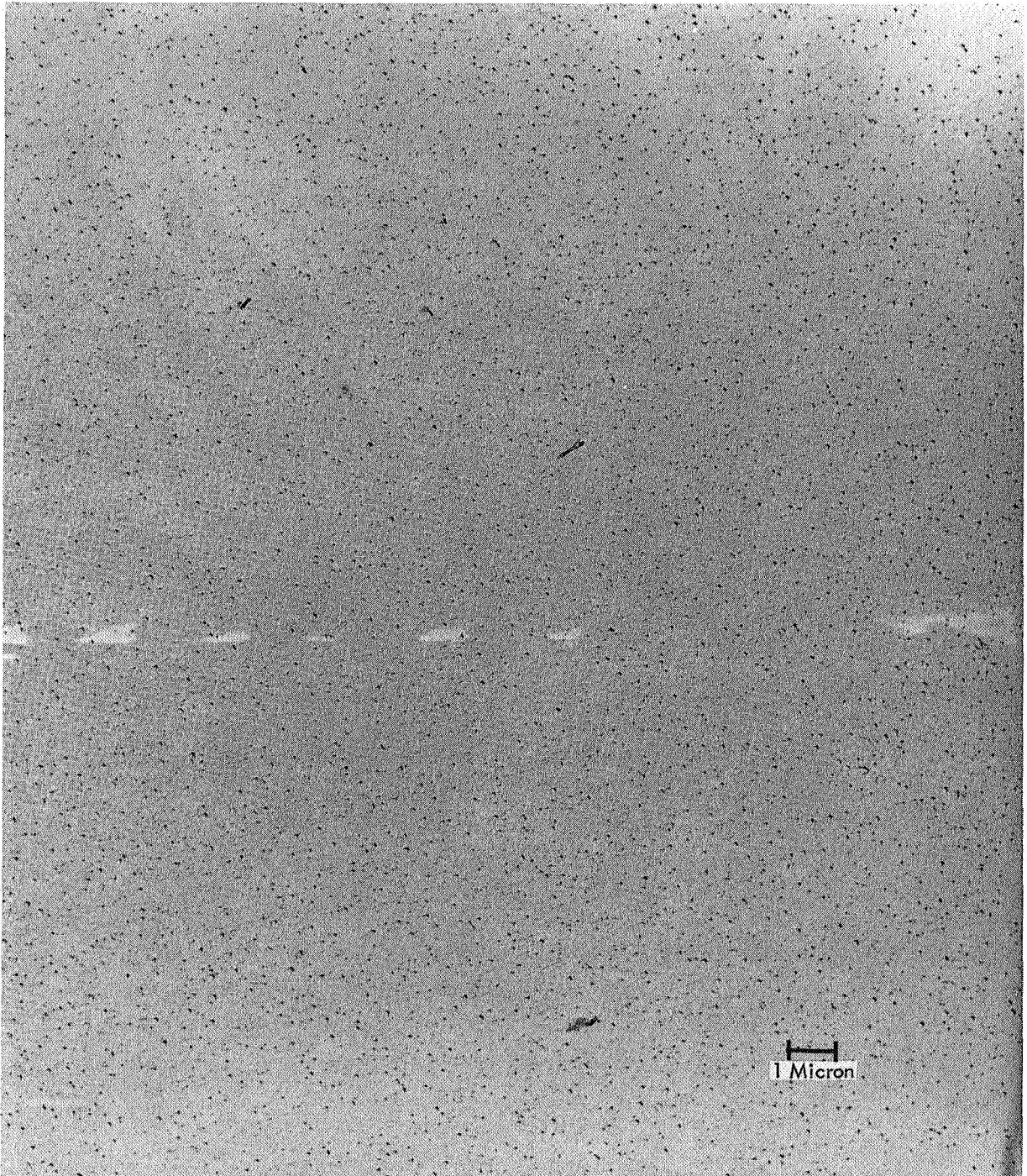


Figure 48: PHOTOMICROGRAPH OF BARE ALUMINUM COATED, ALUMINUM SUBSTRATE MIRROR IRRADIATED WITH 21.3 keV PROTONS (1×10^{17} protons cm^{-2})

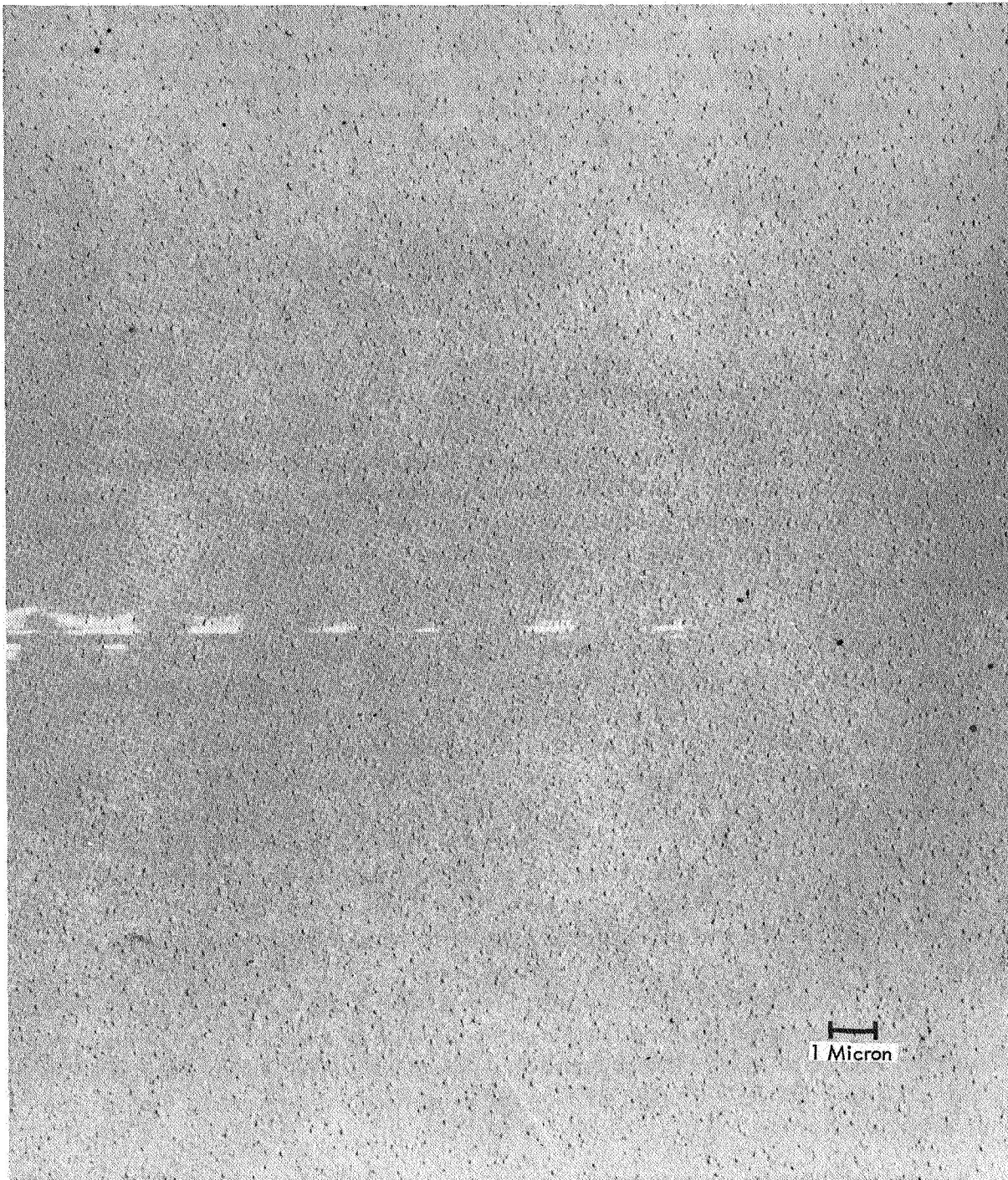


Figure 49: PHOTOMICROGRAPH OF BARE ALUMINUM COATED, ALUMINUM SUBSTRATE MIRROR IRRADIATED WITH 27 keV PROTONS (1×10^{17} protons - cm^{-2})

a similar change in reflectance; (2) the mirror samples irradiated with 6.4 and 13.3 keV protons have two distinctly different size groups of blisters; and (3) energies in excess of about 20 keV produce only small blisters which appear to be in a size class of their own. The distinctly different size classes of blisters suggests that agglomeration may be occurring at the aluminum /SiO interface, the SiO/epoxy interface, and in the bulk of the coatings. Since insufficient time was available prior to completion of the contract, interferometric blister-height and size distribution measurements could not be performed. It is recommended that additional work be performed to correlate the blister size distributions and height-to-diameter ratios to proton energies and agglomeration sites.

Integrated Flux and Mirror Temperature Experiments:

In the study to determine the effects of proton integrated flux and mirror temperature on the optical degradation of stretch-formed aluminum mirrors, integrated flux levels of from 1×10^{15} to 2×10^{17} protons-cm⁻² and temperatures of -195°, 0°, and 50°C were evaluated. This selection of temperatures was made based on results of temperature-only tests on the epoxy-coated aluminum substrates. These tests showed that severe reticulation of the reflective surface occurred at temperatures in excess of 80°C. Since it was desired to study radiation-induced effects, temperatures below the 80°C threshold were used. Similar to the other experiments, a particle energy of 16 keV and a flux of about 1×10^{13} protons-cm⁻² sec⁻¹ were used. Data will be presented in respective order for the bare aluminum and Si₂O₃ overcoated mirrors.

The effects of integrated flux and mirror temperature on the change in solar specular reflectance are shown in Figure 50. As noted in the figure, a large dependence of proton-induced optical damage on temperature was found for the aluminum substrates with bare aluminum reflective surfaces. Surprisingly, temperatures of -195° and 50°C both produced much more damage than 0°C. The mechanism of degradation was blister formation as discussed earlier. A temperature of 50°C produced severe spallation of the aluminum film during irradiation. Visual observations during irradiation of samples at 50°C indicated that the threshold of spallation was at an integrated flux of about 7×10^{16} protons-cm⁻². The appearance of small blisters, as noted by the diffuseness of the surface, was at an integrated flux that was only several percent lower. Thus, a very sharp threshold of damage is shown for the 50°C curve in Figure 50. A 50°C sample was measured several hours after irradiation and again after 890 hours to determine whether the blisters continued to form. It was found that the reflectance did not change in that time period; therefore, it is assumed that the blister formation process did not continue after irradiation.

The blisters produced on the 0°C samples formed during the irradiation, but did not cause spallation of the reflective surface. Similar to the 50°C samples, reflectance measurements made after several hours and 1490 hours showed no further blister formation after irradiation.

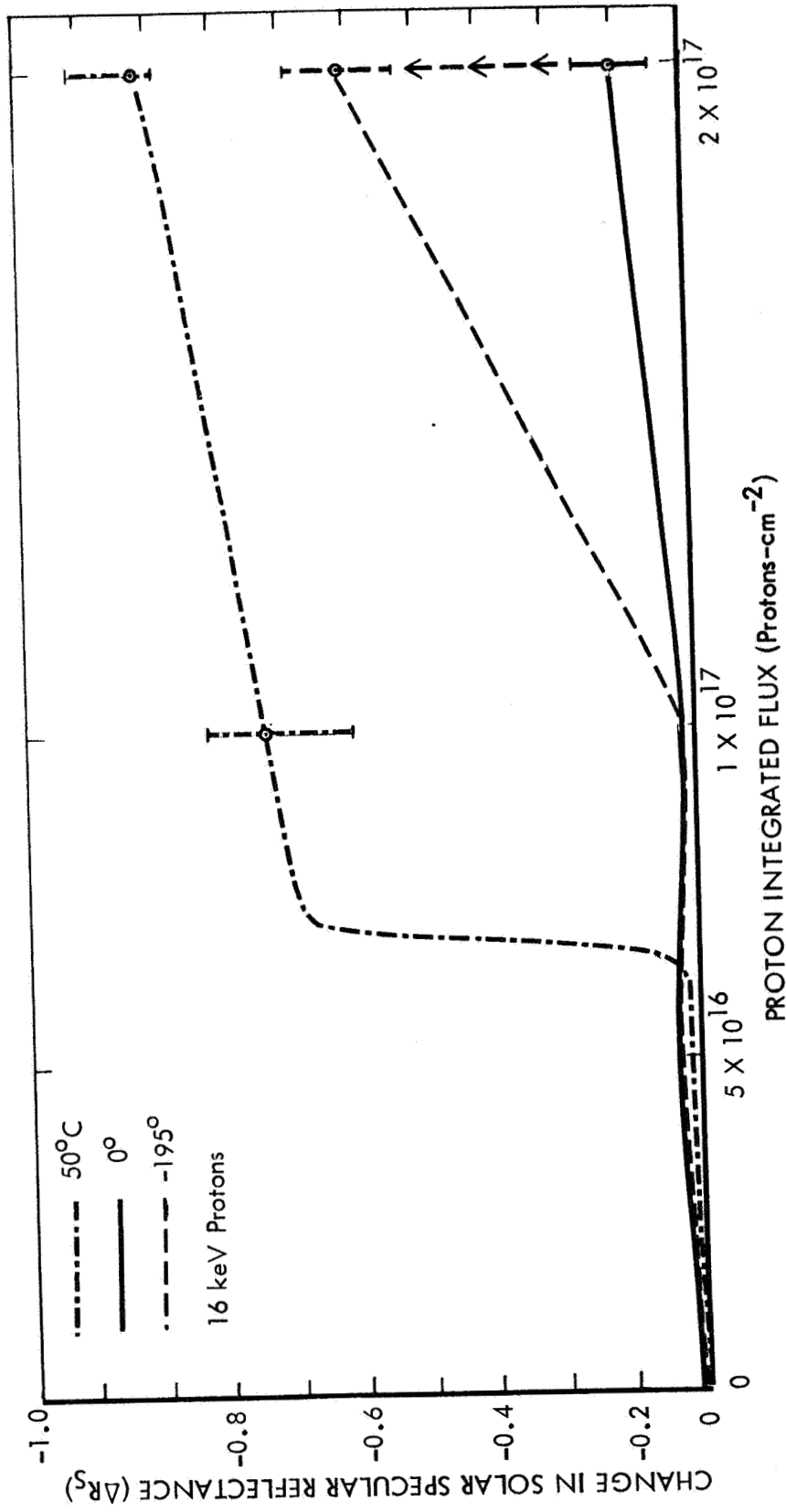


Figure 50: EFFECT OF PROTONS ON SOLAR SPECULAR REFLECTANCE OF BARE ALUMINUM COATED, ALUMINUM SUBSTRATE MIRRORS

It was found that the aluminum coatings that were irradiated at -195°C did not blister during irradiation. However, blistering as evidenced by diffuseness of the reflective surfaces began to occur within an hour after irradiation. Mirror samples were returned to ambient pressure and temperature immediately after irradiation. Reflectance measurements performed on mirrors of this type after several hours and 600 hours showed a significant change in ΔR_s as noted by the data point (with arrows) in Figure 50. A 1200-hour time check on two mirrors which were irradiated at -195°C and 5×10^{16} protons- cm^{-2} showed that their reflectances had decreased slightly (1 to 2 percent). A visual observation of three mirrors which had been exposed to 1×10^{17} protons- cm^{-2} at -195°C revealed that sparse visible blistering had occurred after about 9 to 14 months. It is probable that the reflectance change shown in Figure 50 for -195°C and 1×10^{17} protons- cm^{-2} would be slightly larger if the mirrors had been remeasured near the end of the program.

In regard to the delayed blistering on the cold-irradiated samples, the observed effects may be due to subsequent warming of the mirror sample. In other words, in-situ reflectance measurements would probably show little or no degradation in the same time period. The delayed-blistering phenomenon is probably caused by "freezing" of hydrogen atoms in the lattice during irradiation and their increased mobility when the sample is returned to ambient temperature. The increased mobility allows the hydrogen to diffuse to the interface where agglomeration occurs. The fact that the cold-irradiated surfaces eventually degrade more than the surfaces irradiated at 0°C indicates that less hydrogen escaped from the cold material than the warm material during irradiation. It may be speculated that when the sample temperature is sufficiently high to permit the diffusion of hydrogen during irradiation, the diffusion is aided by thermal spikes produced by the protons. The effect of proton-induced thermal spikes on the diffusion of hydrogen has been discussed by Zeller, et al. (Reference 28).

The phenomena of blistering requires considerable additional investigation to obtain a better understanding of the processes involved. In addition to being dependent on the various parameters mentioned earlier in the discussion on angle-of-incidence effects, it is quite probable that the blistering is also exposure-rate dependent. No proton rate studies were undertaken in this program. Since the space exposure rate is normally 3 to 5 orders of magnitude lower than the laboratory exposure rates, a rate study is highly recommended to determine whether the above data is valid.

The results shown in Figure 51 for silicon-oxide overcoated aluminum-substrate mirrors show comparable reflectance changes at 0° and 50°C where no blistering occurred. Little or no temperature dependence was found for those two temperatures where it is assumed that the decrease in reflectance was due to increased absorption in the silicon-oxide overcoating. A comparison of the results for the 0°C samples between Figures 50 and 51 shows that less damage actually occurred in the silicon-oxide overcoated surfaces because blistering did not occur.

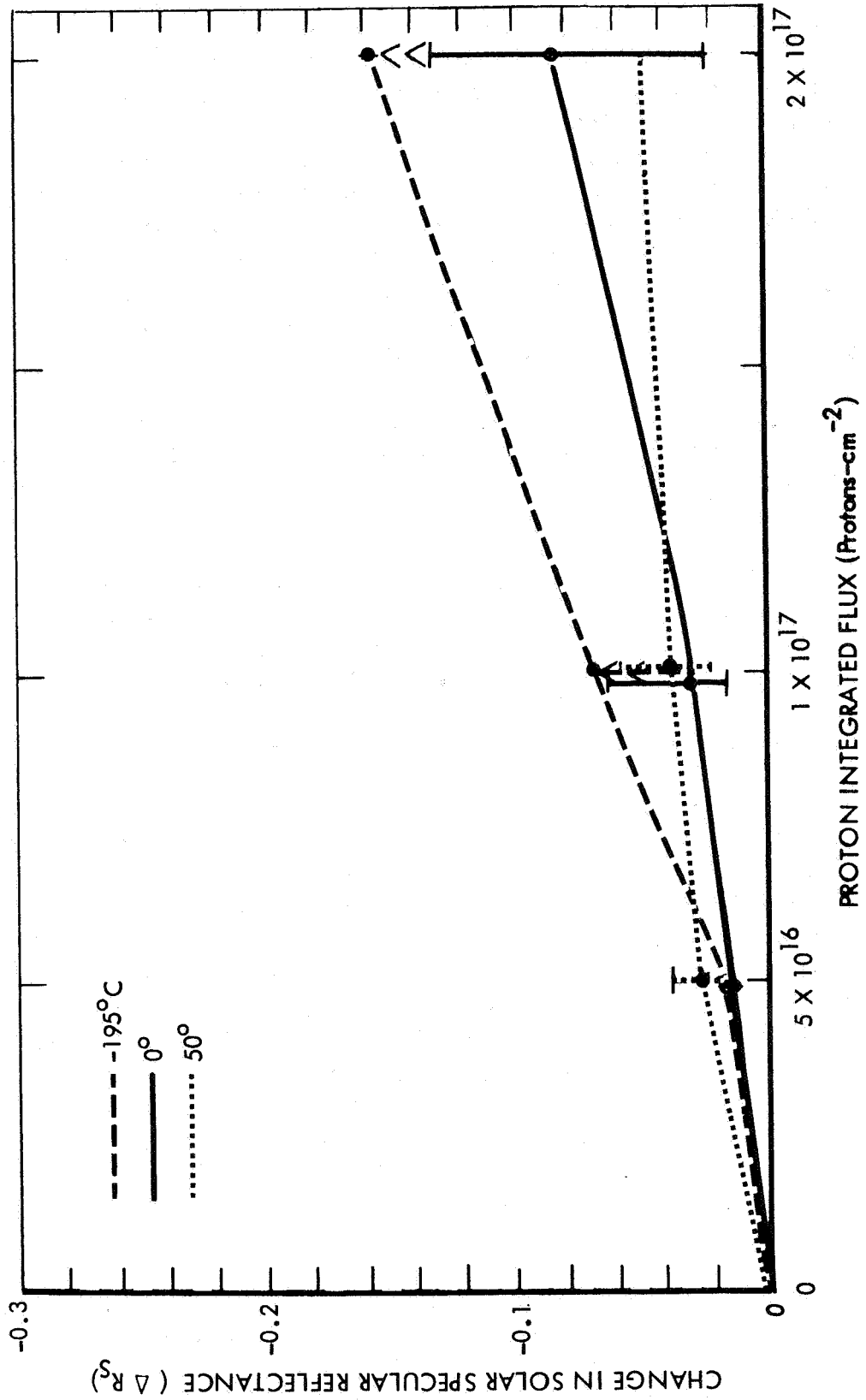


Figure 51: EFFECT OF PROTONS ON SOLAR SPECULAR REFLECTANCE OF SILICON-OXIDE OVERCOATED, ALUMINUM SUBSTRATE MIRRORS

The silicon-oxide overcoated aluminum samples that were irradiated at -195°C changed reflectance with time after irradiation. However, the overall reflectance change was considerably smaller than for the bare aluminum surfaces. The arrows on the data points in Figure 51 indicate the change in ΔR_s with time. Reflectance measurements were performed at various time increments after irradiation on two samples which were irradiated with 1×10^{17} protons- cm^{-2} at -195°C to determine the length of time required for stabilization. It was found that the reflectance continued to decrease on one of the mirrors for about 120 hrs and on the other for about 5700 hrs. Measurements on a mirror which was irradiated with 2×10^{17} protons- cm^{-2} at -195°C indicated a decrease in reflectance during a 1000-hr. time increment after irradiation, but no further changes between 1000 hrs. and 8000 hrs. A reflectance check on a mirror irradiated at 0°C showed no reflectance change with time after irradiation.

In general, the delayed blistering phenomena was noted on both bare aluminum and Si_2O_3 overcoated mirrors which had been irradiated at -195°C . The overall degradation which occurred, however, was considerably larger on the bare aluminum surfaces.

As stated earlier a maximum critical operating temperature was observed on epoxy-coated stretch-formed aluminum mirrors. This critical temperature was found to be about 80°C in both vacuum and air tests. Exceeding this temperature would cause surface failure within several minutes. Photographs of mirrors which were maintained at 100° and 200°C in vacuum are shown in Figures 52 and 53, respectively. The appearance of 100°C surface is similar to that of a mirror exposed to 80°C .

6.3.3 Ultraviolet Radiation Effects---A general outline of the ultraviolet radiation tests conducted on stretch-formed aluminum mirrors was given in Table III. Detailed test data are given in Appendix B. Results of ultraviolet radiation tests on stretch-formed aluminum mirrors are given in Figures 54 and 55. Figure 55 shows data for bare aluminum and Si_2O_3 overcoated mirrors irradiated at 0°C , bare aluminum mirrors irradiated at 50°C , and magnesium substrate mirrors (to be discussed later). Data were not presented from the tests conducted at 100°C because of the severe temperature-induced failure of the reflective surfaces. As a matter of record, the magnitude of the changes obtained at 100°C varied from $\Delta R_s = -0.214$ to -0.339 . It was interesting to note that even though the high temperature produced a visible reticulation of the reflective surfaces in a few minutes, the degradation in measured reflectance continued to increase gradually even up to about 875 hours after irradiation.

The results of ultraviolet radiation tests at -195°C on the Si_2O_3 overcoated mirror samples given in Figure 54 show that the maximum change in solar specular reflectance was only on the order of $\Delta R_s = -0.05$ after a 9800 ESSH exposure. As noted in the figure, the maximum rate of change was during the first 1000-2000

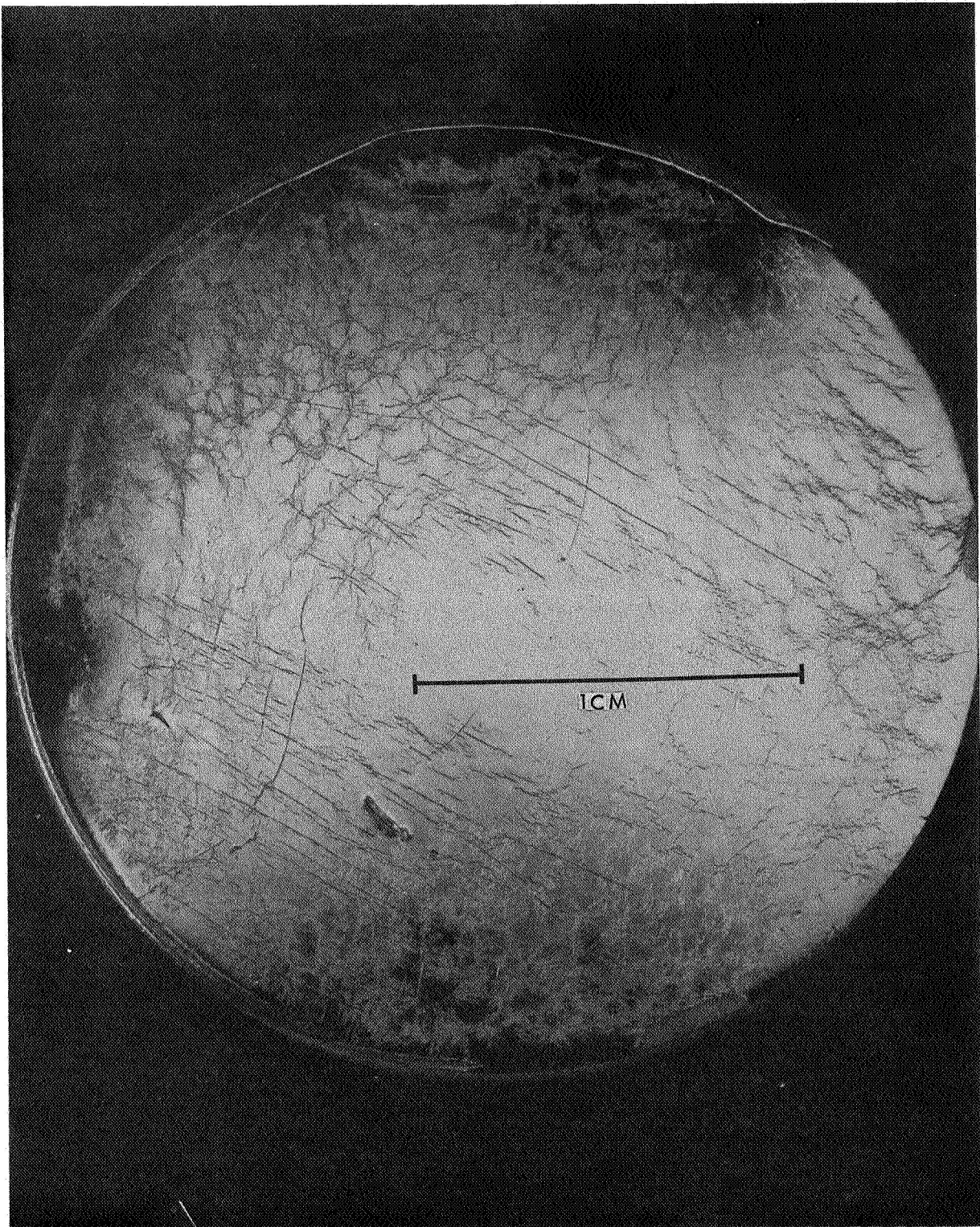


Figure 52: STRETCH-FORMED ALUMINUM MIRROR AFTER HEATING TO 100°C



Figure 53: STRETCH-FORMED ALUMINUM MIRROR AFTER HEATING TO 200°C

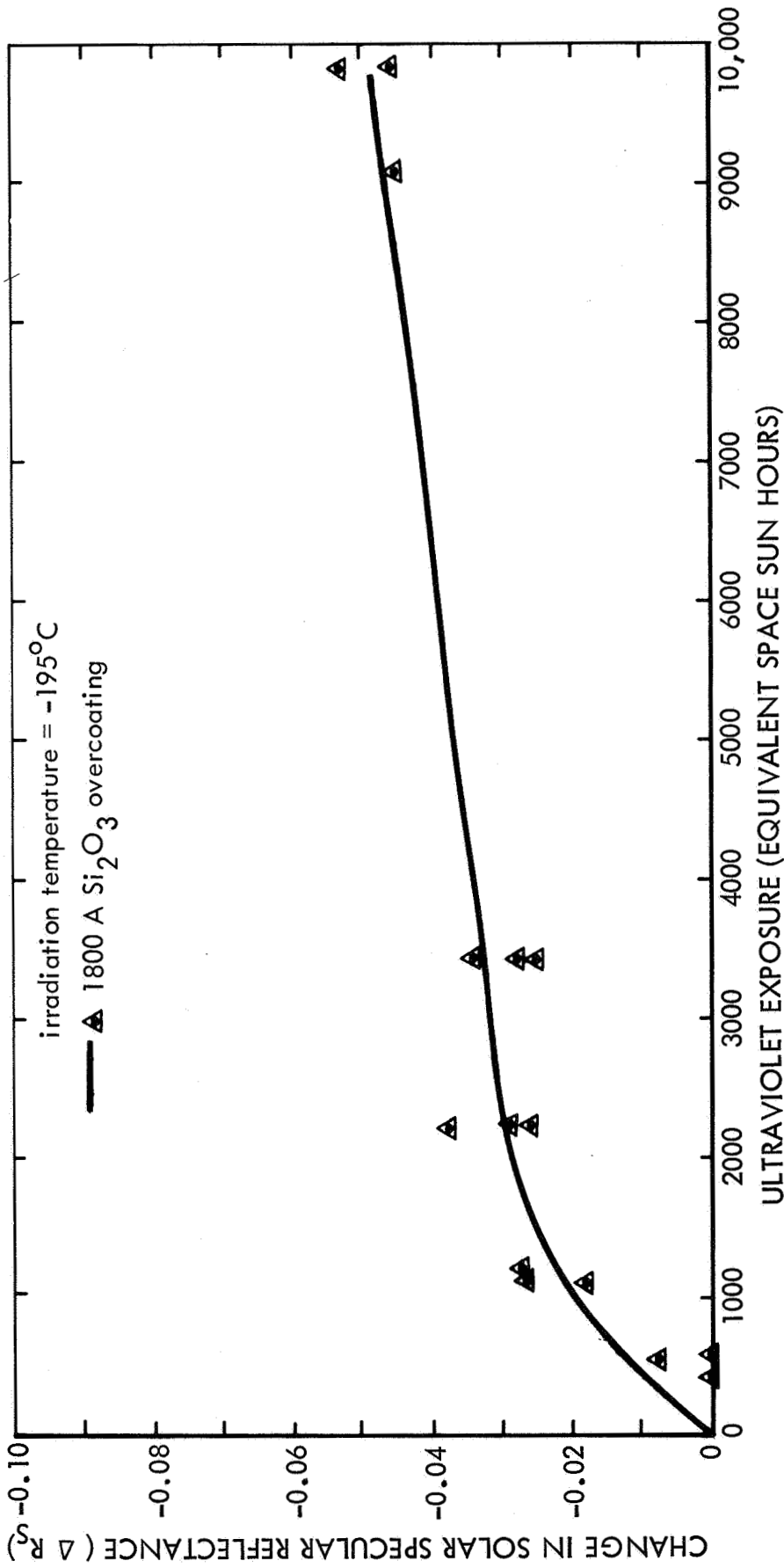


Figure 54: EFFECT OF ULTRAVIOLET RADIATION ON STRETCH-FORMED ALUMINUM MIRRORS

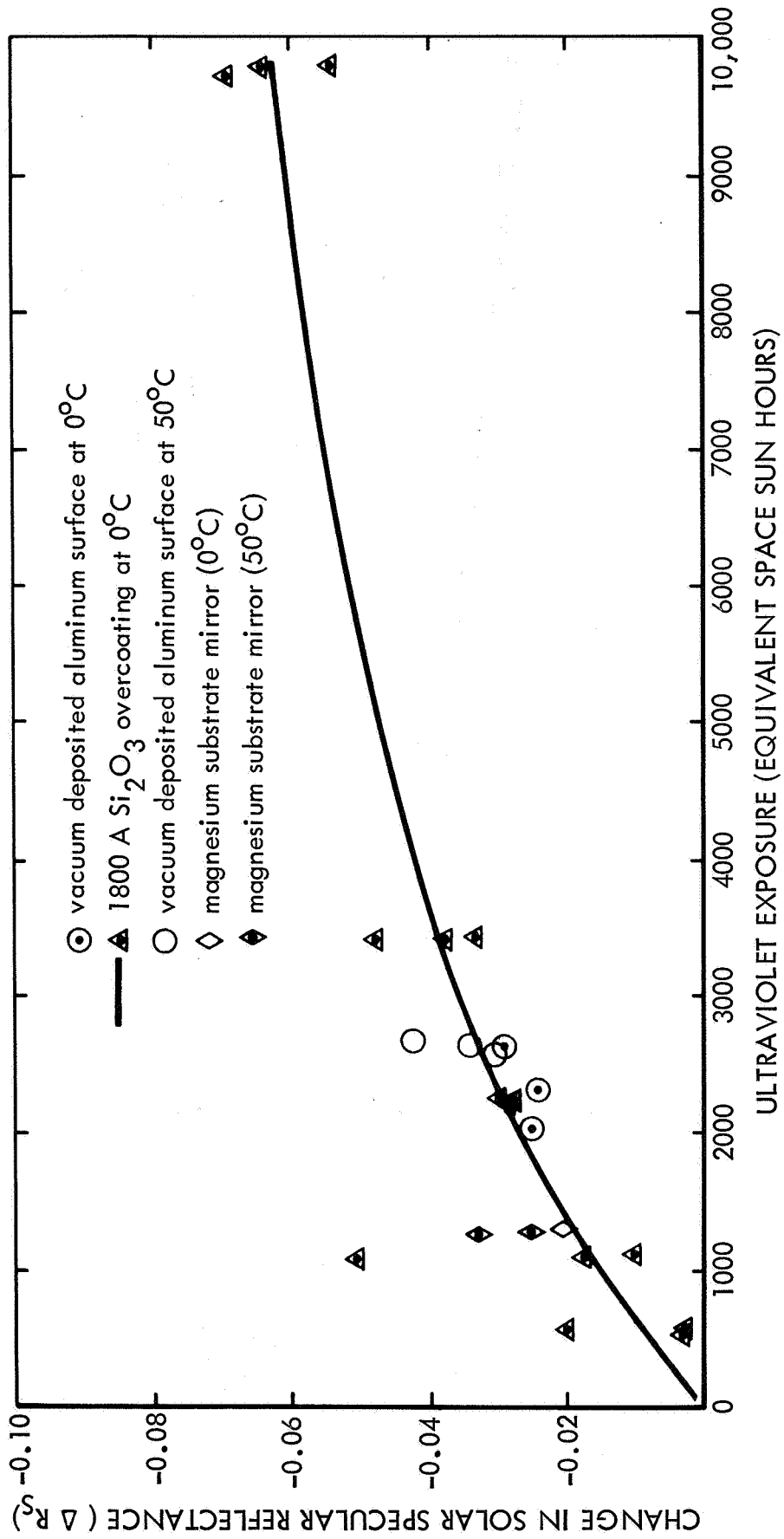


Figure 55: EFFECT OF ULTRAVIOLET RADIATION ON STRETCH-FORMED ALUMINUM MIRRORS

ESSH of irradiation, although a small rate of change continued up to 9800 ESSH. Good agreement was obtained for the three identical mirrors which were identically irradiated.

Results of experiments at 0°C on the Si₂O₃ overcoated mirror samples given in Figure 55 show comparable results to the -195°C tests. This indicates a negligible dependence of radiation damage on temperature in the -195° to 0°C range. Surprisingly, data points for the bare aluminum surfaces irradiated at both 0° and 50°C nearly coincide with the data on the Si₂O₃ surface.

The reflectance of stretch-formed aluminum mirrors was measured in air, in vacuum, and after about 400 ESSH of ultraviolet radiation in vacuum. It was concluded from this experiment and results of similar measurements on nickel mirrors that no significant annealing of radiation-induced optical absorption occurred when these mirrors were returned from vacuum to ambient pressure.

6.3.4 Combined Proton-Ultraviolet Radiation Effects---Results of combined and sequential radiation effects on stretch-formed aluminum mirrors are given in Figures 56 through 59. Data shown in Figure 56 for bare aluminum coated mirrors indicate that the combined environment produced a slightly larger spectral change than the sum of the two individual environments. Data spread bars on the proton-only data show the uncertainty involved with concluding whether a synergistic effect occurred. Thus it can only be concluded that a small synergistic effect may have occurred on the bare aluminum surfaces, and that more samples need to be irradiated at a higher integrated flux to get conclusive results. A similar conclusion was reached for the electroformed-nickel mirrors which were coated with bare aluminum.

The results of the experiment on bare aluminum surfaces wherein a mirror which had been irradiated with protons was subsequently irradiated with ultraviolet radiation are shown in Figure 57. For comparison purposes, data are shown for a similar mirror which was irradiated with ultraviolet only. As noted in the figure the mirror which had been preirradiated with protons degraded slightly more ($\Delta R_s = -0.035$ vs -0.025). This is in agreement with results obtained on electroformed-nickel mirrors.

The combined radiation environment experiments on Si₂O₃ overcoated mirrors (Figure 58) indicated that the combined environment produced more damage than the sum of the two individual environments. However, as discussed for electroformed-nickel mirrors, additional combined-environment tests should be run to confirm this result.

Ultraviolet tests on the Si₂O₃ overcoated mirrors (Figure 59) showed that the mirror which had been pre-irradiated with protons degraded more during ultraviolet exposure than similar mirrors which had not been preirradiated ($\Delta R_s = -0.047$ vs -0.038). These results, which were similar for both bare aluminum and Si₂O₃ over-coated surfaces on both types of mirrors, suggest that the protons do establish some

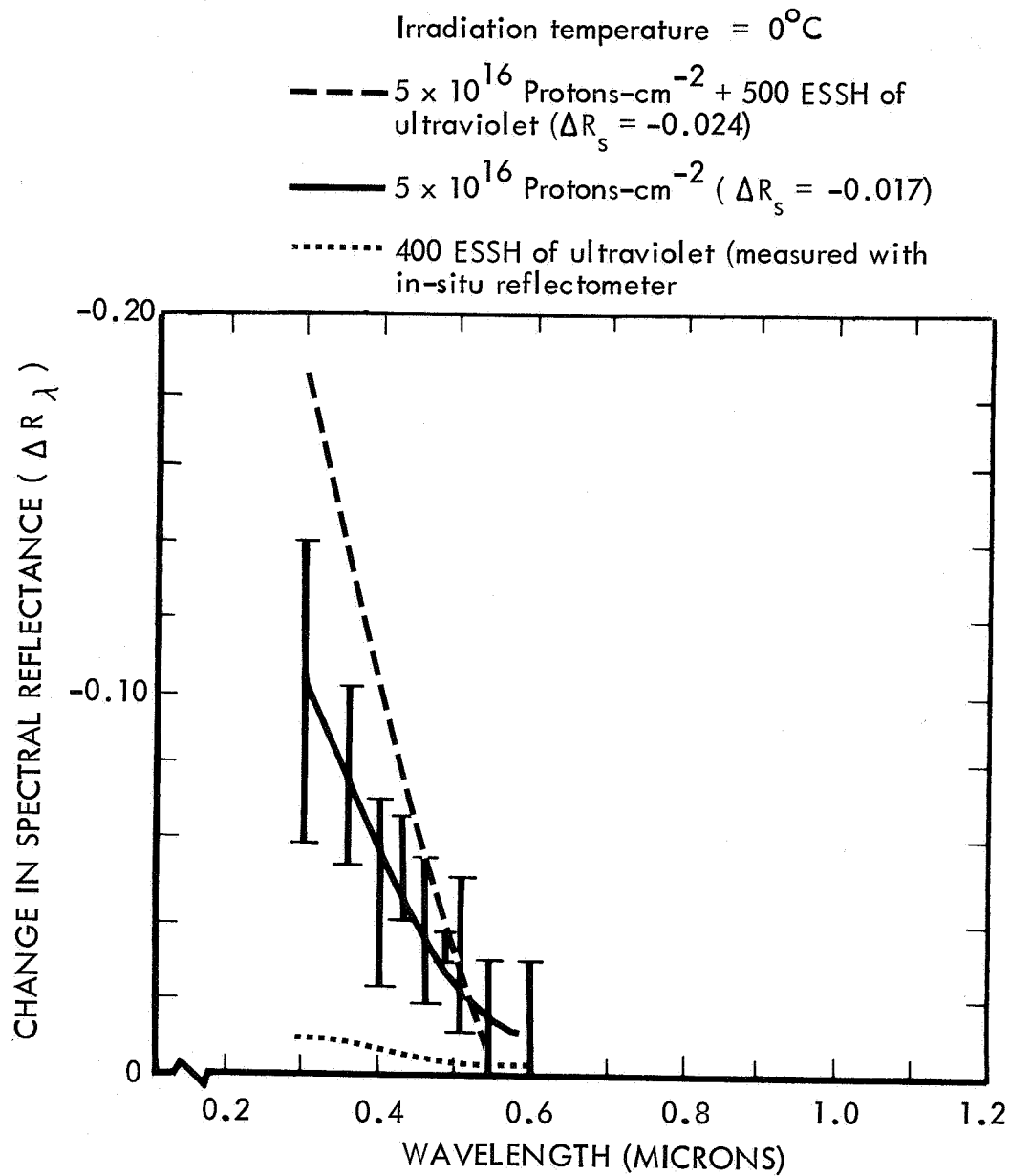


Figure 56: EFFECT OF COMBINED PROTON-ULTRAVIOLET RADIATION ENVIRONMENT ON BARE ALUMINUM COATED, ALUMINUM SUBSTRATE MIRRORS

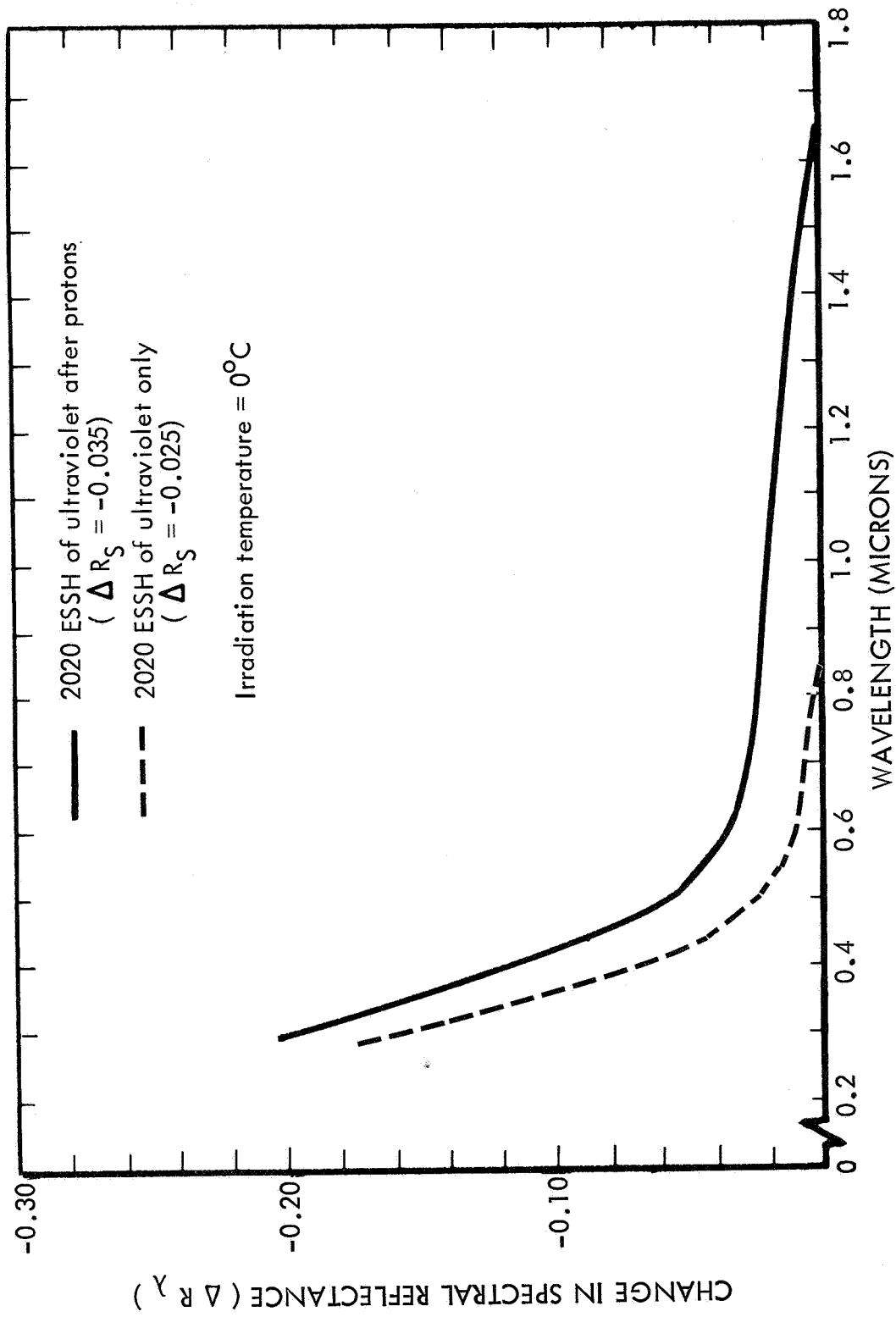


Figure 57: EFFECT OF PROTON IRRADIATION ON ULTRAVIOLET DEGRADATION OF BARE ALUMINUM COATED, ALUMINUM SUBSTRATE MIRRORS

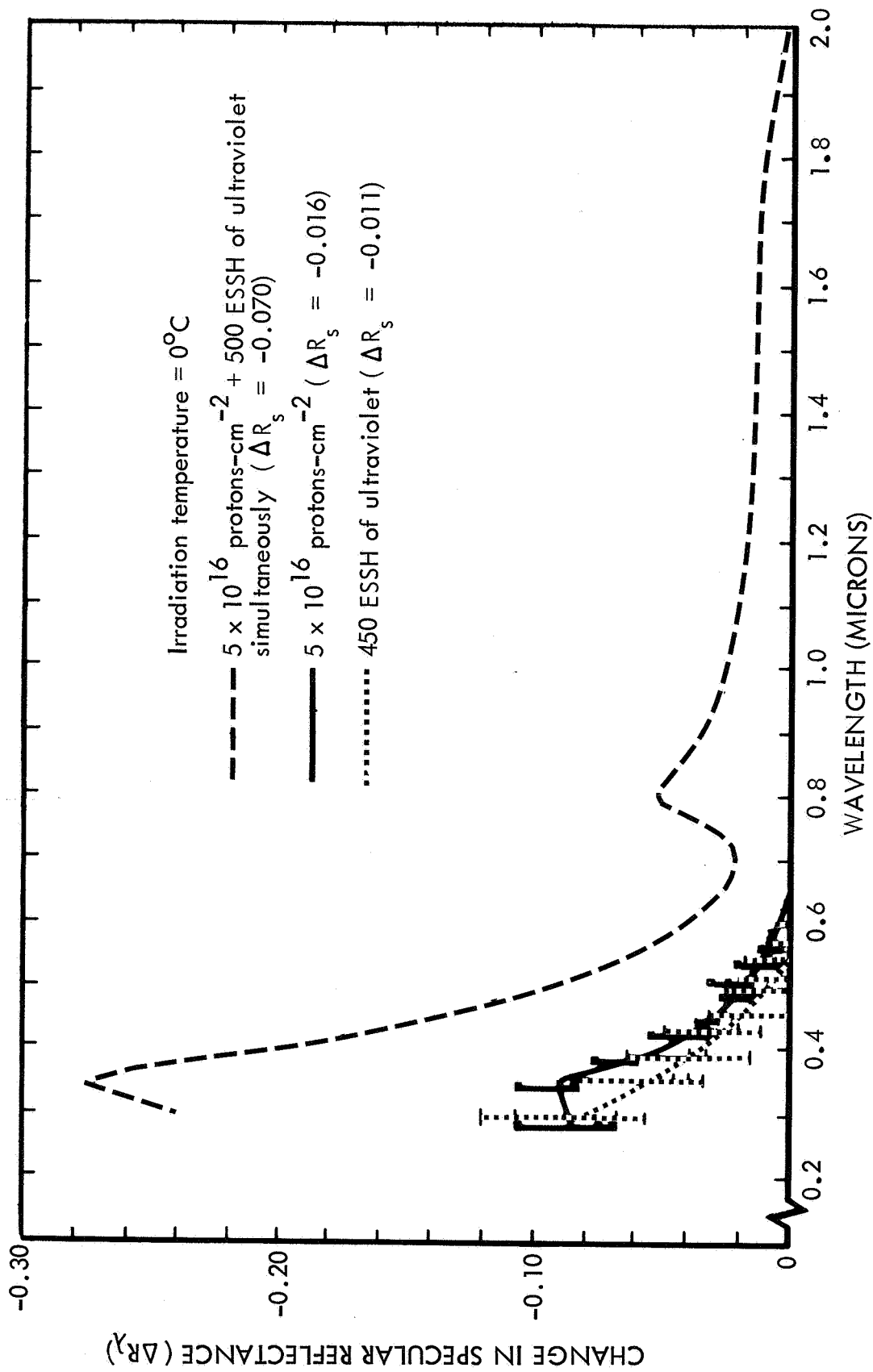


Figure 58: EFFECT OF COMBINED PROTON-ULTRAVIOLET RADIATION ENVIRONMENT ON Si₂O₃ OVERCOATED, ALUMINUM SUBSTRATE MIRRORS

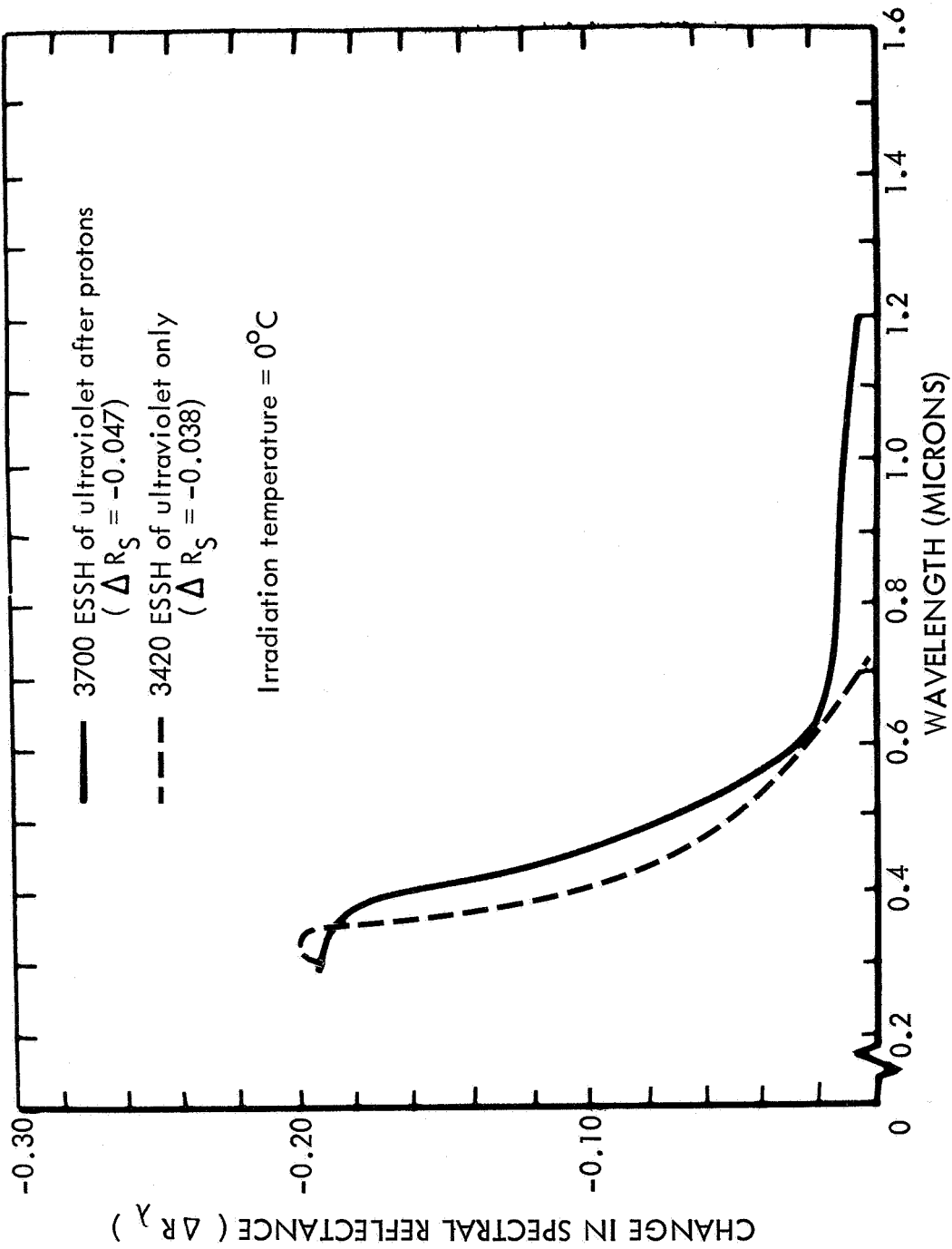


Figure 59: EFFECT OF PROTON IRRADIATION ON ULTRAVIOLET DEGRADATION OF SiO_2 OVERCOATED, ALUMINUM SUBSTRATE MIRRORS

defects which subsequently cause increased light absorption during ultraviolet irradiation. This observation along with the actual combined-environment exposure data indicates that a small synergistic effect occurred on the mirror surfaces. In other words, simultaneous irradiation produced more degradation than the algebraic sum of the degradation produced by the two environments on two test samples. In general, since the amount of degradation in solar specular reflectance obtained in all experiments was small, the significance of synergistic effects is probably more of scientific interest than practical interest unless higher radiation doses are encountered.

6.4 Magnesium Substrate Mirrors

6.4.1 Typical Reflectance Data---Typical specular and diffuse reflectance data for an unirradiated Si_2O_3 -overcoated, magnesium substrate mirror are shown in Figure 60. The solar specular reflectance of unirradiated magnesium mirrors has been found to be in the range of 0.828 to 0.837 with an average of 0.830. This value of solar specular reflectance is lower than that obtained for other mirrors which had been overcoated with thin Si_2O_3 (0.86 to 0.88). The lower reflectance on the magnesium mirrors is probably due to their having an improper Si_2O_3 coating thickness. The reflectance data indicate that the first order reflectance maximum occurred in the 0.6 to 0.7 micron range, whereas, it should occur at 0.55 micron (the peak of the solar spectrum). As a result of the position of the first order maximum, a minimum occurred at about 0.42 micron which caused considerable absorption of the solar spectrum. Based on the above results, it would appear that a physical thickness of about 1250 Å of Si_2O_3 would produce a higher solar reflectance.

6.4.2 Proton Radiation Effects---A general description of the proton tests conducted on magnesium substrate mirrors was given in Table II. Detailed test data are tabulated in Appendix C. Tests were conducted at temperatures of -195° , 0° , and 40°C . A maximum temperature of 40°C was chosen based on results of preliminary tests where it was found that severe reticulation of the reflective surface occurred at 50°C or higher.

Typical effects of protons on the specular and diffuse spectral reflectances are shown in Figure 60. The primary effects of the protons were to decrease the specular reflectance in the wavelength region of 0.3 to 0.5 micron and to increase it in the region from 0.5 to 0.7 micron. The characteristics of the degradation indicate a change in optical properties of the Si_2O_3 film which affects the interference characteristics. The data suggest either a decrease in the refractive index or in film thickness. Superimposed on the interference effects may be an increase in absorption in the Si_2O_3 oxide layer in the ultraviolet wavelength region.

A summary of results obtained on the magnesium-substrate mirrors is shown in Figure 61 which is a plot of the change in solar specular reflectance vs integrated

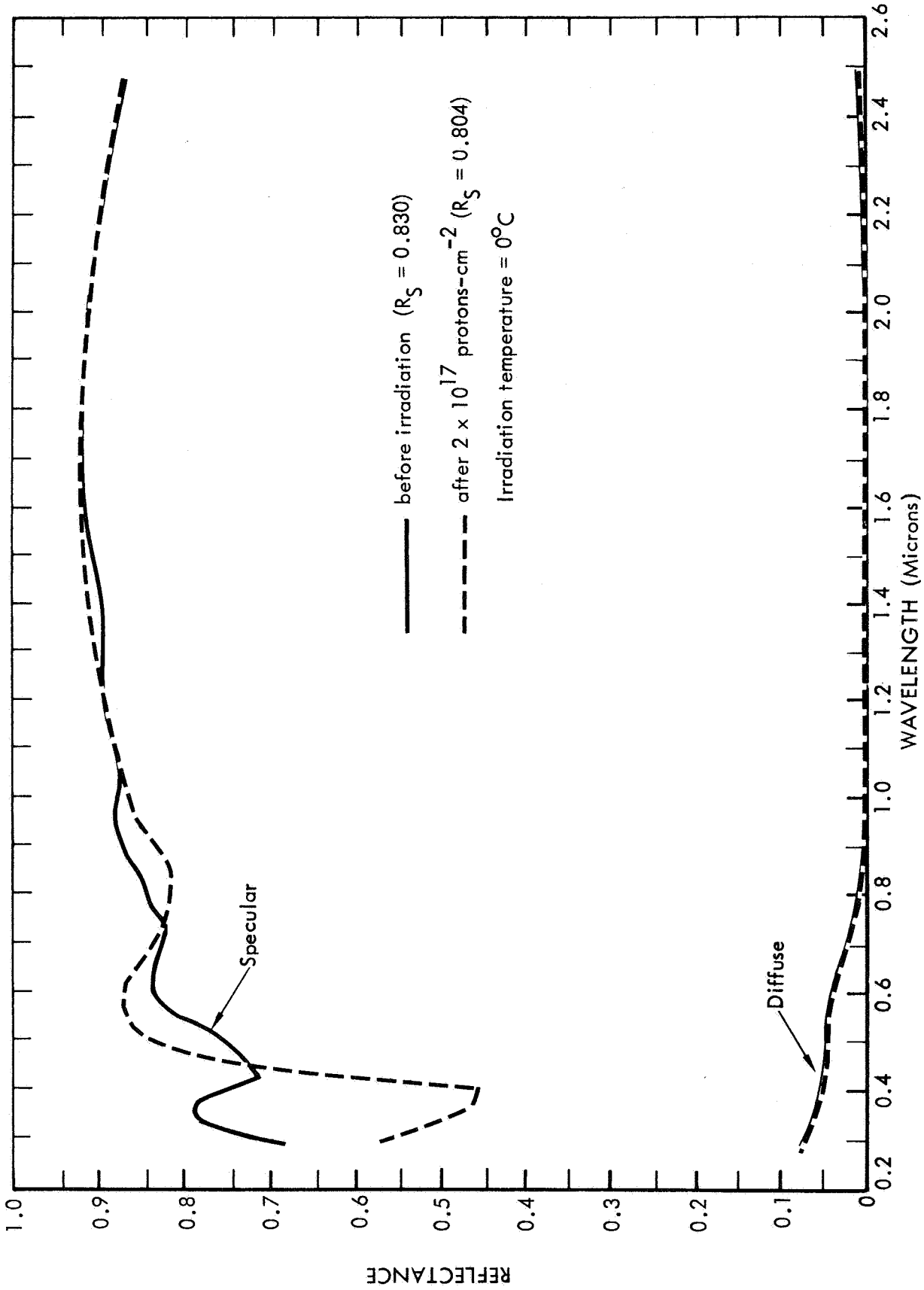


Figure 60: EFFECT OF PROTONS ON THE SPECTRAL REFLECTANCE OF MAGNESIUM SUBSTRATE MIRRORS

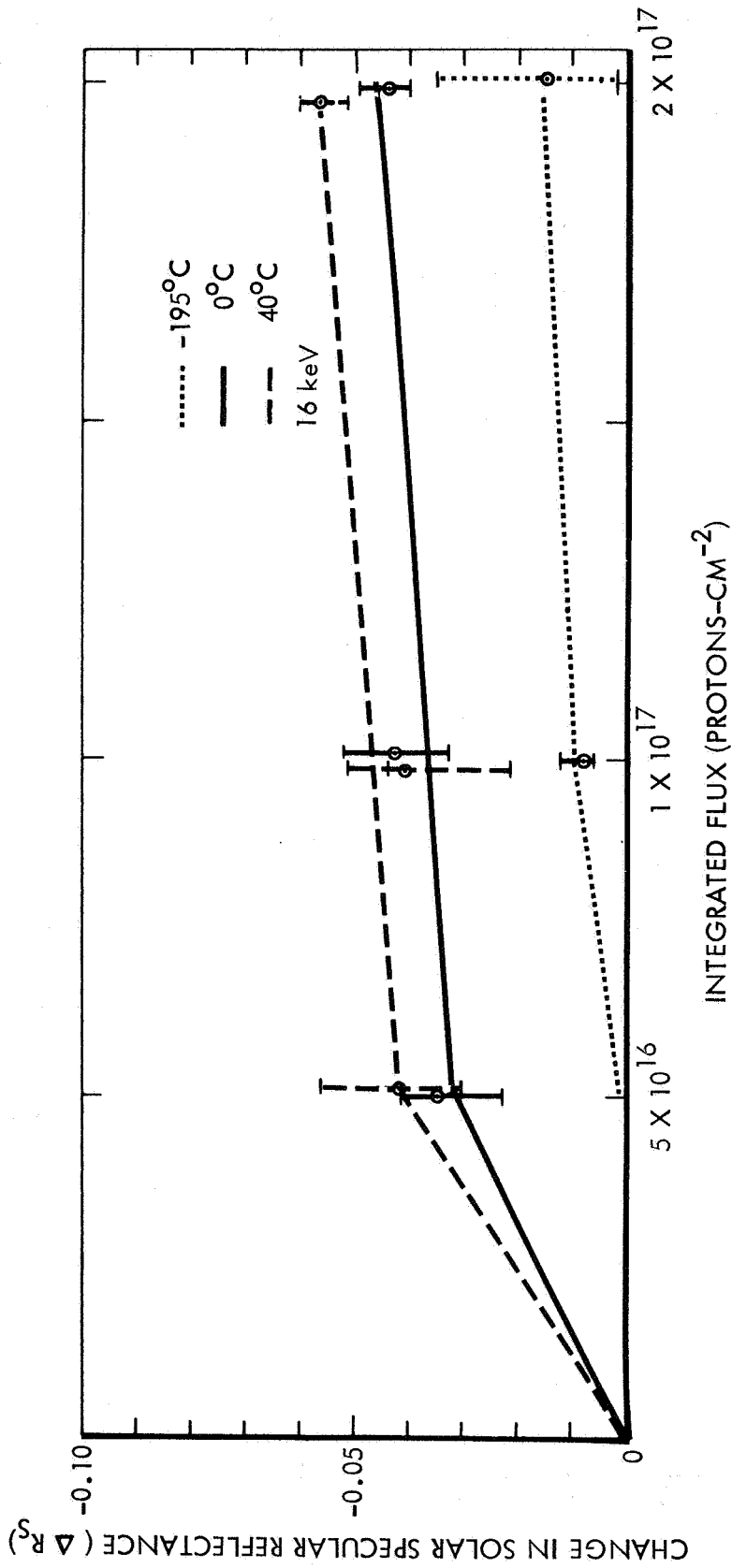


Figure 61: EFFECT OF PROTONS ON SOLAR SPECULAR REFLECTANCE OF SILICON-OXIDE OVERCOATED, MAGNESIUM SUBSTRATE MIRRORS

flux. The reflectance data show a decrease in reflectance as the temperature increased. Data from the mirrors irradiated at -195° , 0° , and 40°C indicated degradation in the order of $\Delta R_s = -0.015$, -0.044 , and -0.055 respectively. It is interesting to note that a saturation of damage occurred somewhere below an integrated flux level of 5×10^{16} protons -cm^{-2} . This suggests that additional tests should be run on these mirrors at lower integrated fluxes to determine the threshold of damage.

6.4.3 Ultraviolet Radiation Effects---A general summary of ultraviolet test conditions was given earlier in Table III and a complete tabulation of ultraviolet test data for magnesium substrate mirrors is given in Appendix B.

Ultraviolet tests were run at -195° , 0° , and 50°C on these mirrors. All test samples irradiated at 0° and 50°C exhibited a reflective surface reticulation which was believed to be due to dimensional changes in the epoxy undercoat. The failure of the reflective surfaces with irradiation time and temperature was not consistent in that the 50°C samples had degraded by the end of 120-test hours and the 0° samples degraded during the 120- to 360-test-hour increment. It should also be pointed out that the change in reflectance given for the -195°C samples between the 120- and 240-test-hour increments is probably not valid due to contamination effects. The data given for the 120-hour increment appears valid. It is suspected that the vacuum chamber became contaminated between the end of the 120-hour increment and the start of the next exposure increment. The mirror samples had been removed for reflectance measurements and another spacecraft hardware test was run in the chamber in the interim. As a result of the thermal effects and contamination, only three valid data points were obtained on the magnesium substrate mirrors.

The three data points which are believed to represent typical radiation effects on the magnesium-substrate mirrors are plotted in Figure 55 along with data from aluminum-substrate mirrors. A comparison of results from the two types of mirrors at the 1200 ESSH exposure increment shows that comparable degradation was experienced. The fact that the amount of degradation experienced on two different mirrors was about the same is of significance because the vacuum deposited films were applied in two different laboratories.

An ultraviolet in-situ reflectance experiment was also performed on the magnesium-substrate mirrors. In the first test the specular-plus-diffuse reflectance of the mirror was measured in air, in vacuum, and in vacuum after 400 ESSH of ultraviolet radiation. Data from these reflectance measurements are given in Figure 62. A leak developed in the chamber which contaminated the surfaces and prevented a valid measurement of reflectance in air after irradiation. In the second test a complete sequence of specular-plus-diffuse reflectance measurements were made before and after ultraviolet radiation; however, the chamber pressure rose to the 1- to 100-micron pressure range several times during the test. Since rather severe degradation was experienced in this test the results are questionable. Thus, a post-

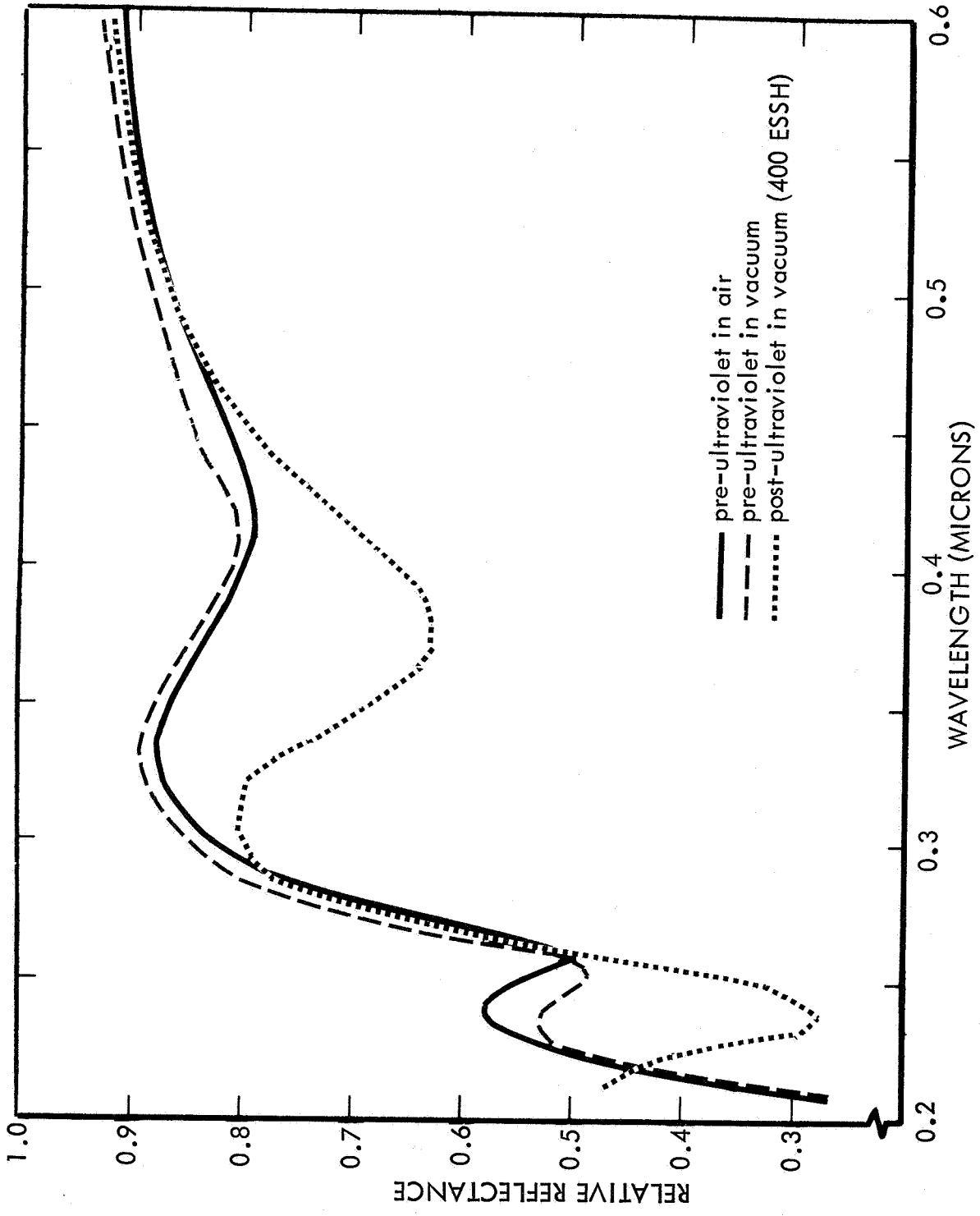


Figure 62: IN-SITU REFLECTANCE DATA ON MAGNESIUM-SUBSTRATE MIRRORS

irradiation curve measured in-air is not given in Figure 62. Despite the problems which were encountered the following observations were made concerning the in-situ reflectance experiment on magnesium substrate mirrors:

1) A negligible shift of interference maxima and minima to shorter wavelengths occurred during pumpdown;

2) A major shift in interference maxima and minima occurred during irradiation which was comparable to the shift measured in air on prior proton and ultraviolet tests; and

3) A minor shift to longer wavelengths occurred immediately upon backfilling the chamber. (A reflectance measurement performed about 11 hours after exposure to ambient pressure, in the latter test described above, indicated a small additional shift to longer wavelengths.)

In general, the results of the in-situ reflectance experiment on these mirrors indicate that no significant changes in solar specular reflectance occurred during either pumpdown or backfilling the vacuum chamber.

6.4.4 Combined Proton-Ultraviolet Radiation Effects---Results of the combined proton-ultraviolet radiation tests on the magnesium substrate mirrors are shown in Figure 63. It was noted in spectral reflectance plots that the change in reflectance, as shown in Figure 63, resulted from the shift in wavelength of interference maxima and minima. Considerable spread was experienced between similarly irradiated mirror samples, thus precluding the possibility of making conclusions regarding synergistic effects.

6.5 Space Radiation Effects

6.5.1 Introduction---Since it is important to relate the results of this test program to space missions and the expected effects of the space radiation environment, a brief description of this environment is necessary. Energy deposition of the environment at synchronous altitude (19,300 n.mi.) will be presented, and equivalence of exposure in space to that employed in the test program discussed. Results of the test will then be compared with those of other researchers. Some conclusions will be drawn and several recommendations for further analysis given.

6.5.2 Particulate Radiation Environment---The radiation environment encountered in space missions consists of geomagnetically trapped protons and electrons, untrapped solar event protons, galactic cosmic rays and - outside the magnetosphere - the solar wind. The proton component of this environment is the most effective for producing damage. Hence we are especially concerned with this component. The low energy

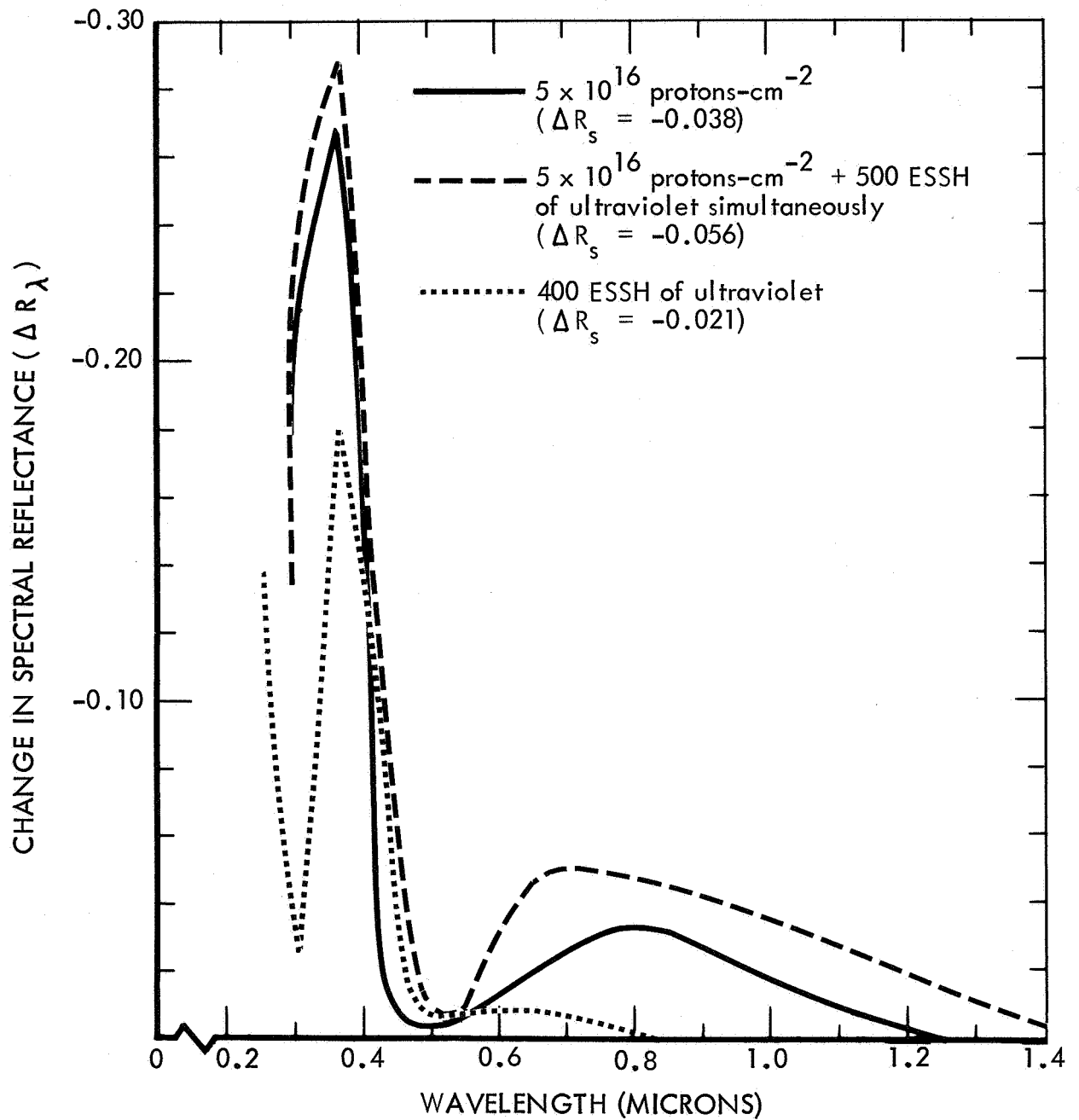


Figure 63: EFFECT OF COMBINED PROTON-ULTRAVIOLET RADIATION ENVIRONMENT ON MAGNESIUM SUBSTRATE MIRRORS

protons ($1 \leq E \leq 100$ keV) outnumber the high energy protons in most space missions. In addition, the protons in this low energy range are the most effective in producing damage to the optically reflecting surfaces considered in this study.

Inside the magnetosphere the peak intensity of these low energy protons occurs near synchronous altitude and is predominantly trapped. The integral f , and differential df/dE energy flux spectra of these trapped protons are given in Figure 64. These spectra are based primarily upon the low energy results reported by L. Frank (Reference 29). These spectra are suggested as a worst case exposure to spacecraft surfaces inside the magnetosphere. Thus, a mission in synchronous orbit for a year (3.15×10^7 sec) may expect to encounter an omnidirectional integrated flux of 1.1×10^{16} protons-cm⁻² with roughly 70 percent of them having energies less than 30 keV. A spacecraft surface which views only a 180 degree solid angle is thereby exposed to about 5.5×10^{15} protons-cm⁻² year⁻¹ in such a mission.

The composite model of the trapped electron environment has been presented by J. I. Vette in NASA SP 3024, Volume 3 (Reference 30). The time-averaged integral spectrum of the omnidirectional flux of energetic electrons is less than or equal to:

$$J(>E) = 10^8 \exp(-E/0.215) \text{ Electrons-cm}^{-2} \text{ sec}^{-1} \quad (1)$$

Based on this spectrum, there are less than 3×10^{15} electrons-cm⁻² year⁻¹ with a mean energy of 215 keV. The low energy spectrum is steeper and is more uncertain. However, a conservative estimate appears to be $\sim 2 \times 10^{16}$ electrons-cm⁻² year⁻¹ with a mean energy of ~ 10 keV. The ionization dose from these electrons is only a fraction of that due to the protons, and the displacement damage is orders of magnitude less. Hence this cryptic conservative estimate of the electron environment is sufficient for our discussion.

Outside the magnetosphere the continual bombardment by the solar wind protons provides the most severe exposure to low energy protons. The solar wind provides an average exposure of 6×10^{15} protons-cm⁻² to a spacecraft surface during a year mission. The energy of the solar wind fluctuates between 0.7 keV and 3 keV. Thus the spectrum of the integrated flux is broader than that of the instantaneous flux but is still quite narrow. For purposes of this study a monoenergetic solar wind model spectrum was chosen.

6.5.3 Energy Deposition---The incident protons interact both inelastically and elastically with the atoms of the solid. Ionization is the principal result of the inelastic scattering while displacement of the atom is the principal effect of the elastic collisions. The energy lost by ionization reaches a maximum of ~ 500 Mev-cm⁻² gm⁻¹ between 40 and 100 keV in Si₂O₃ ($\rho \approx 2.5$ gm-cm⁻³), and decreases as $\sim 1/E$ at higher energies. Below 25 keV the proton is moving slower than the electrons in the atoms, and therefore spends a considerable portion of its path neutra-

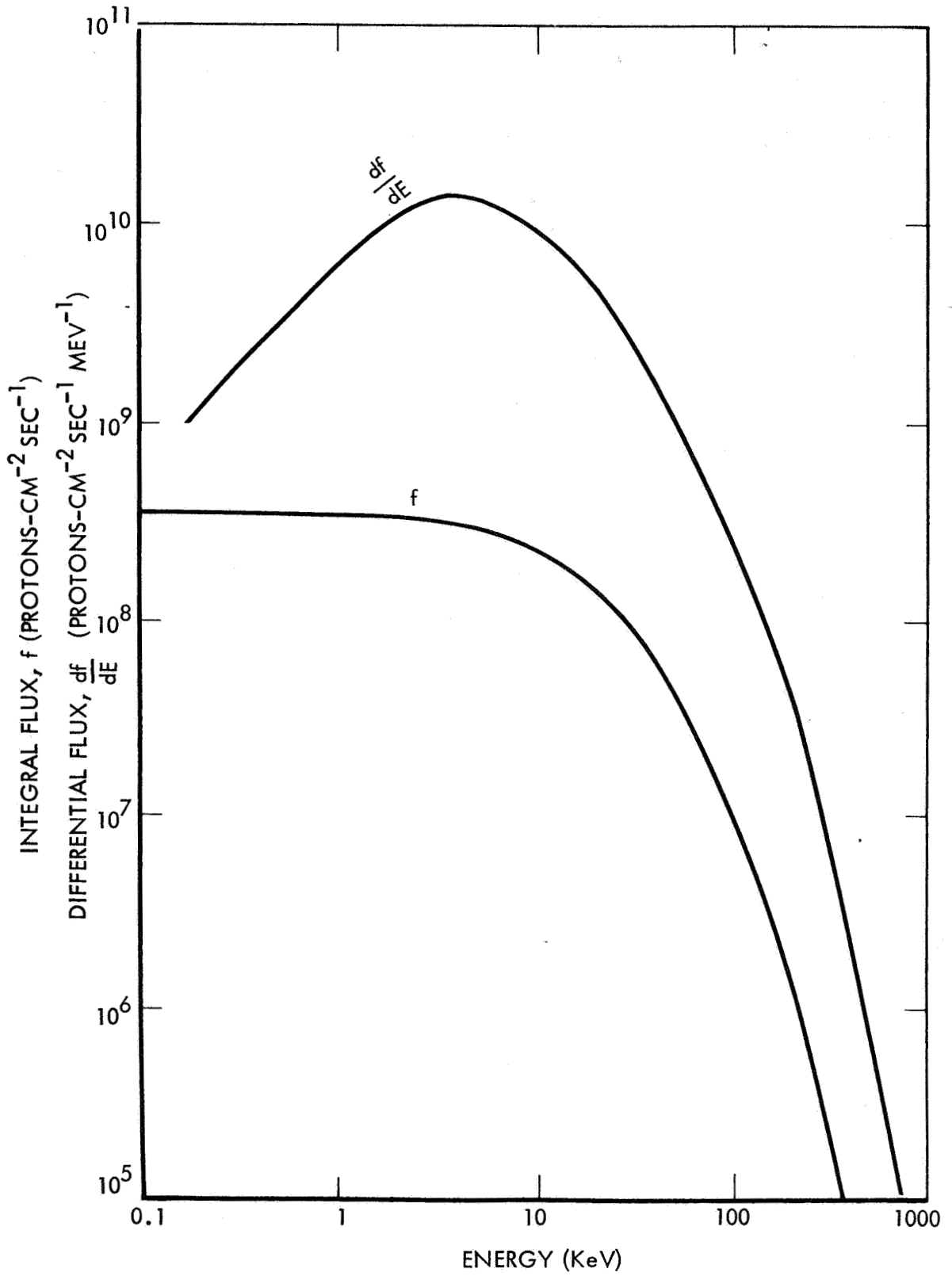


Figure 64: TRAPPED PROTON SPECTRA AT SYNCHRONOUS ALTITUDE

lized by electron capture. The theoretical stopping power based upon the Thomas-Fermi model is given by Lindhard and Scharff (Reference 31) as:

$$\frac{dE}{dX} = N \frac{8\pi Z e^2 a_0}{(1+Z^{2/3})^{3/2}} \frac{\sqrt{E}}{5} = G \left\{ \frac{4}{5} \frac{1+A}{1+Z^{2/3}} \sqrt{E} \right\} \quad (2)$$

where

$$G = N \frac{2\pi Z \lambda_c^2 mc^2}{(1+Z^{2/3})^{1/2} (1+A)}, \quad N = \text{atomic density}$$

$$a_0 = \text{Bohr radius } (5.292 \times 10^{-9} \text{ cm})$$

$$e = \text{electron charge } (4.8 \times 10^{-10} \text{ esu})$$

$$m = \text{mass of electron } (9.11 \times 10^{-28} \text{ g})$$

$$Z = \text{atomic number}$$

$$A = \text{atomic weight}$$

$$E = \text{proton incident energy, keV}$$

$$\lambda_c = \text{reduced compton wavelength of electron } (3.86 \times 10^{-11} \text{ cm})$$

The stopping power due to elastic scattering in a weakly screened and intermediate screened coulomb field was given by N. Bohr (Reference 32) and K. O. Nielson (Reference 33), respectively, as follows:

$$\frac{dE}{dX} = G \left(S \ln \frac{2}{S} \right) \text{ for } S \ll 1 \quad (3)$$

and

$$\frac{dE}{dX} = G (0.582) \text{ for } S > 1$$

where S is the screening parameter given by

$$S = \frac{Ze^2 (1+A)(1+Z^{2/3})^{1/2}}{a_0 A E} = 2.72 \times 10^{-2} \frac{Z(1+A)(1+Z^{2/3})^{1/2}}{A E} \quad (4)$$

Employing Braggs rule for the stopping power of Si_2O_3 ,

$$\left(\frac{dE}{dX}\right)_{\text{Si}_2\text{O}_3} \frac{1}{N} = \frac{2}{5} \left(\frac{dE}{dX}\right)_{\text{Si}} \frac{1}{N_{\text{Si}}} + \frac{3}{5} \left(\frac{dE}{dX}\right)_0 \frac{1}{N_0} \quad (5)$$

a density of 2.5 gm-cm^{-3} which gives $N_{\text{Si}} = 3 \times 10^{22}/\text{cc}$, and $N_0 = 4.5 \times 10^{22}/\text{cc}$, the stopping power for weak screening is

$$\frac{dE}{dX} = \frac{1}{E} \left\{ 0.234 \ln (3.88E) + 0.2733 \ln (1.94E) \right\} + 2.138 \sqrt{E} \text{ ev/A}$$

When the screening is strong the expression for the stopping power becomes

$$\frac{dE}{dX} = 0.4182 + 2.138 \sqrt{E} \text{ ev/A} \quad (6)$$

The contributions from both elastic and inelastic scattering and the total stopping power are presented in Figure 65. A power law expression for $1 < E < 16$ keV of $dE/dx = 2.52 E^{0.499}$ is seen to fit fairly well. This compares well with results obtained for Al_2O_3 by Van Wijngaarden and Duckworth (Reference 34). The results of Nielson and Bohr are compared between 0.5 keV and 2 keV. Nielson's result is employed for $E \leq 2$ keV and Bohr's result above 2 keV. Integrating the inverse stopping power over the energy, the mean path length R of the proton in silica is obtained. Integration of the inverse inelastic stopping power leads to the well known square root relation. The effect on the path length of neglecting elastic collisions is presented in Figure 66. At high energies the protons are losing energy almost exclusively to the electrons in the atom and hence suffer little deflection from their initial direction until they have lost all but a keV or so of their energy, whereupon elastic collisions become important. Thus the penetration depth of these protons is almost equal to the pathlength. At low energies the scattering is quite pronounced. The average center-of-mass scattering angle θ is very nearly 90° for elastic collisions with massive atoms ($\overline{\cos \theta} = 2/(3A)$), thus, diffusion theory is applicable. Under these conditions Nielson has shown that the penetration depth may be estimated by

$$d \approx \frac{0.7}{\sqrt{\xi (1 - \overline{\cos \theta})}} \frac{(1 + Z^{2/3})^{1/2} A^2}{Z (1+A)} E \text{ g/cm}^2 \quad (7)$$

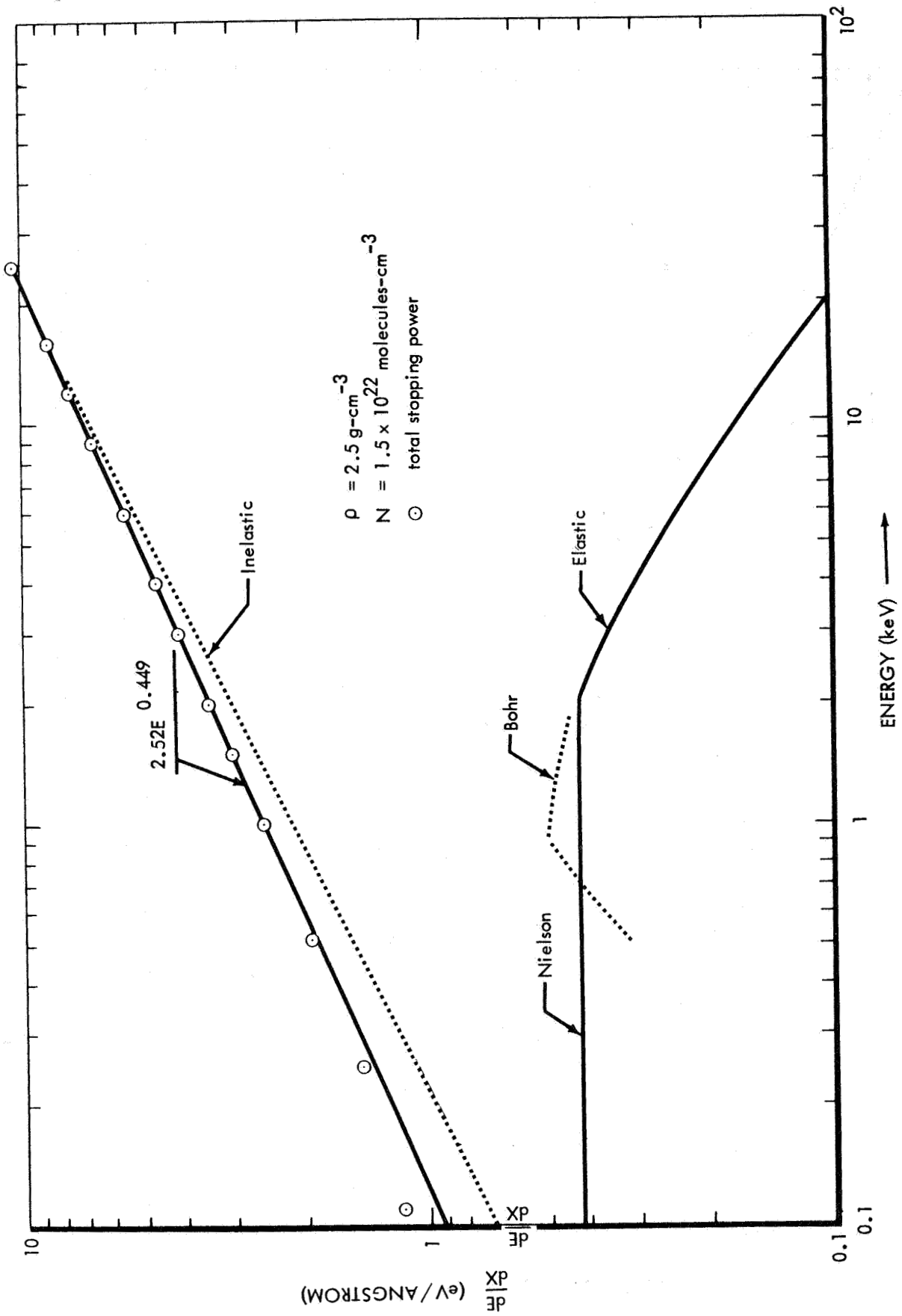


Figure 65: PROTON STOPPING POWER IN SILICA

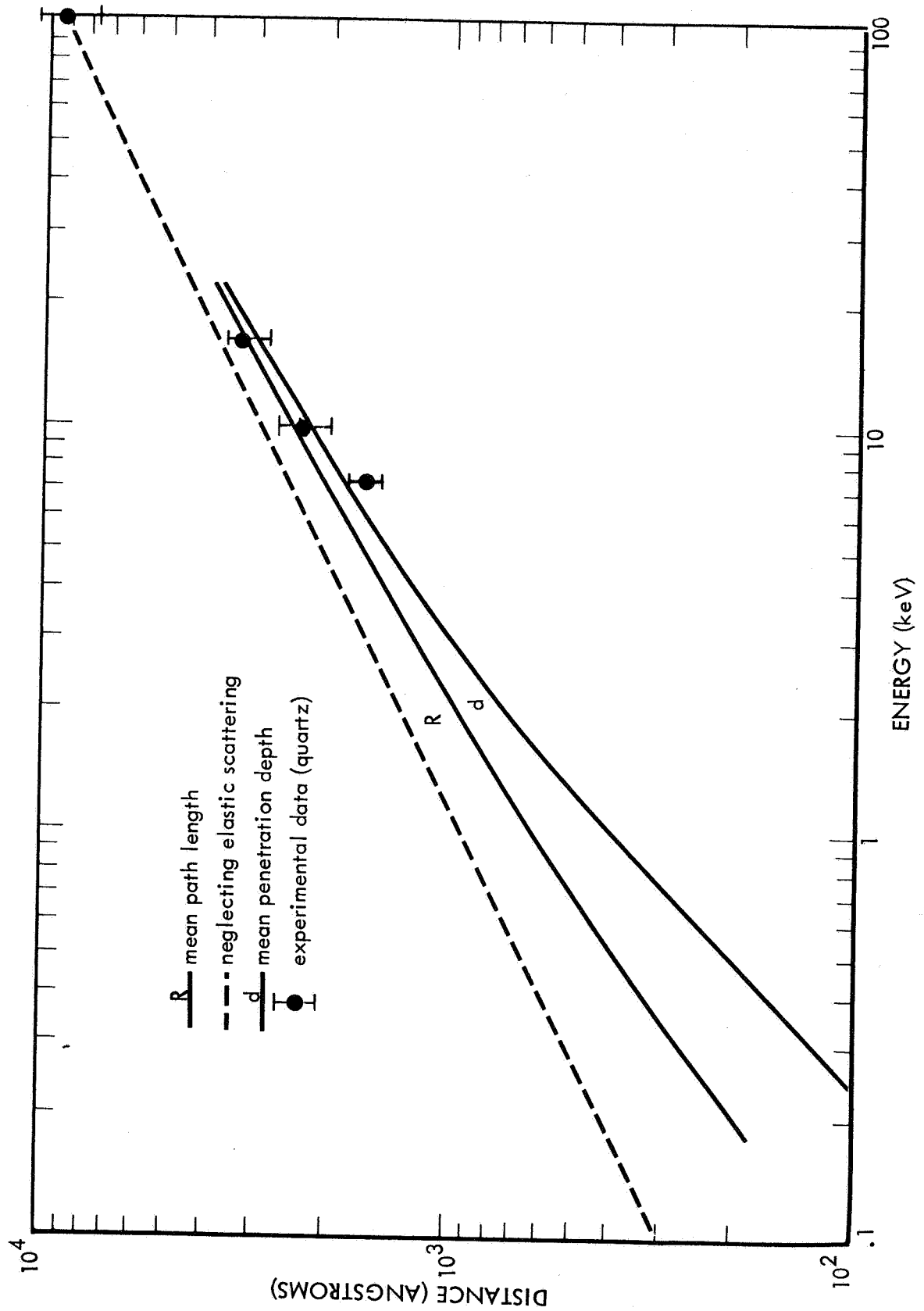


Figure 66: PATH LENGTH AND PENETRATION DEPTH OF PROTONS IN SILICA

where ξ is the average logarithmic decrement of energy loss per collision. This may be approximated by $\xi \approx 2/A$ in elastic collisions with large A atoms (Reference 35). Thus

$$d \approx \frac{1}{2} \frac{\sqrt{1 + Z^{2/3}}}{Z} A^{3/2} E \quad \mu\text{g}/\text{cm}^2 \quad (8)$$

This leads to $10.9 \mu\text{g}\text{-cm}^{-2}$ in silica or 430 \AA for the penetration depth of a 1 keV proton. An accurate treatment of the penetration depth (Reference 36) is beyond the scope of this study. For purposes of this study the penetration depth $d(E)$ will be approximated by

$$\begin{aligned} d(E) &= R(E) - R(1) + 400 \text{ \AA} & E \geq 1 \text{ keV} \\ &= 400 E \text{ \AA} & E \leq 1 \text{ keV} \end{aligned}$$

The depth thus obtained is also presented in Figure 66. The penetration depths deduced from changes in the reflection coefficient of quartz obtained by Hines and Arndt (Reference 11) are shown for comparison. The range of values obtained at 100 keV as presented by V. J. Linnebo (Reference 37) is also given. Fairly good agreement is obtained. The steeper slope of the quartz results can be expected because of the greater importance of elastic scattering in quartz (66.7 percent oxygen) over that in silica (~ 60 percent oxygen). A modest literature search did not reveal any additional experimental determinations of the penetration depth in quartz or silica. Some penetration studies through metal foils (References 38 and 39) indicate smaller penetration depths for few kilovolt protons. However, these studies depend upon large corrections for either the charge state or the induced scintillation probability of kilovolt protons and hence are inconclusive. The energy deposition in the present analysis will be based upon the crudely obtained curve for $d(E)$ given in Figure 66. As a result of this study it is recommended that: (1) a test be conducted with 1 keV protons to properly simulate the solar wind environment; and (2) additional proton depth-of-penetration studies be conducted in the energy region from about 0.8 to 30 keV.

The relative dose contribution to the mirror surface from protons of various energies in the space environment can now be estimated. Multiplying the stopping power by the omnidirectional differential spectrum, we obtain the differential surface dose rate (dD/dE) presented in Figure 67. It is seen to peak between 6 and 11 keV. The logarithmic energy scale visually weights the low energies heavily. For visualization the function $dD/d(\ln E)$ is also presented. This curve represents the contribution to the dose integral per unit change in the abscissa. It is seen from the $dD/d(\ln E)$ curve that the protons in the energy range $15 < E < 40$ keV are giving the most important contribution to the surface dose. Integrating this function and using 0.5 for the solid angle factor, a surface dose of $2.75 \times 10^{14} \text{ keV}\text{-cm}^{-3}\text{-sec}^{-1}$

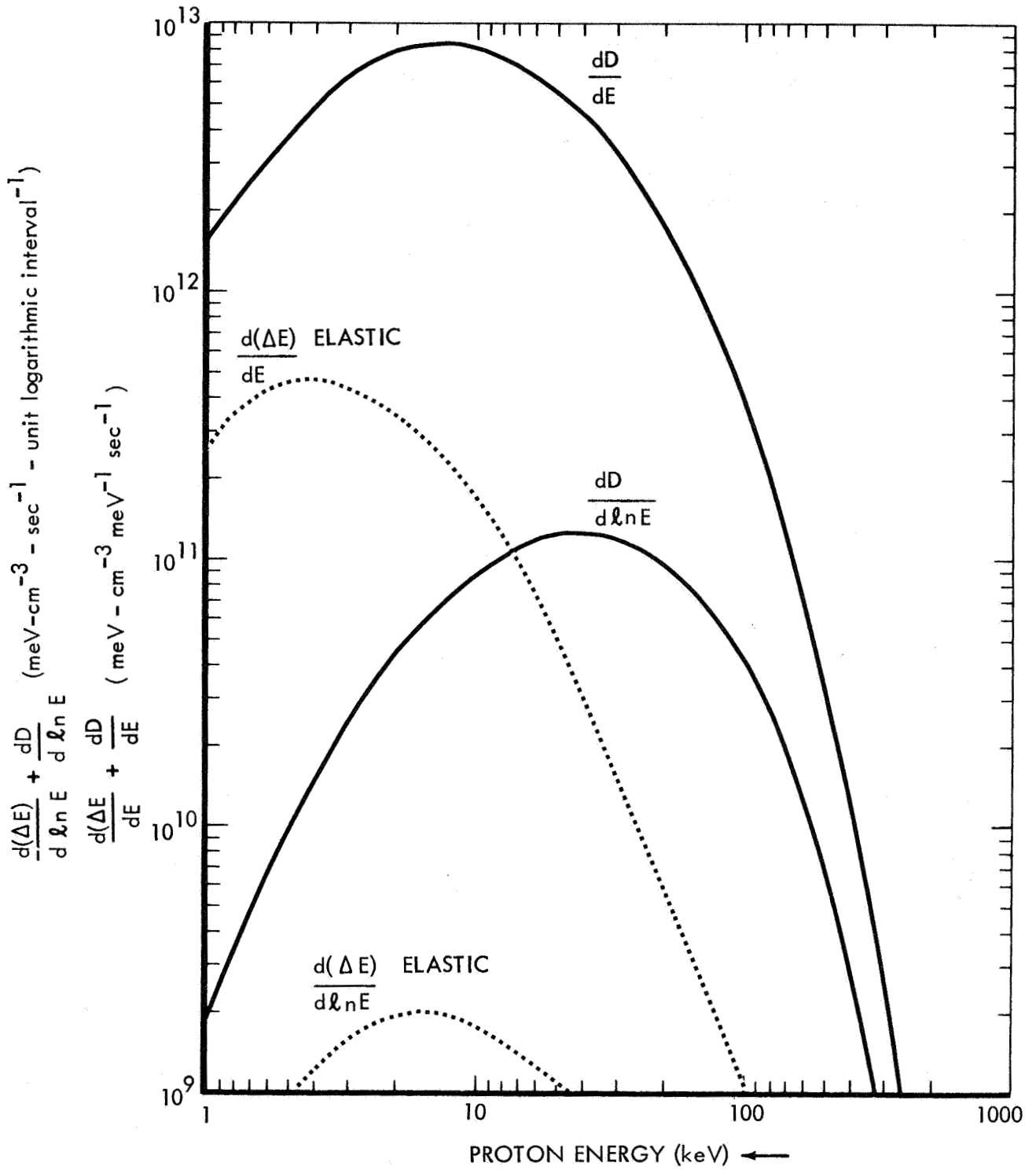


Figure 67: DIFFERENTIAL-DOSE AND ELASTICALLY-DEPOSITED ENERGY TO AN Si_2O_3 SURFACE AT SYNCHRONOUS ORBIT

or 5.4×10^{10} rad-year⁻¹ is obtained for the protons. A conservative estimate of the electron surface dose is 5×10^9 rad-year⁻¹. Hence, the electron dose is negligible. For comparison purposes the energy deposited in the silicon oxide film due to ultra-violet radiation was calculated to be about 6×10^{16} rad-year⁻¹, considerably higher than the proton and electron doses.

The differential energy deposited ($d(\Delta E)/dE$ elastic) by elastic collisions can be obtained similarly. This is also presented in Figure 67. The maximum of the elastic contribution lies between 2 and 4 keV. By plotting a $d(\Delta E)/d \ln E$ curve, it is seen that the maximum contribution to an elastic energy-deposition integral is coming from protons of 4 to 15 keV energy. The integration leads to 8×10^{19} keV-cm⁻³-year⁻¹ at the surface.

Based upon the above energy deposition considerations, a test with protons in the energy range of 10 to 20 keV should be best for representing the radiation effects in a synchronous mission. Mirror samples were irradiated in this program with 16 keV protons. For discussion purposes, the exposure (F) will be expressed in units of 10^{16} protons-cm⁻²; that is, a time integrated flux of 2×10^{17} protons - cm⁻² corresponds to $F = 20$. An exposure (F) gives $5.5 \times 10^{10}F$ rad to the surface and deposits $12 \times 10^{19}F$ keV-cm⁻³ at the surface via elastic collisions. An equivalence to a space exposure can then be estimated for surface effects. Letting Y_{ion} be the years equivalent for ionization effects and Y_d be the years equivalent for displacement damage, one obtains for synchronous orbit;

$$Y_{ion} = \frac{5.5 \times 10^{10} F}{5.4 \times 10^{10}} = \sim 1.0 \text{ years}$$

and

$$Y_d = \frac{12 \times 10^{19} F}{8 \times 10^{19}} = 1.5 \text{ years}$$

The difference between Y_{ion} and Y_d is somewhat greater at a 1500 to 2000 Å depth. Here the space environment dose is only reduced from 5.4×10^{10} rad-year⁻¹ to 5×10^{10} rad-year⁻¹ while the dose from 16 keV protons is reduced from $5.4 \times 10^{10}F$ rad to $3.85 \times 10^{10}F$ rad. The space elastic energy deposition has only increased from 8×10^{19} keV-cm⁻³-year⁻¹ to 10.6×10^{19} keV-cm⁻³-year⁻¹ while that for the 16 keV protons has doubled to $24 \times 10^{19}F$ keV-cm⁻³. Thus, at 1500-2000 Å depths the equivalences are $Y_{ion} = 0.77F$ years and $Y_d = 2.2F$ years. It is presumed that Y_d is more significant for an indication of the degradation of the reflectance of the surface. If one averages Y_d over a 3000 Å thick layer, a value of 2F is obtained. Therefore, it is suggested that the equivalence of the 16 keV proton beam for synchronous missions be estimated by 2F years.

Outside the magnetosphere the solar wind particle flux of 6×10^{15} protons- cm^{-2} year $^{-1}$ gives only 10^{10} rad/year to the surface. This would give $Y_{\text{ion}} \approx 5.5F$ years. However, the elastic collisions are more important outside the magnetosphere since the solar wind deposits 2.5×10^{20} keV- cm^{-3} year $^{-1}$ by elastic scattering throughout their depth of penetration. This would give $Y_d = 0.5F$ years for a layer $\sim 400 \text{ \AA}$ thick in missions outside the magnetosphere. This equivalence, however, may not be valid because of the gross differences in the thickness of the damaged layer in space from that in the test samples. Considering all factors, an equivalence factor of $0.5 F$ years appears reasonable for relating 16 keV proton test results to the extra-magnetospheric environment.

Based on the above equivalences, a plot was made of the equivalent years in both interplanetary space (1.0 A.U.) and at synchronous orbit (19,300 N. Mi.) as shown in Figure 68. Also given in the figure are the approximate thresholds of solar reflectance degradation due to absorption in the thin Si_2O_3 overcoated mirrors, and blistering on bare aluminum surfaces. The threshold of degradation due to absorption in the Si_2O_3 overcoatings was not accurately established because data points were only taken at 1×10^{15} , 5×10^{15} , and 5×10^{16} protons- cm^{-2} . The maximum degradation appeared to occur between 5×10^{15} and 5×10^{16} protons- cm^{-2} , thus, only a broad band can be shown in the figure. For an interplanetary mission the maximum degradation would then occur in a time period of 0.25 to 2.5 years. Similarly, the maximum damage in synchronous orbit would occur in a 1 to 10 year period. The threshold of degradation for blistering of bare aluminum coated, aluminum substrate mirrors is shown at about 7×10^{16} protons- cm^{-2} .

Since the majority of the nickel substrate mirrors did not blister up to the maximum integrated flux used, the crosshatched area on the graph is shown extending up to 2×10^{17} protons- cm^{-2} .

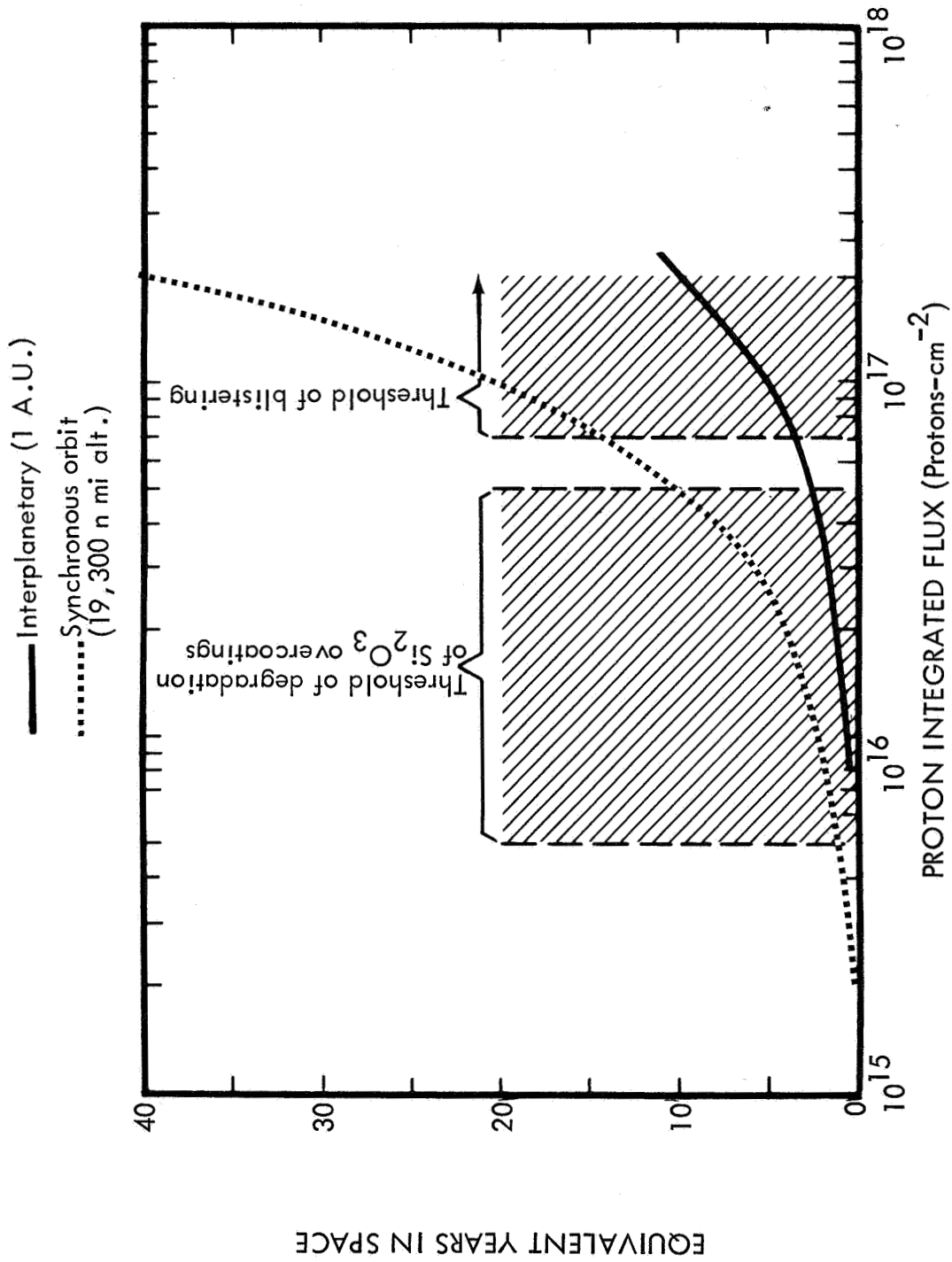


Figure 68: SPACE MISSION EQUIVALENCE FOR 16 keV PROTON TEST DATA

7.0 CONCLUSIONS

As a result of experiments conducted in this program, the following conclusions have been reached:

- 1) Mirror surfaces employing an epoxy surface improvement coating reticulated at high temperatures (80°C maximum for stretch-formed aluminum and 50°C maximum for magnesium-substrate mirrors);
- 2) The most significant mechanism of radiation-induced degradation is proton blistering;
- 3) The amount of optical degradation produced by the blistering phenomena is highly temperature dependent and is a function of the proximity of the stopped protons to the interface at which agglomeration occurs;
- 4) When blistering does not occur, the optical degradation of bare-aluminum and silicon-oxide overcoated surfaces is not strongly temperature dependent and shows saturation at relatively low exposure values;
- 5) The diffuse reflectance of silicon-oxide coated surfaces is reduced by proton bombardment, an effect which is believed to be due to a smoothing of the oxide surface;
- 6) The infrared absorption spectra of vacuum-deposited Si_2O_3 and SiO_2 films changes slightly under proton bombardment; however, the resulting changes in emittance are negligible;
- 7) The calculation of solar specular reflectances from spectral reflectance data measured in-air appears valid with the exception of aluminum-substrate mirrors irradiated with protons at -195°C.

8.0 RECOMMENDATIONS

The following recommendations are presented as a result of research performed in this program:

1) An investigation should be conducted to establish the relationships between vacuum coating conditions and radiation-induced degradation of aluminum- and silicon-oxide films.

2) An investigation should be conducted to determine the mechanism associated with the wavelength shift of interference characteristics during pressure changes and irradiation. Also, other typical optical interference coatings should be evaluated for similar effects.

3) Additional analyses should be performed on electron photomicrographs to correlate blister size distributions and height-to-diameter ratios to proton energies and agglomeration sites.

4) A proton exposure-rate study should be conducted to determine the effect of flux on blister formation and other mechanisms of degradation.

5) Additional work should be conducted to develop polymeric surface improvement coatings for mirror surfaces that can withstand higher temperatures.

6) During preparation of mirror samples, thickness control samples should be prepared from which film thicknesses can be measured with an interferometer.

7) Additional experiments should be conducted to determine the effects of 1 keV protons on solar mirror surfaces.

8) Additional experiments should be conducted to determine the depth of penetration of protons in the energy range of 0.8 to 30 keV.

9) An ultraviolet spectral sensitivity study should be conducted and/or mirror samples should be irradiated with a close-match solar spectrum to determine the validity of tests made in this program with a line-spectrum lamp.

9.0 REFERENCES

1. "60-Inch Stretch-Formed Aluminum Solar Concentrator," NASA CR-47, June 1964.
2. Pichel, M.A.: "Research and Development Techniques for Fabrication of Solar Concentrators," Electro-Optical Systems Inc., Report No. 1587---Final, submitted under Contract NAS7-10, December 1961.
3. Bradford, A. P. and Hass, G.: "Increasing the Far-Ultraviolet Reflectance of Silicon-Oxide-Protected Aluminum Mirrors by Ultraviolet Irradiation," J. Opt. Soc. Am., vol. 53, no. 9, September 1963.
4. Edwards, D. K., Gier, J. T., Nelson, K. E., and Roddick, R. D.: "Integrating Sphere for Imperfectly Diffuse Samples," Applied Optics, vol. 51, November 1961.
5. Arvesen, J. C.: "Spectral Dependence of Ultraviolet-Induced Degradation of Coatings for Spacecraft Thermal Control," AIAA Paper No. 67-340, Presented at the AIAA Thermophysics Specialist Conference, New Orleans, April 1967.
6. Johnson, F. S.: "The Solar Constant," Journal of Meteorology, vol. 11, no. 6, December 1954.
7. Ennos, A. E.: British J. Appl. Phys., vol. 4, p. 101, 1953.
8. Koenig, H., and Helwig, G.: Z. Phys., vol. 129, p. 491, 1951.
9. Ennos, A. E.: British J. Appl. Phys., vol. 5, p. 27, 1954.
10. Hines, R. L.: J. Appl. Phys., vol. 28, no. 5, May 1957.
11. Hines, R. L., and Arndt, R.: Phys. Rev., vol. 119, no. 2, July 1960.
12. Primak, W., and Luthra, J.: J. Appl. Phys., vol. 37, no. 6, May 1966.
13. Dushman, S., and Lafferty, J. M.: Scientific Foundations of Vacuum Technique, 2nd Ed., Wiley & Sons, New York, 1962.
14. Hass, G., Ramsey, J. B., Triolo, J. J., and Albright, H. T.: Thermophysics and Temperature Control of Spacecraft and Entry Vehicles, pp. 47-60, Academic Press, New York, 1966.
15. Bradford, A. P., and Hass, G.: Solar Energy, vol. 9, no. 1, pp. 32-38, January 1965.

REFERENCES (Cont.)

16. Bradford, A. P., Hass, G., McFarland, M., and Ritter, E.: *Applied Optics*, vol. 4, no. 8, pp. 971-976, August 1965.
17. Redus, J. R.: *Sputtering of a Vehicle's Surface in a Space Environment*, NASA TN D-1113, June 1962.
18. Moore, W. J.: "The Ionic Bombardment of Solid Surface," *American Scientist*, June 1960.
19. Wehner, G. K., KenKnight, C., and Rosenberg, D. L.: "Sputtering Rates Under Solar-Wind Bombardment," *Planetary Space Science*, vol. 11, pp. 885-895, 1963.
20. Schroeder, J. B., Bashkin, S., and Nester, J. G.: "Ionic Polishing of Optical Surface," *Applied Optics*, vol. 5, no. 6, June 1966.
21. Gillette, R. B., Brown, R.R., et al.: "Effects of Protons and Alpha Particles on Solar Concentrator Reflective Surface," *Progress in Astronautics and Aeronautics*, vol. 18, Pergamen Press, 1966.
22. Milacek, L. H., and Wolfe, J. R.: "A Study of the Blistering of Metal Surfaces by Solar System Ions," Final Report under Contract NASw-1431, prepared by AVCO Electronics Division, June 1967.
23. Lippincott, E. T.: *J. of Res. of the National Bureau of Standards*, vol. 61, no. 1, p. 66, July 1958.
24. Private communication with Dr. George Hass of the U. S. Army Engineering Research and Development Lab., Ft. Belvoir, Virginia, April 21, 1967.
25. Madden, R. P., Canfield, L. R., and Hass, G.: *J. Opt. Soc. Am.*, vol. 53, no. 5, pp. 620-625, May 1963.
26. Anderson, D. L., and Dahms, R. G.: *J. Spacecraft and Rockets*, vol. 4, no. 3, pp. 364-369, March 1967.
27. Hacskaylo, M., and Giamati, C. C.: "Visible Radiation Damage Effects of 40 Mev Alpha Particles on Sodium Chloride Crystals," NASA TN D-2329, June 1964.
28. Zeller, E. J., Ronca, L. B., and Levy, P. W.: "Proton-Induced Hydroxyl Formation on the Lunar Surface," *Journal of Geophysical Research*, vol. 71, no. 21, October 15, 1966.

REFERENCES (Cont.)

29. Frank, L.: Paper presented at the 48th Annual Meeting of the American Geophysical Union, April 1967.
30. Vette, J. I., NASA SP-3024, vol. III, 1967.
31. Lindhard, J., and Scharff, M., Phys. Rev., vol. 124, no. 128, 1961.
32. Bohr, N.: Math-fys. Medd., vol. 18, no. 8.
33. Nielson, K. O.: Electromagnetically Enriched Isotopes and Mass Spectroscopy, Academic Press, New York, 1956.
34. Van Wijngaarden, A., and Duckworth, H. E.: Can. J. Phys., vol. 40, pp. 1749-1764, 1962.
35. Fermi, E.: Nuclear Physics, University of Chicago Press, Revised Edition, p. 183, 1950.
36. Baroody, E.: Journ. Appl. Phys., vol. 35, p. 2074, 1964.
37. Linnenbom, V. J.: Range-Energy Relations for Protons and Electrons in Al, Si, and SiO₂, Naval Research Lab. Report 5828, Sept. 1962.
38. Young, J. R.: J. Appl. Phys., vol. 27, no. 1, 1956.
39. Roecklin, et al.: ORNL-3702, TID-4500, 1962.

10.0 APPENDICES

APPENDIX A

VACUUM COATING DATA

Sample Type	Sample Numbers	Coating	Pressure (torr)	Coating Thickness (Å)	Deposition Time (sec)	Deposition Rate (Å/sec)	Temperature During Coating (°C)
A	1-4 ⁶	SiO	5×10^{-5}	1500	300	5.0	ambient
A	1-4	Aluminum	1×10^{-5}	1000	10	100	ambient
A	1-15	SiO	5×10^{-5}	1500	420	3.6	ambient
A	1-15	Aluminum	1×10^{-5}	1000	11	91	ambient
A	16-60	SiO	5×10^{-5}	1500	360	4.2	ambient
A	16-60	Aluminum	1×10^{-5}	1000	11	91	ambient
A	61-100 ¹	(Same as A 1-15)					
B	1-5	SiO	5×10^{-5}	1500	300	5.0	ambient
B	1-5	Aluminum	1×10^{-5}	1000	10	100	ambient
B	1-5	Si ₂ O ₃ ²	8×10^{-5}	1820	1500	1.2	ambient
B	1-60	SiO	5×10^{-5}	1500	420	3.6	ambient
B	1-60	Aluminum	1×10^{-5}	1000	11	91	ambient
B	1-60	Si ₂ O ₃ ²	8×10^{-5}	2000	1200	1.7	ambient
B	61-100 ³	(Same as B.1-60)					
C	1-66	Chromium	1×10^{-5}	500	30	16	250
C	1-66	SiO	5×10^{-5}	1500	240	6.3	250
C	1-66	Aluminum	5×10^{-6}	1000	10	100	100
C	67-100	(Same as C 1-66)					
C	1a-16a ⁴	Chromium	1×10^{-5}	500	25	20	270
C	1a-16a	SiO	5×10^{-5}	1500	270	5.6	270

APPENDIX A (Cont.)

Sample Type	Sample Numbers	Coating	Pressure (torr)	Coating Thickness (Å)	Deposition Time (sec)	Deposition Rate (Å/sec)	Temperature During Coating (°C)
C	1a-16a	Aluminum	1×10^{-5}	1000	12	83	100
C	17a-40a	Chromium	1×10^{-5}	500	30	17	270
C	17a-40a	SiO	5×10^{-5}	1500	300	5.0	270
C	17a-40a	Aluminum	5×10^{-6}	1000	10	100	80
D	1-66	Chromium	1×10^{-5}	500	30	16	250
D	1-66	SiO	5×10^{-5}	1500	240	6.3	250
D	1-66	Aluminum	5×10^{-6}	1000	10	100	100
D	1-66	Si ₂ O ₃	8×10^{-5}	2000	1200	1.7	100
D	67-155	(Same as D 1-66)					
D(A)	1a-16a	Chromium	1×10^{-5}	500	30	17	270
D(A)	1a-16a	SiO	5×10^{-5}	1500	300	5.0	270
D(A)	1a-16a	Aluminum	1×10^{-5}	1000	12	83	80
D(A)	1a-16a	Si ₂ O ₃	8×10^{-5}	1820	1260	1.4	80
D(A)	17a-34a	Chromium	1×10^{-5}	500	30	17	270
D(A)	17a-34a	SiO	5×10^{-5}	1500	300	5.0	270
D(A)	17a-34a	Aluminum	5×10^{-6}	1000	10	100	80
D(A)	17a-34a	Si ₂ O ₃	8×10^{-5}	1820	1500	1.2	80
E	1a-30a	Chromium	1×10^{-5}	500	45	11	200
E	1a-30a	SiO	5×10^{-5}	1500	270	5.5	200
E	1a-30a	Aluminum	1×10^{-5}	1000	15	67	100
E	1a-30a	Si ₂ O ₃	1×10^{-4}	8000	6600	1.2	100
E	31a-36a	(Same as E 1a-30a)					

APPENDIX A (Cont.)

Sample Type	Sample Numbers	Coating	Pressure (torr)	Coating Thickness (Å)	Deposition Time (sec)	Deposition Rate (Å/sec)	Temperature During Coating (°C)
F	1a-30a	Chromium	1×10^{-5}	500	45	11	200
F	1a-30a	SiO	5×10^{-5}	1500	270	5.5	200
F	1a-30a	Aluminum	1×10^{-5}	1000	30-40	25-33	100
F	1a-30a	SiO ₂	1×10^{-4}	² 17000	3000	5.6	100
F	31a-36a	⁶ (Same as F 1a-30a)					
G	1 to 58	SiO	8×10^{-5}	1528 ⁷	unknown	100	ambient
G	1 to 58	Aluminum	5×10^{-5}	1000	5	200	ambient
G	1 to 58	Si ₂ O ₃	8×10^{-5}	1400 ²	280	5	50

- ¹ Sample Nos A97-A100 are NASA samples
- ² Backfilled with oxygen dynamically
- ³ Sample Nos B96-B100 are NASA samples
- ⁴ Sample Nos C11-C16 are NASA samples
- ⁵ Sample Nos D11-D16 are NASA samples
- ⁶ NASA samples
- ⁷ 1/2 wave at 5500Å. Physical thickness calculated assuming a refractive index of 1.8
- ⁸ 1/2 wave at 5500Å. Physical thickness measured by interferometry

APPENDIX B

ULTRAVIOLET TEST DATA

Sample No.	Exposure Time (Hrs)	Exposure Rate (ESS)*	Total Exposure (ESSH)**	Sample Temperature (°C)	Solar Specular Reflectance (R _S)	Change In Reflectance (-ΔR _S)***
A75	0	-	-	-	0.894	-
A75	240	11.0	2640	0	0.865	0.029
A78	0	-	-	-	0.894	-
A78	240	9.9	2380	0	0.870	0.024
A73	0	-	-	-	0.894	-
A73	240	8.4	2020	0	0.869	0.025
A72	0	-	-	-	0.894	-
A72	240	11.2	2690	50	0.851	0.043
A63	0	-	-	-	0.894	-
A63	240	11.1	2660	50	0.864	0.030
A76	0	-	-	-	0.894	-
A76	240	11.0	2640	50	0.860	0.034
B7	0	-	-	-	0.863	-
B7	50	11.1	555	-195	0.867	-0.004
B7	100	11.1	1110	-195	0.845	0.018
B7	200	11.1	2220	-195	0.834	0.029
B7	308	11.1	3420	-195	0.836	0.027
B7	875	11.1	9710	-195	0.818	0.045
B8	0	-	-	-	0.865	-
B8	50	11.2	560	-195	0.869	-0.004
B8	100	11.2	1120	-195	0.838	0.027
B8	200	11.2	2240	-195	0.839	0.026
B8	308	11.2	3450	-195	0.850	0.015
B8	875	11.2	9800	-195	0.812	0.053
B9	0	-	-	-	0.866	-
B9	50	11.2	560	-195	0.858	0.008
B9	100	11.2	1120	-195	0.839	0.027
B9	200	11.2	2240	-195	0.828	0.038
B9	308	11.2	3450	-195	0.840	0.026
B9	875	11.2	9800	-195	0.820	0.046
B4	0	-	-	-	0.865	-
B4	50	11.1	555	0	0.862	0.003
B4	100	11.1	1110	0	0.849	0.016
B4	200	11.1	2220	0	0.836	0.029
B4	308	11.1	3420	0	0.827	0.038
B4	875	11.1	9710	0	0.796	0.069

APPENDIX B (Cont.)

Sample No.	Exposure Time (Hrs)	Exposure Rate (ESS)*	Total Exposure (ESSH)**	Sample Temperature (°C)	Solar Specular Reflectance (R_S)	Change In Reflectance ($-\Delta R_S$)***
B5	0	-	-	-	0.864	-
B5	50	11.2	560	0	0.861	0.003
B5	100	11.2	1120	0	0.854	0.010
B5	200	11.2	2240	0	0.836	0.028
B5	308	11.2	3450	0	0.831	0.033
B5	875	11.2	9800	0	0.800	0.064
B6	0	-	-	-	0.865	-
B6	50	11.2	560	0	0.845	0.020
B6	100	11.2	1120	0	0.815	0.050
B6	200	11.2	2240	0	0.835	0.030
B6	308	11.2	3450	0	0.817	0.048
B6	875	11.2	9800	0	0.811	0.054
B1	0	-	-	-	0.864	-
B1	50	11.1	555	100	0.628	0.236
B1	100	11.1	1110	100	0.642	0.222
B1	200	11.1	2220	100	0.605	0.259
B1	308	11.1	3420	100	0.582	0.282
B1	875	11.1	9710	100	0.571	0.293
B2	0	-	-	-	0.841	-
B2	50	11.2	560	100	0.751	0.090
B2	100	11.2	1120	100	0.643	0.198
B2	200	11.2	2240	100	0.647	0.194
B2	308	11.2	3450	100	0.641	0.200
B2	875	11.2	9800	100	0.557	0.284
B3	0	-	-	-	0.867	-
B3	50	11.2	560	100	0.823	0.044
B3	100	11.2	1120	100	0.741	0.026
B3	200	11.2	2240	100	0.757	0.110
B3	308	11.2	3450	100	0.740	0.127
B3	875	11.2	9800	100	0.551	0.316
C2	0	-	-	-	0.897	-
C2	50	11.1	555	-195	0.894	0.003
C2	100	11.1	1110	-195	0.884	0.013
C2	200	11.1	2220	-195	0.878	0.019
C2	308	11.1	3420	-195	0.855	0.042
C2	875	11.1	9710	-195	0.874	0.023

APPENDIX B (Cont.)

Sample No.	Exposure Time (Hrs)	Exposure Rate (ESS)*	Total Exposure (ESSH)**	Sample Temperature (°C)	Solar Specular Reflectance (R _S)	Change In Reflectance (-ΔR _S)***
C9A	0	-	-	-	0.853	-
C9A	50	10.9	545	-195	0.834	0.019
C9A	100	10.9	1090	-195	0.825	0.028
C9A	200	10.9	2180	-195	0.802	0.051
C9A	308	10.9	3360	-195	0.808	0.045
C9A	875	10.9	9540	-195	0.789	0.064
C8A	0	-	-	-	0.848	-
C8A	50	10.8	540	-195	0.830	0.018
C8A	100	10.8	1080	-195	0.805	0.043
C8A	200	10.8	2020	-195	0.800	0.048
C8A	308	10.8	3330	-195	0.826	0.022
C8A	875	10.8	9450	-195	0.795	0.053
C1	0	-	-	-	0.898	-
C1	50	11.1	555	0	0.891	0.007
C1	100	11.1	1110	0	0.888	0.010
C1	200	11.1	2220	0	0.874	0.024
C1	308	11.1	3420	0	0.879	0.019
C1	875	11.1	9710	0	0.873	0.025
C5A	0	-	-	-	0.845	-
C5A	50	10.9	545	0	0.818	0.027
C5A	100	10.9	1090	0	0.805	0.040
C5A	200	10.9	2180	0	0.795	0.050
C5A	308	10.9	3360	0	0.809	0.036
C5A	875	10.9	9540	0	0.805	0.040
C6A	0	-	-	-	0.842	-
C6A	50	10.8	540	0	0.820	0.022
C6A	100	10.8	1080	0	0.807	0.035
C6A	200	10.8	2020	0	0.796	0.046
C6A	308	10.8	3330	0	0.805	0.037
C6A	875	10.8	9450	0	0.794	0.048
C99	0	-	-	-	0.870	-
C99	50	11.1	555	100	0.865	0.005
C99	100	11.1	1110	100	0.858	0.012
C99	200	11.1	2220	100	0.856	0.014
C99	308	11.1	3420	100	0.855	0.015
C99	875	11.1	9710	100	0.836	0.034

APPENDIX B (Cont.)

Sample No.	Exposure Time (Hrs)	Exposure Rate (ESS)*	Total Exposure (ESSH)**	Sample Temperature (°C)	Solar Specular Reflectance (R _S)	Change In Reflectance (-ΔR _S)***
C3A	0	-	-	-	0.847	-
C3A	50	10.9	545	100	0.826	0.021
C3A	100	10.9	1090	100	0.821	0.026
C3A	200	10.9	2180	100	0.811	0.036
C3A	308	10.9	3360	100	0.813	0.034
C3A	875	10.9	9540	100	0.799	0.048
C4A	0	-	-	-	0.844	-
C4A	50	10.8	540	100	0.824	0.020
C4A	100	10.8	1080	100	0.821	0.023
C4A	200	10.8	2020	100	0.802	0.042
C4A	308	10.8	3330	100	0.814	0.030
C4A	875	10.8	9450	100	0.800	0.044
C5	0	-	-	-	0.893	-
C5	50	11.1	555	200	0.889	0.004
C5	100	11.1	1110	200	0.886	0.007
C5	200	11.1	2220	200	0.884	0.009
C5	308	11.1	3420	200	0.834	0.059
C5	875	11.1	9710	200	Data Missing	
C1A	0	-	-	-	0.846	-
C1A	50	10.9	545	200	0.809	0.037
C1A	100	10.9	1090	200	0.802	0.044
C1A	200	10.9	2180	200	0.783	0.063
C1A	308	10.9	3360	200	0.780	0.066
C1A	875	10.9	9540	200	0.724	0.122
C2A	0	-	-	-	0.842	-
C2A	50	10.8	540	200	0.817	0.025
C2A	100	10.8	1080	200	0.815	0.027
C2A	200	10.8	2020	200	0.801	0.041
C2A	308	10.8	3330	200	0.822	0.020
C2A	875	10.8	9450	200	0.812	0.030
D34A	0	-	-	-	0.875	-
D34A	240	8.5	2040	0	0.816	0.059
D27A	0	-	-	-	0.875	-
D27A	240	11.1	2660	0	0.834	0.041
D19A	0	-	-	-	0.875	-
D19A	240	11.2	2690	0	0.827	0.048
D24A	0	-	-	-	0.875	-
D24A	240	10.9	2620	50	0.821	0.054

APPENDIX B (Cont.)

Sample No.	Exposure Time (Hrs)	Exposure Rate (ESS)*	Total Exposure (ESSH)**	Sample Temperature (°C)	Solar Specular Reflectance (R_S)	Change In Reflectance ($-\Delta R_S$ ***)
D32A	0	-	-	-	0.875	-
D32A	240	11.1	2660	50	0.824	0.051
D30A	0	-	-	-	0.875	-
D30A	240	11.2	2690	50	0.818	0.057
D21A	0	-	-	-	0.875	-
D21A	240	10.9	2620	200	0.844	0.031
D22A	0	-	-	-	0.875	-
D22A	240	11.1	2660	200	0.852	0.023
D18A	0	-	-	-	0.875	-
D18A	240	11.2	2690	200	0.848	0.027
E11	0	-	-	-	0.764	-
E11	240	10	2400	0	0.757	0.007
E18	0	-	-	-	0.764	-
E18	240	10.8	2590	0	0.762	0.002
F8	0	-	-	-	0.756	-
F8	120	11.2	1340	0	bad data	-
F8	360	11.2	4030	0	0.743	0.013
F22	0	-	-	-	0.758	-
F22	120	11.1	1330	0	0.775	-0.017
F22	360	11.1	3990	0	0.744	0.014
F19	0	-	-	-	0.734	-
F19	120	11.2	1340	0	0.730	0.004
G29	0	-	-	-	0.830	-
G29	120	10.9	1310	-195	0.827	0.003
G29	360	10.9	3930	-195	0.747	0.083
G30	0	0	0	0	0.830	-
G30	120	10.8	1300	-195	bad data	-
G30	360	10.8	3890	-195	0.750	0.08
G14	0	0	0	0	0.830	0
G14	120	10.5	1260	-195	bad data	-
G14	360	10.5	3780	-195	0.737	0.093
G16	0	-	-	-	0.830	-
G16	120	10.9	1310	0	0.830	0
G16	360	10.9	3930	0	0.606	0.224
G31	0	-	-	-	0.830	-
G31	120	10.8	1296	0	0.810	0.020
G31	360	10.8	3890	0	0.669	0.151
G13	0	-	-	-	0.830	-
G13	120	9.9	1190	0	bad data	-
G13	360	9.9	3570	0	0.582	0.261
G11	0	-	-	-	0.830	-
G11	120	10.9	1310	50°	0.538	0.292

APPENDIX B (Cont.)

Sample No.	Exposure Time (hr)	Exposure Rate (ESS)*	Exposure (ESSH)**	Sample Temperature (°C)	Solar Specular Reflectance (R _S)	Change In Reflectance (-ΔR _S)***
G11	360	10.9	3930	50	0.271	0.559
G28	0	--	--	--	0.830	--
G28	120	10.8	1300	50	0.805	0.025
G28	360	10.8	3890	50	0.715	0.115
G42	0	--	--	--	0.830	--
G42	120	10.5	1260	50	0.797	0.033
G42	360	10.5	3780	50	0.628	0.202
A61	1	Before	Protons	--	0.895	--
A61	0	(after protons & before UV)		--	0.882	0.013
A61	240	8.4	2020	50	0.847	0.035
B60	1	Before	Protons	--	0.871	--
B60	0	(after protons & before UV)		--	0.854	0.017
B60	120	11.1	1330	0	0.827	0.027
B60	360	9.9	3710	50	0.807	0.047
C60	1	Before	Protons	--	0.896	--
C60	0	(after protons & before UV)		--	0.896	0
C60	120	11	1320	0	0.888	0.008
C60	360	10	3720	50	0.854	0.042
D54	1	Before	Protons	--	0.78	--
D54	0	(after protons & before UV)		--	0.759	0.021
D54	240	8.5	2040	50	0.727	0.032
D20A	2	Before ultraviolet in air		10	--	--
D20A		Before ultraviolet in vacuum		10	--	0
D20A	68	7.0	476	10	--	0.016
D20A		After ultraviolet in air		10	--	0
E21	2	Before ultraviolet in air		10	--	--
E21		Before ultraviolet in vacuum		10	--	0
E21	73	7.5	550	10	--	0
E21		After ultraviolet in air		10	--	0

* Exposure rate is given in equivalent space suns (ESS) in the wavelength region less than 4000 angstroms

** Total exposure is given in equivalent space sun hours (ESSH)

*** For tabulation simplicity a decrease in absolute solar specular reflectance is shown as a positive value

1 Exposed to protons and ultraviolet radiation sequentially

2 Data from in-situ reflectance measurement experiment

APPENDIX B (Cont.)

Sample No.	Exposure Time (hr)	Exposure Rate (ESS)*	Exposure (ESSH)**	Sample Temperature (°C)	Solar Specular Reflectance (R _S)	Change In Reflectance (-ΔR _S)***
F23	2			10	--	--
F23				10	--	0
F23	115	7.0	805	10	--	0
F23				10	--	0

* Exposure rate is given in equivalent space suns (ESS) in the wavelength region less than 4000 angstroms

** Total exposure is given in equivalent space sun hours (ESSH)

*** For tabulation simplicity a decrease in absolute solar specular reflectance is shown as a positive value

1 Exposed to protons and ultraviolet radiation sequentially

2 Data from in-situ reflectance measurement experiment

APPENDIX C

PROTON TEST DATA

Sample No.	Proton Energy (keV)	Integrated Flux (Protons-cm ⁻²)	Sample Temperature (°C)	Solar Specular Reflectance (R _S)		Change in Reflectance (-ΔR _S)
				Before	After	
A16	2	1 x 10 ¹⁵	0	0.887	0.889	-0.002
A17	2	1 x 10 ¹⁵	0	0.889	0.890	-0.001
A18	2	1 x 10 ¹⁵	0	0.895	0.894	0.001
A19	2	5 x 10 ¹⁵	0	0.899	0.893	0.006
A25	2	5 x 10 ¹⁶	0	0.900	0.880	0.020
A22	4	5 x 10 ¹⁵	0	0.898	0.887	0.011
A23	4	5 x 10 ¹⁶	0	0.896	0.882	0.014
A24	8	5 x 10 ¹⁶	0	0.901	0.892	0.009
A32	14	1 x 10 ¹⁷	0	0.886	0.876	0.010
A41	16	5 x 10 ¹⁶	-195	0.896	0.880	0.016
A46	16	5 x 10 ¹⁶	-195	0.864	0.867	0.000
A12	16	5 x 10 ¹⁶	-195	0.892	0.860	0.032
A52	16	1 x 10 ¹⁷	-195	0.891	0.712	0.179
A54	16	1 x 10 ¹⁷	-195	0.901	0.859	0.042
A28	16	1 x 10 ¹⁷	-195	0.896	0.883	0.013
A65	16	2 x 10 ¹⁷	-195	0.891	0.680	0.211
A64	16	2 x 10 ¹⁷	-195	0.891	0.762	0.129
A31	16	2 x 10 ¹⁷	-195	0.892	0.375	0.517
A61	16	5 x 10 ¹⁶	0	0.908	0.882	0.026
A32	16	1 x 10 ¹⁷	0	0.887	0.876	0.011
A45	16	1 x 10 ¹⁷	0	0.881	0.886	-0.005
A15	16	1 x 10 ¹⁷	0	0.897	0.850	0.047
A13	16	1 x 10 ¹⁷	0	0.891	0.828	0.063
A62	16	2 x 10 ¹⁷	0	0.895	0.895	0
A50	16	2 x 10 ¹⁷	0	0.895	0.852	0.043
A26	16	2 x 10 ¹⁷	0	0.899	0.741	0.158
A44	16	5 x 10 ¹⁶	50	0.891	0.846	0.045
A59	16	5 x 10 ¹⁶	50	0.890	0.889	0.001
A38	16	5 x 10 ¹⁶	50	0.889	0.877	0.012
A35	16	1 x 10 ¹⁷	50	0.895	0.194	0.701
A49	16	1 x 10 ¹⁷	50	0.886	0.159	0.727



APPENDIX C (Cont.)

Sample No.	Proton Energy (keV)	Integrated Flux (Protons-cm ⁻²)	Sample Temperature (°C)	Solar Specular Reflectance (R _S)		Change in Reflectance (-ΔR _S)
				Before	After	
A30	16	1 x 10 ¹⁷	50	0.894	0.363	0.531
A42	16	2 x 10 ¹⁷	50	0.936	Bad Data	Bad Data
A43	16	2 x 10 ¹⁷	50	0.905	0.111	0.794
A29	16	2 x 10 ¹⁷	50	0.897	0.065	0.832
A36	16	5 x 10 ¹⁶	100	0.890	0.120	0.770
A39	0	0	80	0.897	0.757	0.140
A37	0	0	80	0.897	0.613	0.284
A51	16	5 x 10 ¹⁶	0	0.891	0.712	0.179
A27	16	5 x 10 ¹⁶	0	0.902	0.883	0.019
B17	2	1 x 10 ¹⁵	0	0.868	0.867	0.001
B18	2	1 x 10 ¹⁵	0	0.865	0.864	0.001
B19	2	1 x 10 ¹⁵	0	0.874	0.867	0.007
B12	2	5 x 10 ¹⁵	0	0.873	0.866	0.007
B16	2	5 x 10 ¹⁶	0	0.870	0.856	0.014
B13	4	5 x 10 ¹⁵	0	0.868	0.859	0.007
B15	4	5 x 10 ¹⁶	0	0.873	0.866	0.007
B20	8	5 x 10 ¹⁶	0	0.876	0.857	0.019
B31	14	1 x 10 ¹⁷	0	0.866	0.833	0.033
B91	16	5 x 10 ¹⁶	-195	0.869	0.830	0.039
B53	16	5 x 10 ¹⁶	-195	0.865	0.796	0.069
B29	16	5 x 10 ¹⁶	-195	0.866	0.851	0.015
B80	16	1 x 10 ¹⁷	-195	0.870	0.800	0.070
B59	16	1 x 10 ¹⁷	-195	0.863	0.786	0.077
B23	16	1 x 10 ¹⁷	-195	0.863	0.827	0.036
B34	16	2 x 10 ¹⁷	-195	0.872	0.717	0.155
B64	16	2 x 10 ¹⁷	-195	0.870	0.670	0.200
B10	16	2 x 10 ¹⁷	-195	0.871	0.712	0.159
B54	16	5 x 10 ¹⁶	0	0.868	0.858	0.010
B60	16	5 x 10 ¹⁶	0	0.871	0.827	0.044
B14	16	5 x 10 ¹⁶	0	0.865	0.842	0.023
B38	16	1 x 10 ¹⁷	0	0.864	0.844	0.020

APPENDIX C (Cont.)

Sample No.	Proton Energy (keV)	Integrated Flux (Protons-cm ⁻²)	Sample Temperature (°C)	Solar Specular Reflectance(R _S)		Change in Reflectance (- ΔR _S)
				Before	After	
B81	16	1 x 10 ¹⁷	0	0.870	0.812	0.058
B21	16	1 x 10 ¹⁷	0	0.870	0.847	0.023
B33	16	1 x 10 ¹⁷	0	0.863	0.842	0.021
B75	16	5 x 10 ¹⁶	50	0.863	0.845	0.018
B76	16	5 x 10 ¹⁶	50	0.873	0.835	0.038
B28	16	5 x 10 ¹⁶	50	0.871	0.844	0.027
B37	16	1 x 10 ¹⁷	50	0.859	0.843	0.016
B35	16	1 x 10 ¹⁷	50	0.868	0.838	0.030
B11	16	1 x 10 ¹⁷	50	0.873	0.810	0.063
B24	16	2 x 10 ¹⁷	50	0.871	0.827	0.044
B47	16	2 x 10 ¹⁷	0	0.872	0.761	0.111
B48	16	2 x 10 ¹⁷	0	0.866	0.685	0.181
B22	16	2 x 10 ¹⁷	0	0.857	0.339	0.518
B26	16	2 x 10 ¹⁷	50	0.871	0.807	0.064
B27	16	2 x 10 ¹⁷	50	0.868	0.829	0.039
B30	16	2 x 10 ¹⁷	100	0.869	0.468	0.401
B32	0	0	100	0.867	0.749	0.118
C14	2	1 x 10 ¹⁵	0	0.892	0.892	0
C16	2	1 x 10 ¹⁵	0	0.898	0.893	0.005
C17	2	1 x 10 ¹⁵	0	0.892	0.892	0
C18	2	1 x 10 ¹⁵	0	0.897	0.895	0.002
C4	2	5 x 10 ¹⁵	0	0.890	0.883	0.007
C7	2	5 x 10 ¹⁶	0	0.895	0.889	0.006
C10	2	1 x 10 ¹⁷	0	0.892	0.883	0.009
C6	4	5 x 10 ¹⁶	0	0.892	0.890	0.002
C8	8	5 x 10 ¹⁶	0	0.883	0.883	0
C71	16	5 x 10 ¹⁶	-195	0.886	0.889	-0.003
C44	16	5 x 10 ¹⁶	-195	0.892	0.886	0.006
C28	16	5 x 10 ¹⁶	-195	0.891	0.886	0.005
C55	16	1 x 10 ¹⁷	-195	0.892	0.864	0.028
C53	16	1 x 10 ¹⁷	-195	0.889	0.885	0.004

APPENDIX C (Cont.)

Sample No.	Proton Energy (keV)	Integrated Flux (Protons-cm ⁻²)	Sample Temperature (°C)	Solar Specular Reflectance(R _S)		Change in Reflectance (- ΔR _S)
				Before	After	
C24	16	1 x 10 ¹⁷	-195	0.893	0.886	0.007
C76	16	2 x 10 ¹⁷	-195	0.873	0.831	0.042
C56	16	2 x 10 ¹⁷	-195	0.890	0.871	0.019
C22	16	2 x 10 ¹⁷	-195	0.893	0.890	0.003
C60	16	5 x 10 ¹⁶	0	0.894	0.867	0.027
C9	16	5 x 10 ¹⁶	0	0.889	0.888	0.001
C59	16	1 x 10 ¹⁷	0	0.894	0.890	0.004
C54	16	1 x 10 ¹⁷	0	0.894	0.886	0.008
C36	16	1 x 10 ¹⁷	0	0.894	0.887	0.007
C26 	16	1 x 10 ¹⁷	0	0.888	0.887	0.001
C31 	16	1 x 10 ¹⁷	0	0.896	0.888	0.008
C40	16	2 x 10 ¹⁷	0	0.892	0.880	0.012
C39	16	2 x 10 ¹⁷	0	0.897	0.884	0.013
C27	16	2 x 10 ¹⁷	0	0.885	0.865	0.020
C35	16	5 x 10 ¹⁶	50	0.894	0.809	0.085
C57	16	5 x 10 ¹⁶	100	0.891	0.883	0.008
C47	16	5 x 10 ¹⁶	100	0.891	0.887	0.004
C29	16	5 x 10 ¹⁶	100	0.894	0.892	0.002
C72	16	1 x 10 ¹⁷	100	0.856	0.878	-0.022
C58	16	1 x 10 ¹⁷	100	0.891	0.883	0.008
C25	16	1 x 10 ¹⁷	100	0.891	0.887	0.004
C43	16	2 x 10 ¹⁷	100	0.899	0.881	0.018
C33	16	2 x 10 ¹⁷	100	0.894	0.875	0.019
C52	16	5 x 10 ¹⁶	200	0.891	0.887	0.004
C42	16	5 x 10 ¹⁶	200	0.887	-	-
C30	16	5 x 10 ¹⁶	200	0.894	0.884	0.010
C45	16	1 x 10 ¹⁷	200	0.888	0.892	-0.004
C50	16	1 x 10 ¹⁷	200	0.892	0.880	0.012
C3	16	1 x 10 ¹⁷	200	0.897	0.886	0.011
C48	16	2 x 10 ¹⁷	200	0.895	-	-
C49	16	2 x 10 ¹⁷	200	0.892	-	-

APPENDIX C (Cont.)

Sample No.	Proton Energy (keV)	Integrated Flux (Protons-cm ⁻²)	Sample Temperature (°C)	Solar Specular Reflectance(R _S)		Change in Reflectance (-ΔR _S)
				Before	After	
C34	16	2 x 10 ¹⁷	200	0.897	0.888	0.009
C34	16	2 x 10 ¹⁷	200	0.897	0.879	0.018
D3	2	1 x 10 ¹⁵	0	0.591	0.605	-0.014
D4	2	1 x 10 ¹⁵	0	0.608	0.619	-0.011
D5	2	1 x 10 ¹⁵	0	0.722	0.719	0.003
D6	2	5 x 10 ¹⁵	0	0.578	0.573	0.005
D8	2	5 x 10 ¹⁶	0	0.523	0.506	0.017
D23	2	1 x 10 ¹⁷	0	0.715	0.681	0.034
D7	4	5 x 10 ¹⁶	0	0.678	0.668	0.010
D18	4	1 x 10 ¹⁷	0	0.751	0.737	0.014
D13	8	5 x 10 ¹⁶	0	0.575	0.509	0.074
D16	8	1 x 10 ¹⁷	0	0.728	0.712	0.016
D26	28	1 x 10 ¹⁷	0	0.635	0.494	0.141
D24	30	1 x 10 ¹⁷	0	0.616	0.521	0.095
D89	16	5 x 10 ¹⁶	-195	0.767	0.762	0.005
D59	16	5 x 10 ¹⁶	-195	0.787	0.790	-0.003
D25	16	5 x 10 ¹⁶	-195	0.616	0.592	0.024
D42	16	1 x 10 ¹⁷	-195	0.786	0.790	-0.004
D19	16	1 x 10 ¹⁷	-195	0.532	0.522	0.010
D76	16	1 x 10 ¹⁷	-195	0.761	0.752	0.009
D39	16	2 x 10 ¹⁷	-195	0.789	0.783	0.006
D40	16	2 x 10 ¹⁷	-195	0.796	0.791	0.005
D33	16	2 x 10 ¹⁷	-195	0.783	0.755	0.028
D74	16	5 x 10 ¹⁶	0	0.765	0.720	0.045
D11	16	5 x 10 ¹⁶	0	0.464	0.421	0.043
D54	16	5 x 10 ¹⁶	0	0.780	0.759	0.021
D50	16	1 x 10 ¹⁷	0	0.785	0.759	0.026
D15	16	1 x 10 ¹⁷	0	0.769	0.711	0.058
D72	16	1 x 10 ¹⁷	0	0.745	0.719	0.026
D14	16	1 x 10 ¹⁷	0	0.607	0.603	0.004
D20	16	1 x 10 ¹⁷	0	0.655	0.655	0

APPENDIX C (Cont.)

Sample No.	Proton Energy (keV)	Integrated Flux (Protons-cm ⁻²)	Sample Temperature (°C)	Solar Specular Reflectance (R _S)		Change in Reflectance (- ΔR _S)
				Before	After	
D47	16	2 x 10 ¹⁷	0	0.787	0.759	0.028
D21	16	2 x 10 ¹⁷	0	0.676	0.593	0.083
D43	16	2 x 10 ¹⁷	0	0.777	0.748	0.029
D58	16	5 x 10 ¹⁶	100	0.758	0.742	0.016
D37	16	5 x 10 ¹⁶	100	0.758	0.742	0.016
D46	16	5 x 10 ¹⁶	100	0.781	0.760	0.021
D56	16	1 x 10 ¹⁷	100	0.774	0.740	0.034
D31	16	1 x 10 ¹⁷	100	0.791	0.761	0.030
D57	16	1 x 10 ¹⁷	100	0.778	0.749	0.029
D30	16	2 x 10 ¹⁷	100	0.468	0.421	0.047
D27	16	2 x 10 ¹⁷	100	0.763	0.717	0.046
D38	16	2 x 10 ¹⁷	100	0.799	0.755	0.044
D52	16	5 x 10 ¹⁶	200	0.763	0.745	0.018
D29	16	5 x 10 ¹⁶	200	0.745	0.733	0.012
D75	16	5 x 10 ¹⁶	200	0.754	0.731	0.023
D49	16	1 x 10 ¹⁷	200	0.780	0.761	0.019
D45	16	1 x 10 ¹⁷	200	0.776	0.745	0.031
D32	16	1 x 10 ¹⁷	200	0.786	0.757	0.029
D48	16	2 x 10 ¹⁷	200	0.781	0.737	0.044
D60	16	2 x 10 ¹⁷	200	0.784	0.740	0.044
D28	16	2 x 10 ¹⁷	200	0.538	0.494	0.042
D17A	16	5 x 10 ¹⁶	0	0.802	0.778	0.024
D29A	16	1 x 10 ¹⁷	0	0.733	0.705	0.028
D26A	16	2 x 10 ¹⁷	0	0.730	0.675	0.055
E25	16	5 x 10 ¹⁶	0	0.748	0.747	0.001
E26	16	5 x 10 ¹⁶	0	0.771	0.771	0
E28	16	5 x 10 ¹⁶	0	0.763	0.765	-0.002
E4	16	1 x 10 ¹⁷	0	0.772	0.751	0.021
E24	16	1 x 10 ¹⁷	0	0.758	0.749	0.009
E6	16	2 x 10 ¹⁷	0	0.760	0.727	0.033
E1	16	2 x 10 ¹⁷	0	0.767	0.751	0.016

APPENDIX C (Cont.)

Sample No.	Proton Energy (keV)	Integrated Flux (Protons-cm ⁻²)	Sample Temperature (°C)	Solar Specular Reflectance(R _S)		Change in Reflectance (- ΔR _S)
				Before	After	
E2	16	2 x 10 ¹⁷	0	0.756	0.738	0.018
F1	16	5 x 10 ¹⁶	0	0.781	0.792	-0.011
F3	16	5 x 10 ¹⁶	0	0.756	0.766	-0.010
F11	16	5 x 10 ¹⁶	0	0.747	0.772	-0.025
F4	16	1 x 10 ¹⁷	0	0.761	0.772	-0.011
F13	16	1 x 10 ¹⁷	0	0.756	0.769	-0.013
F14	16	1 x 10 ¹⁷	0	0.750	0.769	-0.019
F7	16	2 x 10 ¹⁷	0	0.754	0.738	0.016
F2	16	2 x 10 ¹⁷	0	0.762	0.740	0.022
F9	16	2 x 10 ¹⁷	0	0.748	0.752	-0.004
G2	16	5 x 10 ¹⁶	0	0.838	0.795	0.043
G5	16	5 x 10 ¹⁶	0	0.838	0.804	0.024
G9	16	5 x 10 ¹⁶	0	0.838	0.802	0.039
G1	16	1 x 10 ¹⁷	0	0.838	0.793	0.045
G6	16	1 x 10 ¹⁷	0	0.838	0.805	0.033
G7	16	1 x 10 ¹⁷	0	0.838	0.786	0.052
G3	16	2 x 10 ¹⁷	0	0.838	0.789	0.049
G8	16	2 x 10 ¹⁷	0	0.838	0.801	0.037
G20	16	2 x 10 ¹⁷	0	0.838	0.792	0.046
G21	16	5 x 10 ¹⁶	40	0.838	0.799	0.039
G32	16	5 x 10 ¹⁶	40	0.838	0.809	0.029
G37	16	5 x 10 ¹⁶	40	0.838	0.783	0.055
G18	16	1 x 10 ¹⁷	40	0.838	0.788	0.038
G33	16	1 x 10 ¹⁷	40	0.838	0.794	0.044
G34	16	1 x 10 ¹⁷	40	0.838	0.814	0.022
G22	16	2 x 10 ¹⁷	40	0.838	0.787	0.051
G23	16	2 x 10 ¹⁷	40	0.838	0.778	0.060
G35	16	2 x 10 ¹⁷	40	0.838	0.781	0.057
G15	16	5 x 10 ¹⁶	-195	0.837	0.843	-0.006
G50	16	5 x 10 ¹⁶	-195	0.827	0.831	-0.004

APPENDIX C (Cont.)

Sample No.	Proton Energy (keV)	Integrated Flux (Protons-cm ⁻²)	Sample Temperature (°C)	Solar Specular Reflectance(R _S)		Change in Reflectance (-ΔR _S)
				Before	After	
G26	16	1 x 10 ¹⁷	-195	0.828	0.822	0.006
G39	16	1 x 10 ¹⁷	-195	0.828	0.820	0.008
G40	16	1 x 10 ¹⁷	-195	0.829	0.816	0.013
G38	16	2 x 10 ¹⁷	-195	0.838	0.803	0.035
G4	16	2 x 10 ¹⁷	-195	0.828	0.823	0.005
G10	16	2 x 10 ¹⁷	-195	0.830	0.828	0.002

1 ▸ Irradiated at 30 degrees from normal

2 ▸ Irradiated at 60 degrees from normal

ABSTRACT

The effects of proton and ultraviolet radiation on the specular and diffuse reflectance of stretch-formed aluminum, electroformed nickel and magnesium substrate solar mirrors were studied in high vacuum at temperatures from -195° to 200°C and energies from 2 to 30 keV. Ultraviolet exposures were varied up to one equivalent year in space. The reflective surfaces were vacuum deposited Al, which in some cases were overcoated with Si_2O_3 or SiO_2 . The most severe mechanism of radiation-induced degradation was found to be proton blistering.

FIRST CLASS MAIL

POSTMASTER: If Undeliverable (Section 158
Postal Manual) Do Not Return

"The aeronautical and space activities of the United States shall be conducted so as to contribute . . . to the expansion of human knowledge of phenomena in the atmosphere and space. The Administration shall provide for the widest practicable and appropriate dissemination of information concerning its activities and the results thereof."

—NATIONAL AERONAUTICS AND SPACE ACT OF 1958

NASA SCIENTIFIC AND TECHNICAL PUBLICATIONS

TECHNICAL REPORTS: Scientific and technical information considered important, complete, and a lasting contribution to existing knowledge.

TECHNICAL NOTES: Information less broad in scope but nevertheless of importance as a contribution to existing knowledge.

TECHNICAL MEMORANDUMS: Information receiving limited distribution because of preliminary data, security classification, or other reasons.

CONTRACTOR REPORTS: Scientific and technical information generated under a NASA contract or grant and considered an important contribution to existing knowledge.

TECHNICAL TRANSLATIONS: Information published in a foreign language considered to merit NASA distribution in English.

SPECIAL PUBLICATIONS: Information derived from or of value to NASA activities. Publications include conference proceedings, monographs, data compilations, handbooks, sourcebooks, and special bibliographies.

TECHNOLOGY UTILIZATION PUBLICATIONS: Information on technology used by NASA that may be of particular interest in commercial and other non-aerospace applications. Publications include Tech Briefs, Technology Utilization Reports and Notes, and Technology Surveys.

Details on the availability of these publications may be obtained from:

SCIENTIFIC AND TECHNICAL INFORMATION DIVISION
NATIONAL AERONAUTICS AND SPACE ADMINISTRATION
Washington, D.C. 20546